ECSS-E-HB-31-01 Part 9A
5 December 2011

Space engineering

Thermal design handbook - Part 9: Radiators

ECSS Secretariat
ESA-ESTEC
Requirements & Standards Division
Noordwijk, The Netherlands

Foreword

This Handbook is one document of the series of ECSS Documents intended to be used as supporting material for ECSS Standards in space projects and applications. ECSS is a cooperative effort of the European Space Agency, national space agencies and European industry associations for the purpose of developing and maintaining common standards.

The material in this Handbook is a collection of data gathered from many projects and technical journals which provides the reader with description and recommendation on subjects to be considered when performing the work of Thermal design.

The material for the subjects has been collated from research spanning many years, therefore a subject may have been revisited or updated by science and industry.

The material is provided as good background on the subjects of thermal design, the reader is recommended to research whether a subject has been updated further, since the publication of the material contained herein.

This handbook has been prepared by TEC QR/MT, reviewed by the ECSS Executive Secretariat and approved by the ECSS Technical Authority.

Disclaimer

Published by: ESA Requirements and Standards Division
ESTEC, P.O. Box 299,
2200 AG Noordwijk
The Netherlands

Table of contents

Figures

Tables

1
Scope

Radiators are a significant component of all space vehicles. There are several methods of radiation dissipation. Radiator design in spacecrafts vary for the different stages of a mission and also vary according to mission constraints.

This Part 9 deals with the design and construction of radiators on spacecraft, depending on the energy dissipation requirements. Clause 5 is devoted to fin construction; the rest of this Part is devoted to cooling methods.

Additional methods of radiation dissipation are also discussed in ECSS-E-HB-31-01 Part 8 (heat pipes) and ECSS-E-HB-31-01 Part 10 (phase-change capacitors).

The Thermal design handbook is published in 16 Parts

ECSS-E-HB-31-01 Part 1	Thermal design handbook – Part 1: View factors
ECSS-E-HB-31-01 Part 2	Thermal design handbook – Part 2: Holes, Grooves and Cavities
ECSS-E-HB-31-01 Part 3	Thermal design handbook – Part 3: Spacecraft Surface Temperature
ECSS-E-HB-31-01 Part 4	Thermal design handbook – Part 4: Conductive Heat Transfer
ECSS-E-HB-31-01 Part 5	Thermal design handbook – Part 5: Structural Materials: Metallic and Composite
ECSS-E-HB-31-01 Part 6	Thermal design handbook – Part 6: Thermal Control Surfaces
ECSS-E-HB-31-01 Part 7	Thermal design handbook – Part 7: Insulations
ECSS-E-HB-31-01 Part 8	Thermal design handbook – Part 8: Heat Pipes
ECSS-E-HB-31-01 Part 9	Thermal design handbook – Part 9: Radiators
ECSS-E-HB-31-01 Part 10	Thermal design handbook – Part 10: Phase – Change Capacitors
ECSS-E-HB-31-01 Part 11	Thermal design handbook – Part 11: Electrical Heating
ECSS-E-HB-31-01 Part 12	Thermal design handbook – Part 12: Louvers
ECSS-E-HB-31-01 Part 13	Thermal design handbook – Part 13: Fluid Loops
ECSS-E-HB-31-01 Part 14	Thermal design handbook – Part 14: Cryogenic Cooling
ECSS-E-HB-31-01 Part 15	Thermal design handbook – Part 15: Existing Satellites
ECSS-E-HB-31-01 Part 16	Thermal design handbook – Part 16: Thermal Protection System

2 References

ECSS-S-ST-00-01	ECSS System - Glossary of terms
ECSS-E-HB-31-01 Part 6	Thermal design handbook – Part 6: Thermal Control Surfaces
ECSS-E-HB-31-01 Part 7	Thermal design handbook – Part 7: Insulations
ECSS-E-HB-31-01 Part 11	Thermal design handbook – Part 11: Electrical Heating
ECSS-E-HB-31-01 Part 14	Thermal design handbook – Part 14: Cryogenic Cooling

All other references made to publications in this Part are listed, alphabetically, in the **Bibliography**.

3
Terms, definitions and symbols

3.1 Terms and definitions

For the purpose of this Standard, the terms and definitions given in ECSS-S-ST-00-01 apply.

3.2 Abbreviated terms

The following abbreviated terms are defined and used within this Standard.

ADL	Arthur D. Little
AVHRR	advanced very high resolution radiometer
CRTU	cryogenic radiator test unit
HIRS	high resolution infrared sounder
HP	heat pipe
IR	infrared
ITT	international telephone and telegraph corporation
MERC	
MLI	multilayer insulation
MSS	multispectral scanner
PCM	phase-change material
RCA	radio corporation of America
SCMR	surface composition mapping radiometer
SRET	satellites de recherches et d'etudes technologiques
UV	ultraviolet
VHRR	very high resolution radiometer
VISSR	visible and infrared spin scan radiometer

3.3 Symbols

$\mathbf{A_p}$	patch area in a passive radiator, [m]
D	diameter, [m]
$\mathbf{F_L}$	volume function for fixed fin length, defined in clause 5.2.4
$\mathbf{F_W}$	volume function for fixed Q_L/W ratio, defined in clause 5.2.4
$\mathbf{F_t}$	volume function for fixed fin thickness, defined in clause 5.2.4
H	height, [m]
L	characteristic length of the fin, it is defined more precisely in the sketches, [m]
M	dimensionless thermal conductivity vs. temperature slope, defined in clause 5.2.5
N	dimensionless emittance vs. temperature slope, defined in clause 5.2.5
$\mathbf{P_c}$	detector control power, [W]
Q	heat load, [W]
$\mathbf{Q_E}$	parasitic heat load, [W]
$\mathbf{Q_L}$	Clause 5: heat radiated by the fin per unit time, [W] Clause 6: detector heat output, [W]
$\mathbf{Q_0}$	heat radiated by the fin, per unit time, when at temperature, T_0.= [W]
$\mathbf{Q_T}$	heat radiated by the fin-base system per unit time, [W]
$\mathbf{R_0}$	tube radius, also outer radius of annular fins, [m]
$\mathbf{R_P}$	radius of the planet, [m]
$\mathbf{R_i}$	inner radius of annular fins, [m]
T	temperature, [K]
$\mathbf{T_0}$	temperature at the base of the fin, [K]
$\mathbf{T_1}$	Clause 5: mid-fin temperature, [K]

	Clause 6: passive radiant cooler first stage temperature, [K]
T_C	cold boundary temperature in an MLI, [K]
T_H	hot boundary temperature in an MLI, [K]
T_S	equivalent surrounding temperature, [K]
T_P	patch temperature in a passive radiator, [K]
T_s	sunshield temperature, [K]
W	width of the fin, [m]
X	dimensionless coordinate along the fin, $X = x/L$
f(λ)	conductance function, defined as: $f(\lambda) = 0{,}4(1-\tau_1^5)-2\tau_S(1-\tau_1)$
h	distance from the spacecraft to the planet surface, [m]
i	inclination of the orbital plane, [angular degrees]
k	thermal conductivity of the fin, [$W.m^{-1}.K^{-1}$]
k_{eff}	effective thermal conductivity of an MLI, [$W.m^{-1}.K^{-1}$]
m	number of reflections
t	Clause 5: thickness of the fin, it is defined more precisely in the sketches, [m]
	Clause 6: time, [h]
x	coordinate along the fin, [m]
y	coordinate across the fin platform, [m]
z	coordinate normal to fin platform, [m]
α_s	solar absorptance
β	angle between cone axis and extreme incident rays, [angular degrees]
δ	lengths in finned tube radiators, they are introduced in clause 5.2.6 [m]
ε	emittance, a factor 2 is included for fins emitting on both faces

η	Clause 5: radiating effectiveness of a fin, it is defined as the actual heat flow rate from the fin divided by the ideal rate, the ideal heat flow rate is that from the fin, assuming that its thermal conductivity is infinitely large, and that it radiates without interference at the base temperature T_0 Clause 6: thermal effectiveness of passive radiator, it is defined in clause 6.3.1.
θ	angle, [angular degrees]
λ	conductance parameter, defined as: $\lambda = \sqrt{\frac{\varepsilon\sigma T_0^3 L^2}{kt}}$.
ρ_{IR}	infrared reflectance
ρ_s	solar reflectance
σ,	Stefan-Boltzmann constant, $\sigma = 5{,}6697 \times 10^{-8}$ $W.m^{-2}.K^{-4}$
τ,	dimensionless temperature, $\tau = T/T_0$
ϕ	angle between Earth-vehicle vector and Earth horizon, [angular degrees]

Subscripts

S	equivalent surrounding temperature conditions
1	conditions at $X = 1$

4
General introduction

A radiator is a system which takes the waste thermal energy from a heat source and discharges it, by radiation to the exterior, through radiating surfaces. Normally these radiating surfaces are the fins.

Depending on how the heat is transferred from the source to the radiating surfaces, radiators can be classified as follows:

TYPE	CONNECTION TO THE HEAT SOURCE
Passive Radiators	Direct
	By means of Heat Pipes
	By means of Phase-Change Materials (PCM)
Active Radiators	By means of Fluid Loops
	By means of Fluid Loops plus Heat Pipes

4.1 Passive radiators

Passive radiators do not require power. They can be coupled to the heat source in the following ways.

1. Passive Radiators Directly Connected to the Heat Source.

   In these radiators the radiating surfaces are connected to the heat source by thermal conduction through the walls of the heat source, by radiation, or both.

   The main advantage of these radiators is their simplicity and although they have been mainly used to cool lenses and IR detectors in the range of cryogenic temperatures, there is no reason to overlook possible applications at higher temperatures, provided that the required size does not exceed reasonable limits.

   Since directly connected radiators can be tailored to the system to be cooled it is difficult to define their standard configuration.

2. Passive Radiators Connected to the Heat Source with Heat Pipes.

   In this type of radiators, the heat pipes, whose operating peculiarities are discussed in ECSS-E-HB-31-01 Part 8, carry the heat from the source to the radiating surfaces, as sketched in Figure 4-1

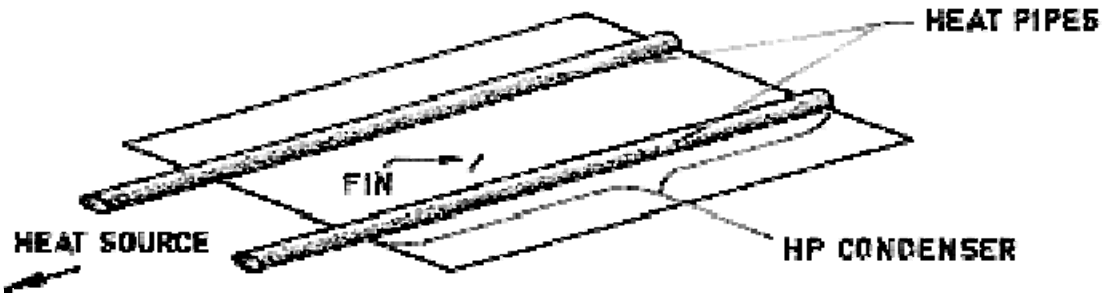

Figure 4-1: Sketch of a Heat Pipe-Radiator

The evaporators of the heat pipes are placed close to the heat source, and the condenser zones are placed in the radiating surfaces.

Joining of the heat pipe to the fin can be made by either of the following methods:

(a) directly,

(b) integrating the heat pipe into a honeycomb structure, or

(c) joining the heat pipe to the fins by means of specially shaped mounting surfaces.

3. Passive Radiators with Phase-Change Materials.

In these systems the heat transfer through the radiator is controlled by a PCM, Figure 4-2, which melts during the high heat dissipation periods and freezes again when the temperature decreases. The performances of the PCMs are discussed in ECSS-E-HB-31-01 Part 8.

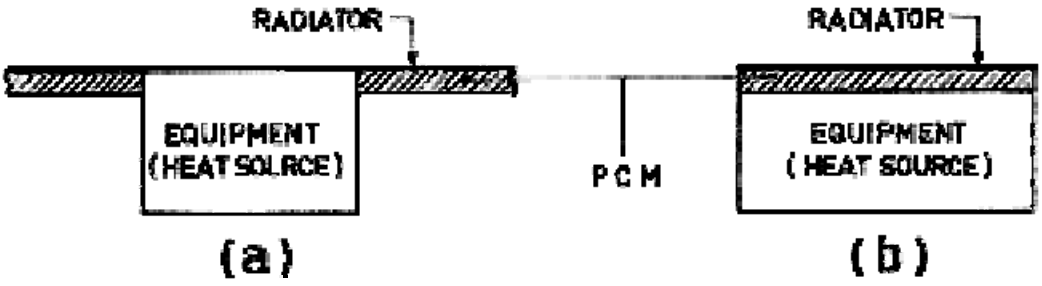

Figure 4-2: Typical configurations of passive radiators with Phase-change materials

System (a) of Figure 4-2 has the PCM attached to the radiator fin, allowing good conductive heat transfer to the surfaces radiating to space. This arrangement provides the maximum heat rejection by radiation directly from the heat source, but decreases the thermal potential at the fin-PCM interface because of the temperature decay along the fin.

In system (b) of Figure 4-2, the PCM is placed between the heat source and the radiator. The radiated heat rate is limited by the fact that the radiator is at-or-below-the PCM melting temperature provided that the material should not be melted. During the whole process the PCM insulates the heat source from the radiator.

4.2 Active radiators

Active radiators require power to pump the fluid convecting the heat. This fluid is pumped from the source either to the radiating surfaces or just to their root. In the later case heat pipes should be used to increase the thermal conductivity of the fins. Coupling with the heat source can be achieved as follows:

1. Active Radiators with the Heat Source Connected to the Radiating Surfaces by Means of Fluid Loops.

   In these radiators a working fluid carries the heat from the source to the radiating surfaces which are of the fin-tube configuration (Figure 4-3). The fluid exchanges heat with the fins while it is being cooled. Generally the working fluid is a two-phase fluid entering into the fin-tube panel in the vapor phase and going out as a liquid which has been condensed when passing through the tubes of the fins.

   These radiators are normally used to dissipate the waste heat in spacecraft power systems.

   Operating peculiarities of fluid loops are discussed in ECSS-E-HB-31-01 Part 13.

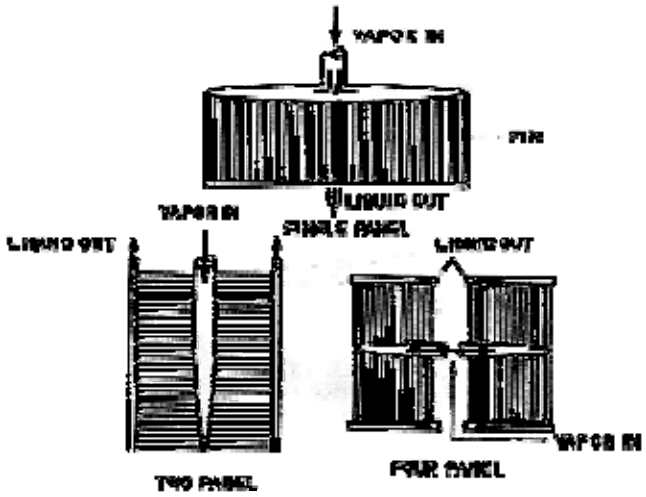

Figure 4-3: Typical configurations of radiators with fluid loops. After Krebs, Winch & Lieblein (1963) [11].

2. Active radiators with the heat source connected to the radiating surfaces by means of fluid loops plus heat pipes.

   In these radiators the working fluid carries the heat from the source to the root of the radiating surfaces, while a system of heat pipes distributes the heat along these surfaces. The evaporator of the heat pipe is braced to the fluid loop and the condenser to the radiating surfaces.

5
Fins

5.1 General

This clause concerns fins formed by flat plates of rectangular or annular plan forms with the common feature of having one or more lines drawn on the surface whose temperature is kept constant. In the case of Figure 5-1a such lines are AA and BB, while in Figure 5-1b they are the inner circles of the annuli. The procedure used to keep the temperature constant along these lines is immaterial, heat pipes or other devices could be used.

The data presented cannot be applied to study the following configurations:

1. Passive radiators in direct contact with the heat source.
2. Passive radiators with phase-change materials.
3. Active radiators with a single-phase coolant.

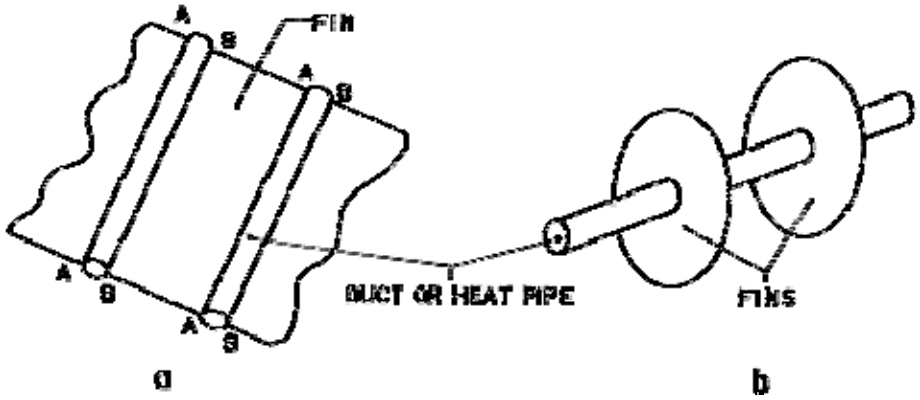

Figure 5-1: Typical configurations of finned radiators.

5.2 Rectangular plan form

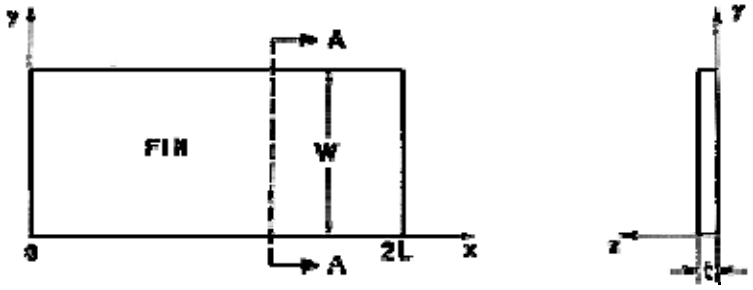

Assumptions:

The following assumptions have been made by Lieblein (1959) [12] to calculate the performances of these fins.

1. The fin is uniformly heated along the edges x = 0 and x = 2L which are at the same temperature.
2. The heat is evacuated from the plate only by radiation through a non-absorbing medium.
3. Thermal properties of the materials are constant, unless otherwise indicated.
4. the plate temperature is constant across the thickness t for each x position.
5. In order to take into account the heat received by the fin both directly from the space and reflected from the other parts of the spacecraft, an equivalent temperature, T_S, is used.

5.2.1 Temperature distribution along the fin

Differential Equation:

$$\frac{d^2\tau}{dX^2} = \lambda^2\left(\tau^4 - \tau_S^4\right) \qquad [5\text{-}1]$$

Boundary Conditions:

$\tau = 1$ on $X = 0$

$d\tau/dX = 0$ on $X = 1$ (symmetry boundary condition).

Values of $\tau = T/T_0$ vs. $X = x/L$ for several values of T_S/T_0 and of the conductance parameter, λ, which have been obtained by solving the above differential equation, are plotted in Figure 5-2 to Figure 5-4. The ratio T_1/T_0 (mid-fin temperature) vs. the conductance parameter, λ, for several values of the ratio T_S/T_0 is shown in Figure 5-5.

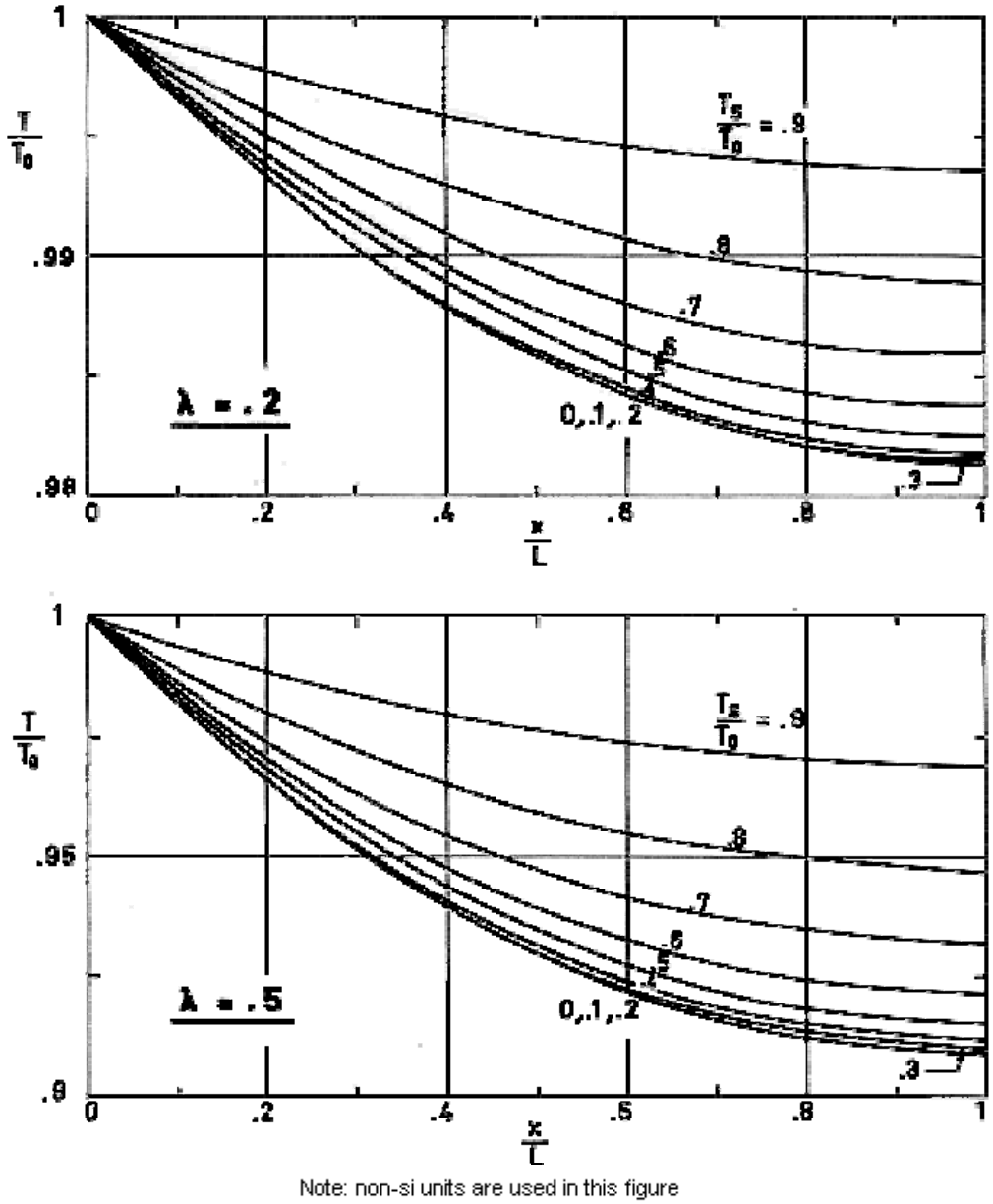

Figure 5-2: Dimensionless temperature distribution, T/T_0, along the fin, for several values of the dimensionless surrounding temperature, T_s/T_0. Calculated by the compiler.

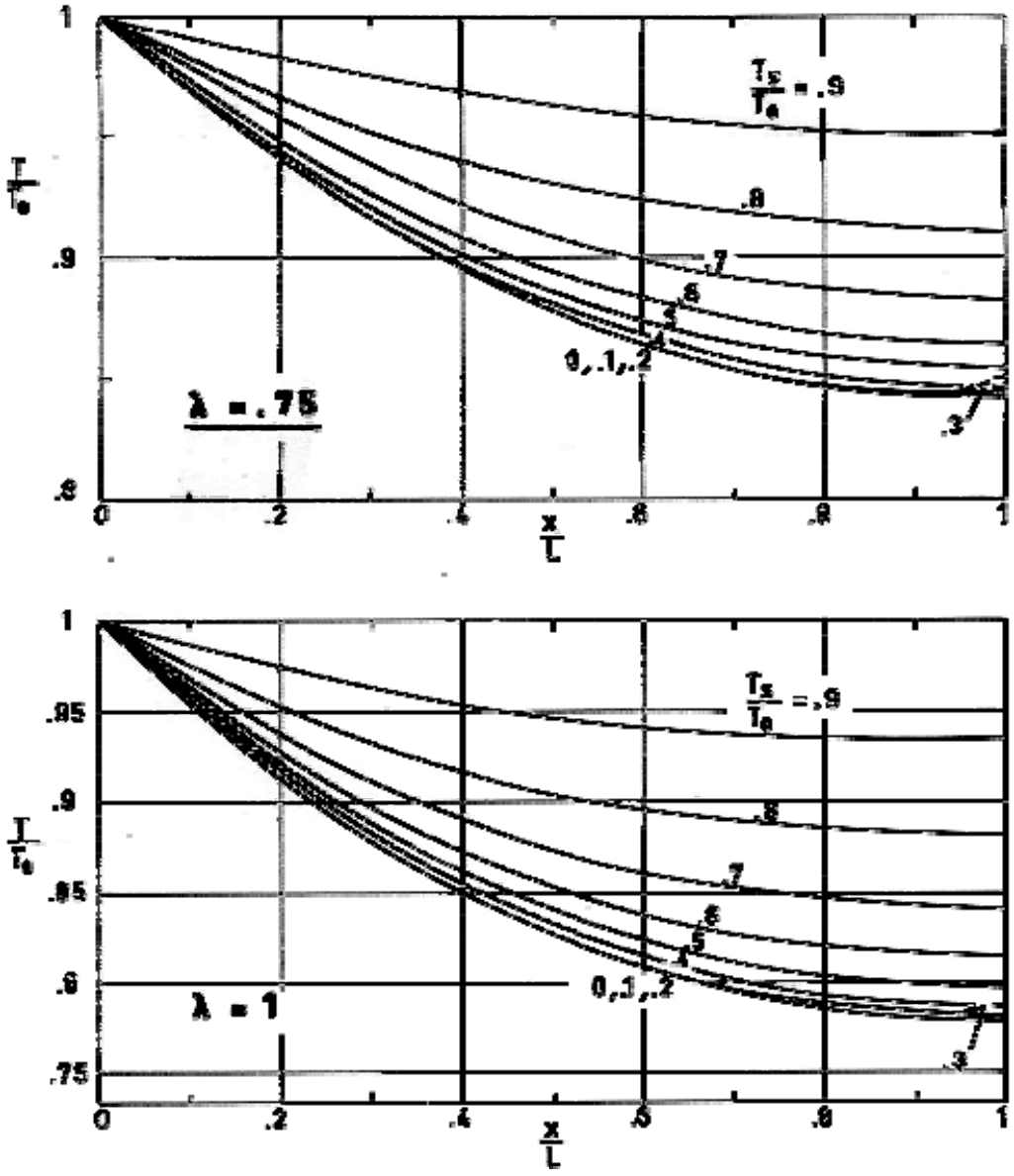

Figure 5-3: Dimensionless temperature distribution, T/T_0, along the fin, for several values of the dimensionless surrounding temperature, T_S/T_0. Calculated by the compiler.

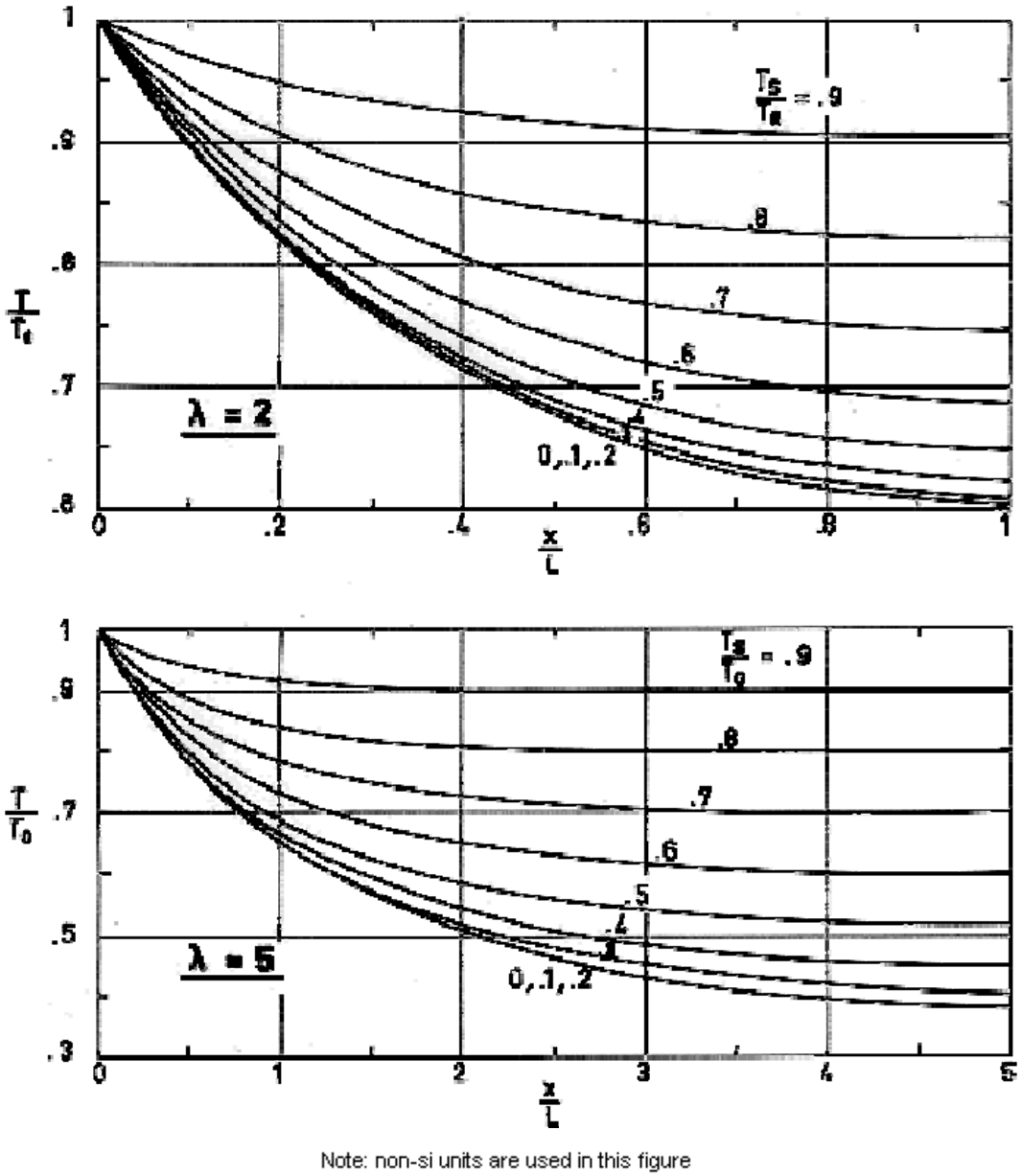

Note: non-si units are used in this figure

Figure 5-4: Dimensionless temperature distribution, T/T_0, along the fin, for several values of the dimensionless surrounding temperature, T_S/T_0. Calculated by the compiler.

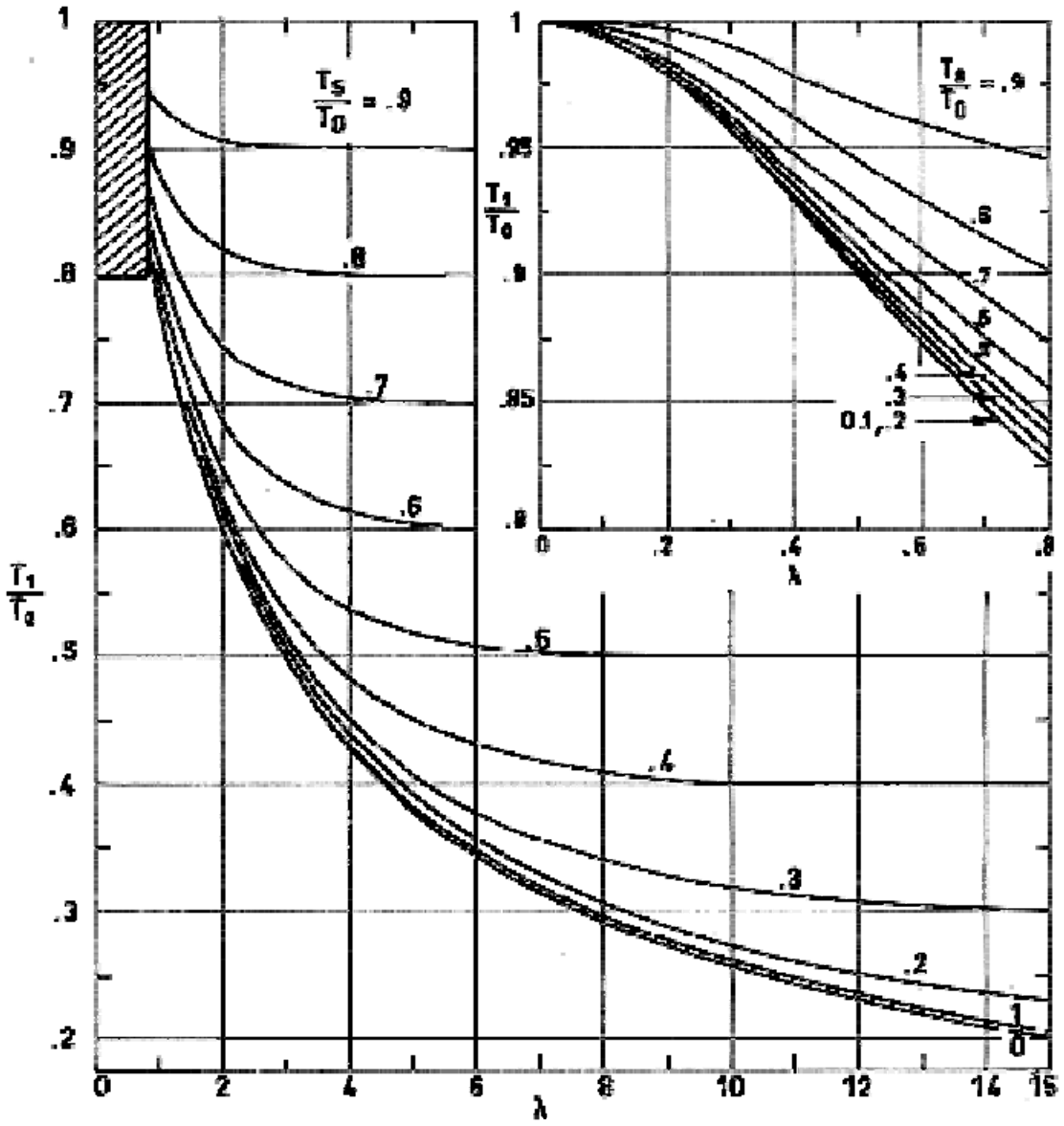

Figure 5-5: Dimensionless mid-fin temperature, T/T_0, vs. conductance parameter, λ, for several values of the dimensionless surrounding temperature, T_S/T_0. Calculated by the compiler.

5.2.2 Radiated heat

The heat radiated by the fin, between positions $x = 0$ and $x = L$, is given by the following expression:

$$\frac{Q_L / W}{\sqrt{kt\varepsilon\sigma T_0^5}} = \sqrt{\frac{2}{5}\left[1-\tau_1^5-5\tau_S^4(1-\tau_1)\right]} \qquad [5\text{-}2]$$

If the fin temperature, T_0, were uniform, the heat radiated would be:

$$\frac{Q_0 / W}{\sqrt{kt\varepsilon\sigma T_0^5}} = \lambda\left(1-\tau_S^4\right) \qquad [5\text{-}3]$$

The ratios of the first members of both equations are plotted in Figure 5-6 and Figure 5-7 respectively, vs. the conductance parameter, λ, for different values of the ratio T_S/T_0.

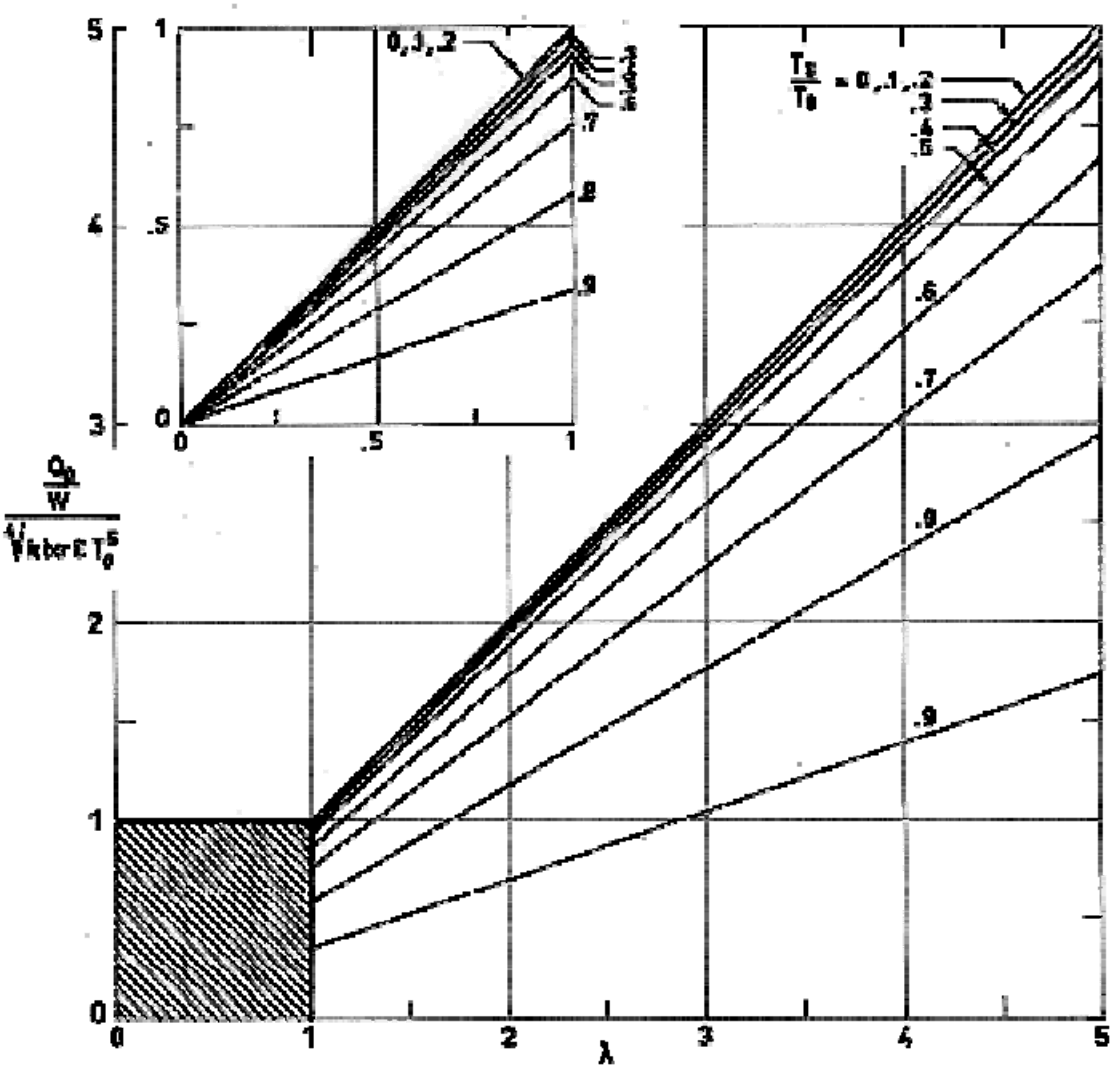

Note: non-si units are used in this figure

Figure 5-6: Dimensionless radiated heat from a rectangular fin at temperature T_0, vs. conductance parameter, λ, for several values of the dimensionless surrounding temperature, T_S/T_0. Calculated by the compiler.

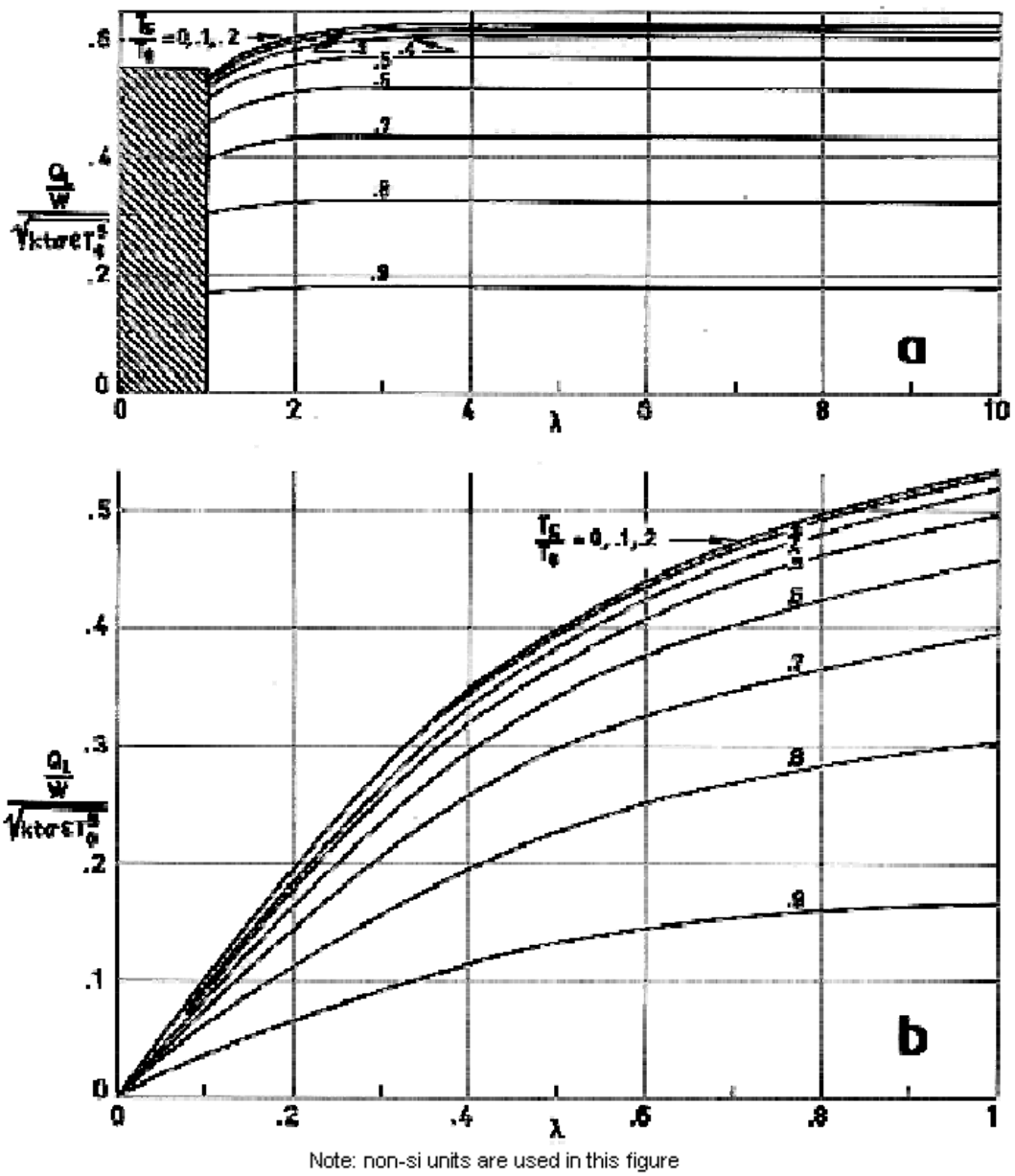

Figure 5-7: Total dimensionless radiated heat vs. conductance parameter, λ, for several values of the dimensionless surrounding temperature, T_S/T_0. Zone shade in a) is enlarged in b). Calculated by the compiler.

5.2.3 Radiating effectiveness

According to the definition given in the List of Symbols, the radiating effectiveness, η, may be written as:

$$\eta = \frac{Q_L}{Q_0} = \frac{\sqrt{\frac{2}{5}\left[1-\tau_1^5-5\tau_S^4\left(1-\tau_1\right)\right]}}{\lambda\left(1-\tau_S^4\right)} \qquad [5\text{-}4]$$

η is plotted vs. λ in Figure 5-8 for several values of the ratio T_S/T_0.

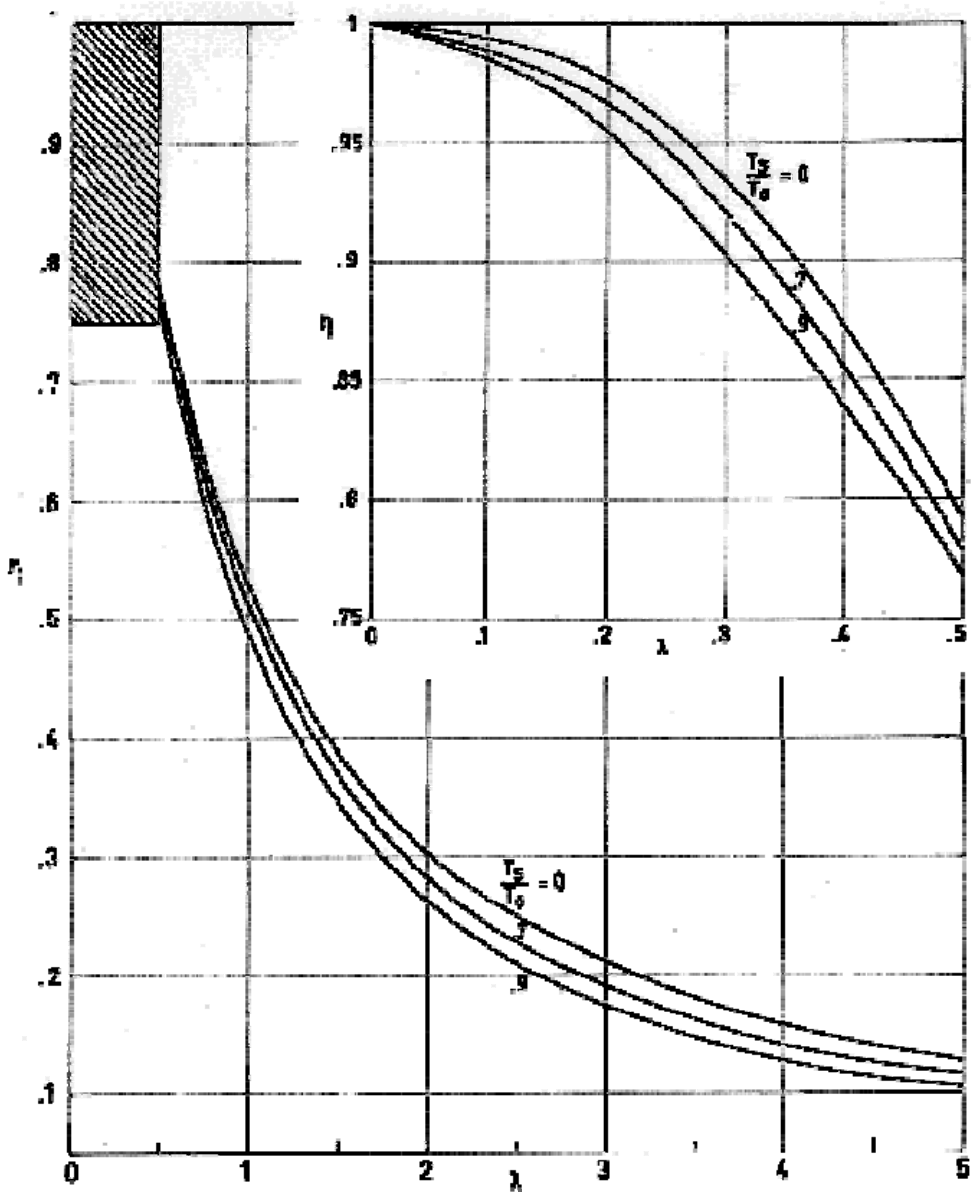

Figure 5-8: Radiating effectiveness, η, vs. conductance parameter, λ, for several values of the dimensionless surrounding temperature, T_S/T_0. Calculated by the compiler.

5.2.4 Volume functions

In order to estimate the values of the thickness, width, and length of the fin that results in a minimum fin volume for a given amount of the heat radiated, the following volume functions could be introduced.

1. For a given length, the volume functions is:

$$F_L = \frac{kT_0}{L^2}\frac{WLt}{Q_L} = \frac{1}{\lambda\sqrt{f(\lambda)}} \qquad [5\text{-}5]$$

According to the definition of λ, $t \sim \lambda^2$ in this particular case.

2. When the thickness is fixed, the volume function is given by:

$$F_t = \frac{\varepsilon\sigma T_0^4}{t}\frac{WLt}{Q_L} = \frac{\lambda}{\sqrt{f(\lambda)}} \qquad [5\text{-}6]$$

while the length, L, is proportional to λ.

3. Sometimes the ratio Q_L/W is given. In these cases the volume function may be written as:

$$F_W = \frac{\varepsilon\sigma T_0^4 k T_0}{(Q_L/W)^2}\frac{WLt}{Q_L} = \frac{\lambda}{[f(\lambda)]^{3/2}} \qquad [5\text{-}7]$$

$L/t^{1/2}$ being a linear function of λ.

The volume functions F_L, F_t, and T_W are plotted in Figure 5-9, Figure 5-10, and Figure 5-11 as functions of λ^2 (proportional to t), λ (proportional to L), and λ (proportional to $L/t^{1/2}$) respectively, for several values of the dimensionless surrounding temperature, T_S/T_0.

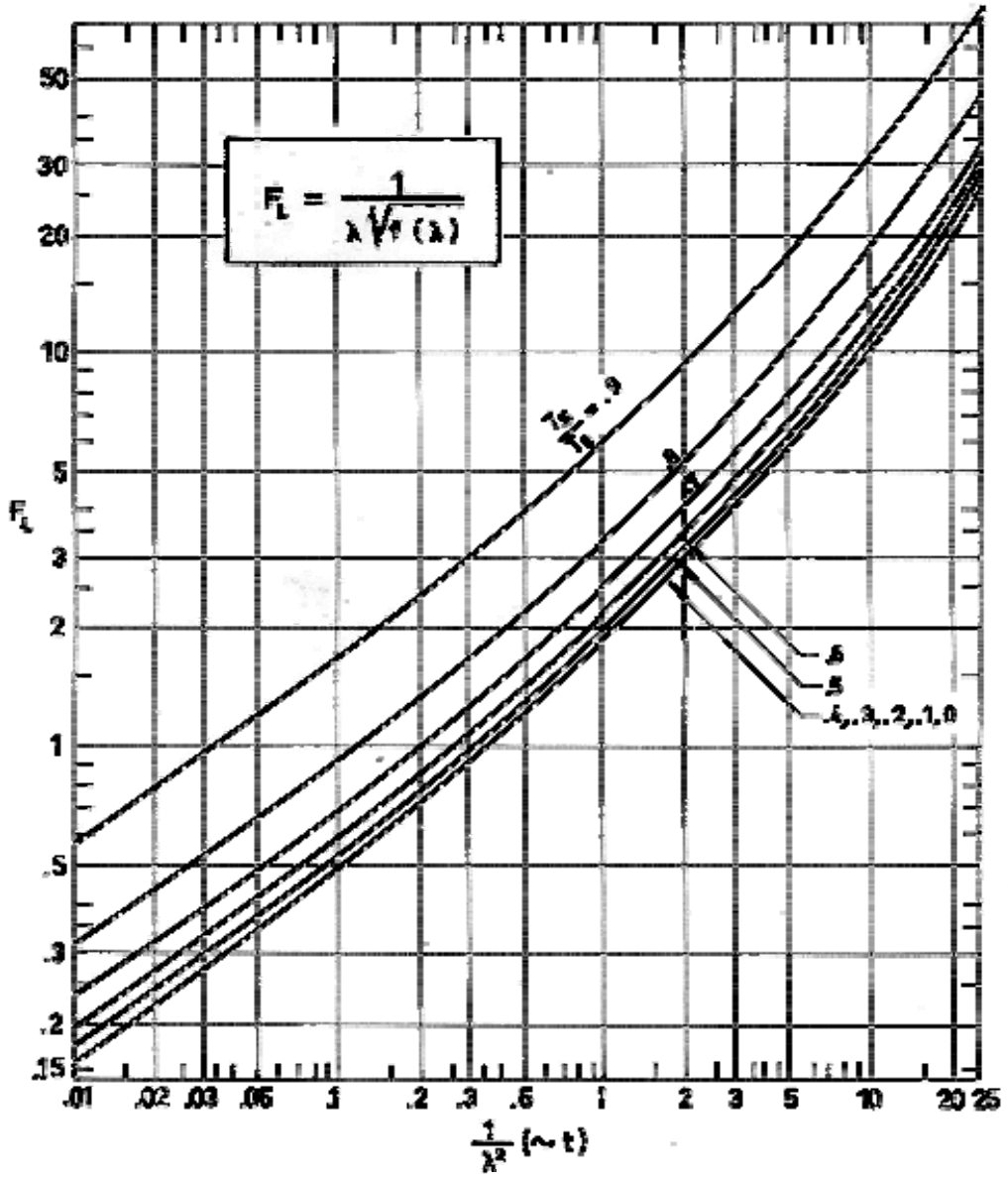

Figure 5-9: Volume function, F_L, when the length of the fin is fixed, vs. $1/\lambda^2$ (proportional to thickness, t) for several values of the dimensionless surrounding temperature, T_S/T_0. Calculated by the compiler.

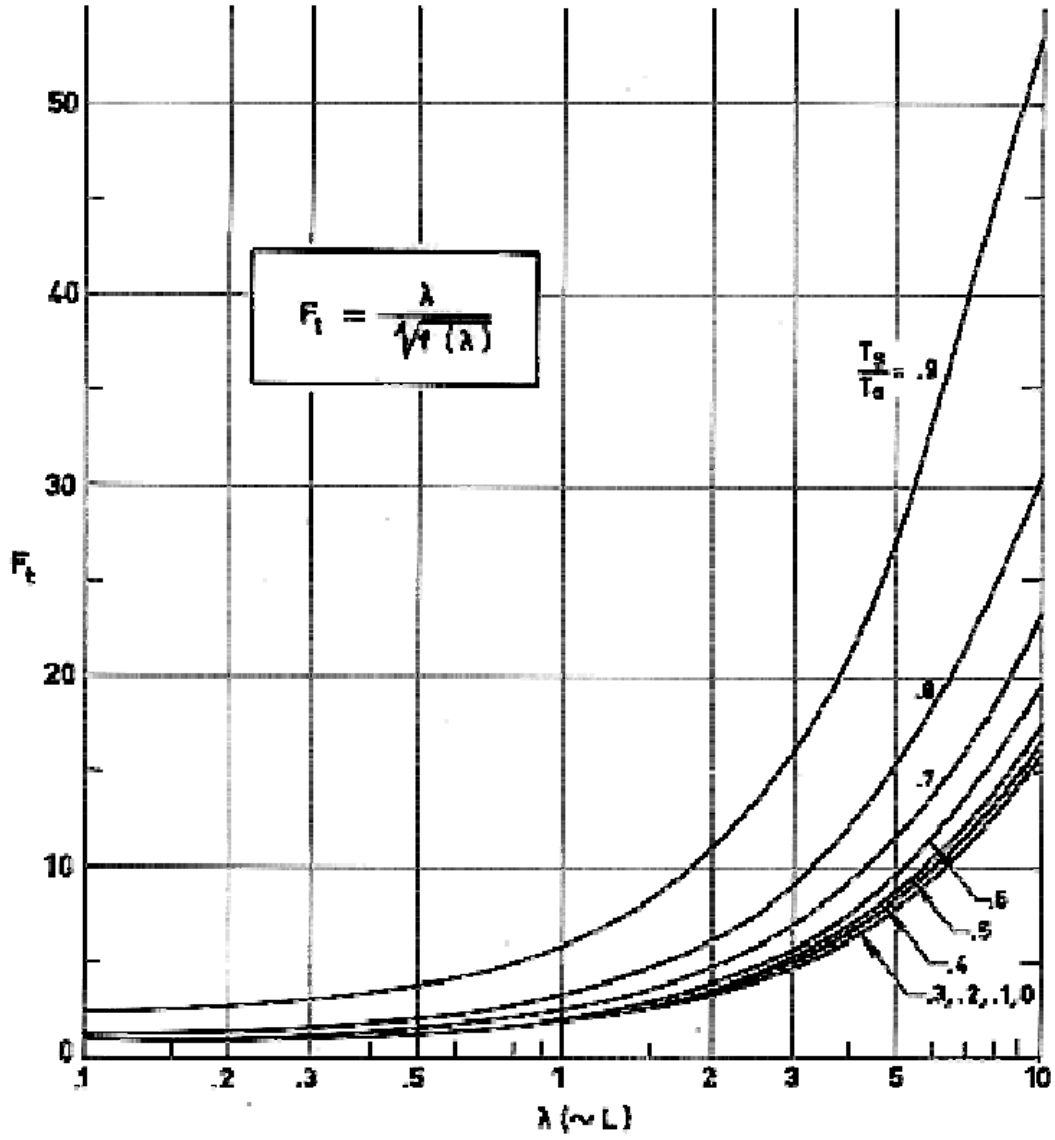

Note: non-si units are used in this figure

Figure 5-10: Volume function, F_t, when the thickness of the fin is fixed, vs. conductance parameter, λ (proportional to length, L) for several values of the dimensionless surrounding temperature, T_s/T_0. Calculated by the compiler.

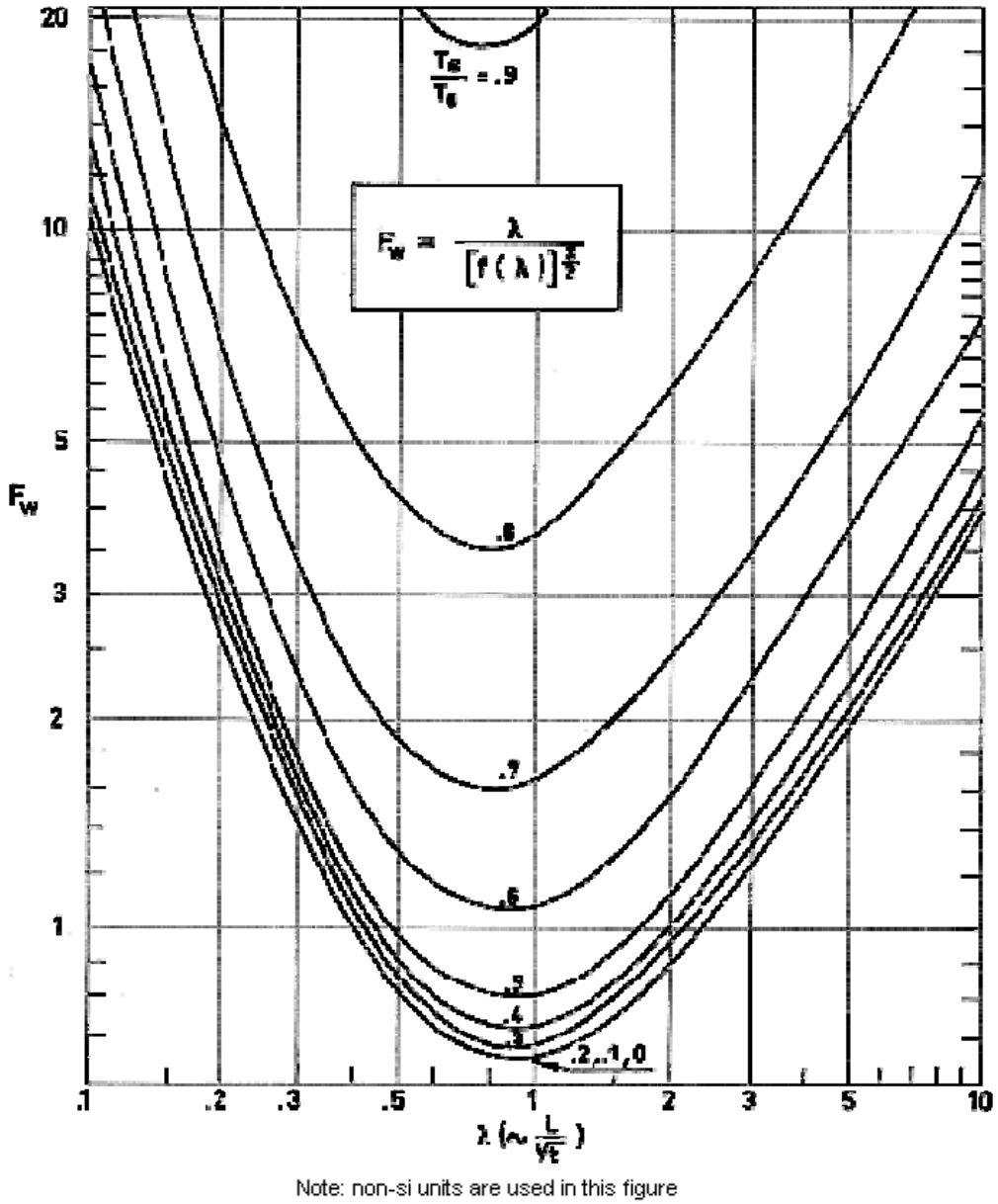

Note: non-si units are used in this figure

Figure 5-11: Volume function, F_W, when the ratio Q_L/W is fixed, vs. conductance parameter, λ, (proportional to $L/(t)^{1/2}$) for several values of the dimensionless surrounding temperature, T_S/T_0. Calculated by the compiler.

5.2.5 Effect of variable thermal properties

When thermal properties are not constant, the effect of temperature on the radiating effectiveness of the fin, for zero surrounding temperature and several values of the conductance parameter, τ, can be deduced from Figure 5-12 to Figure 5-14.

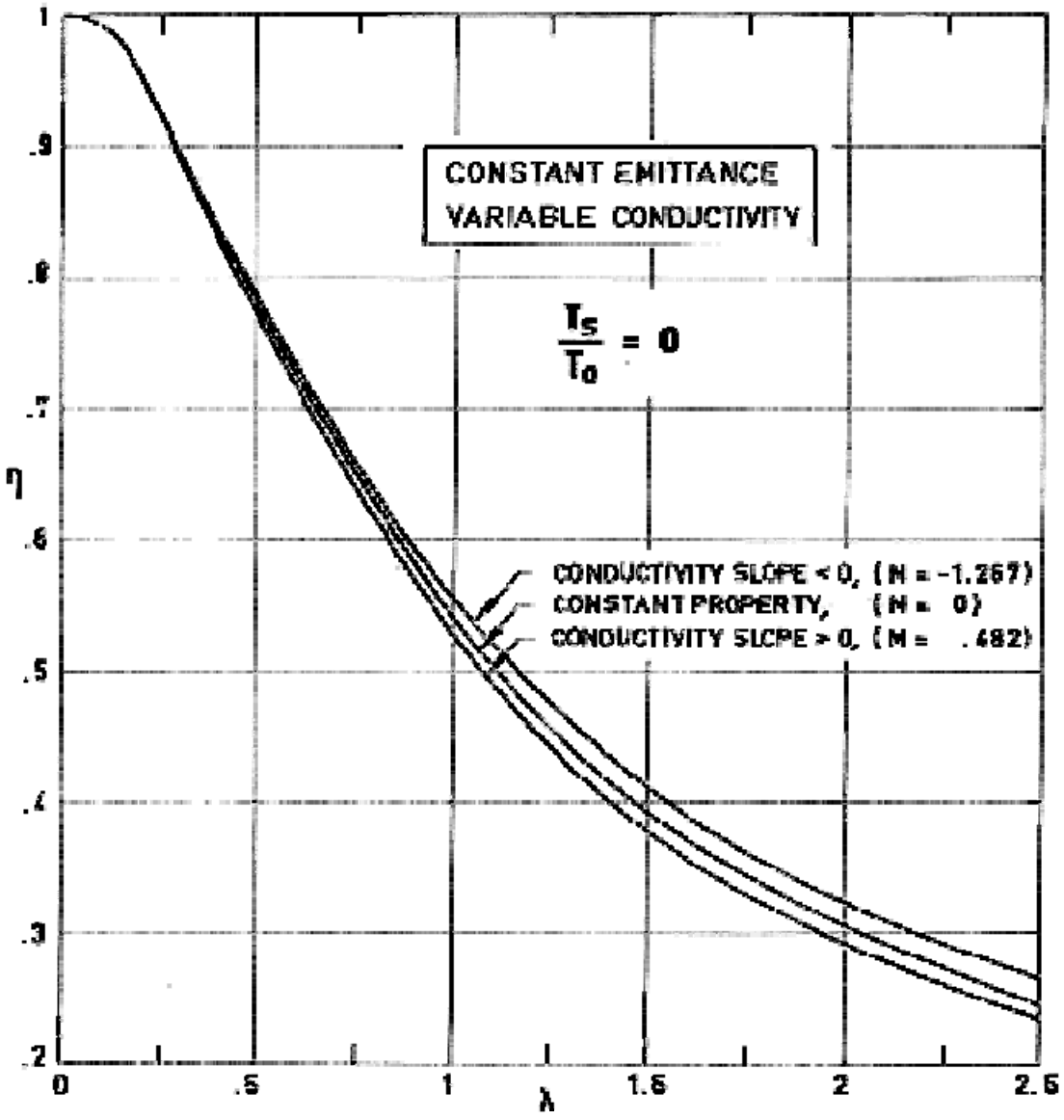

Note: non-si units are used in this figure

Figure 5-12: Radiating effectiveness, η, vs. conductance parameter, λ, for different values of the conductivity slope, M. From Stockman & Kramer (1963) [18].

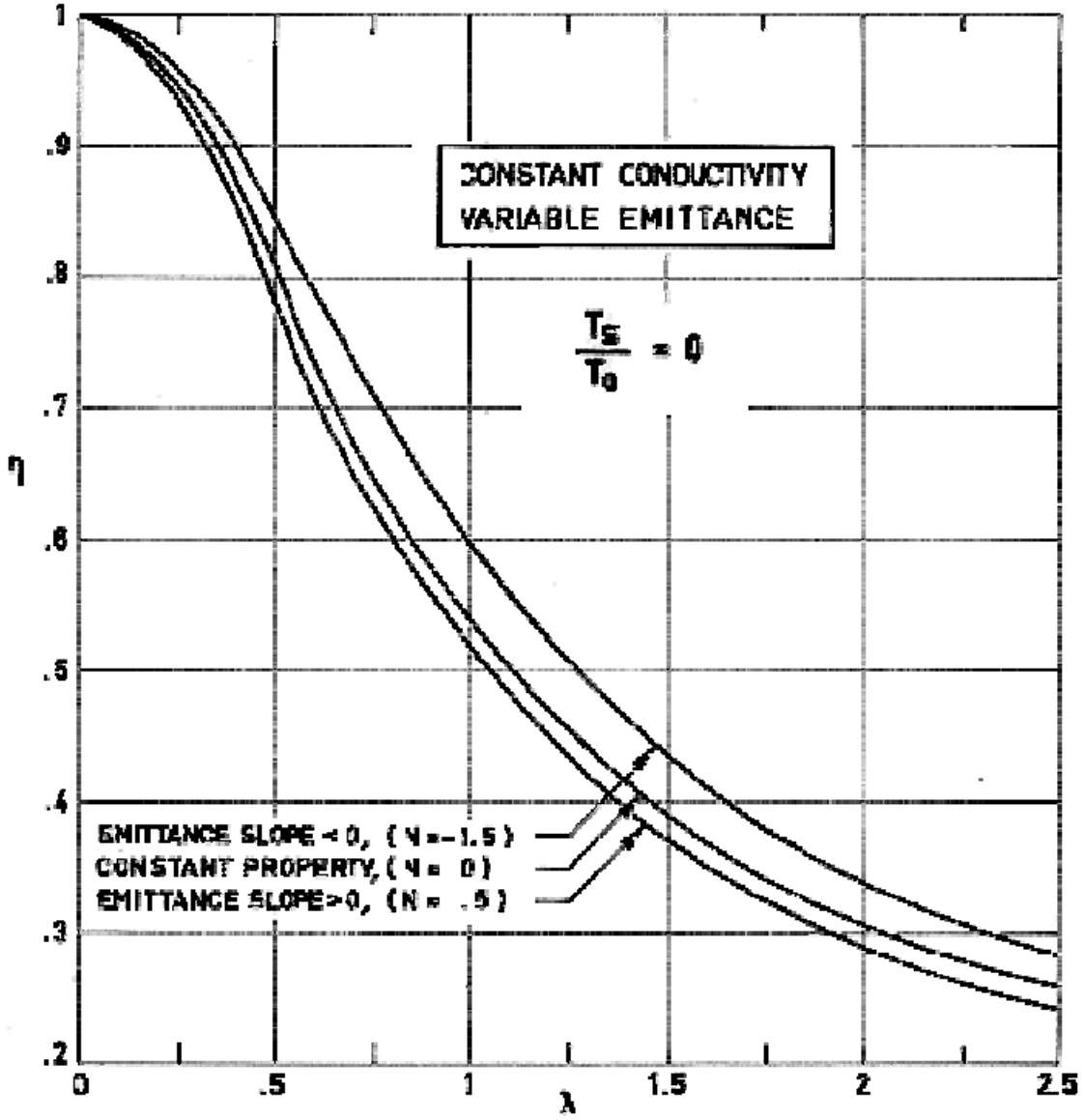

Note: non-si units are used in this figure

Figure 5-13: Radiating effectiveness, η, vs. conductance parameter, λ, for different values of the emittance slope, *N*. From Stockman & Kramer (1963) [18].

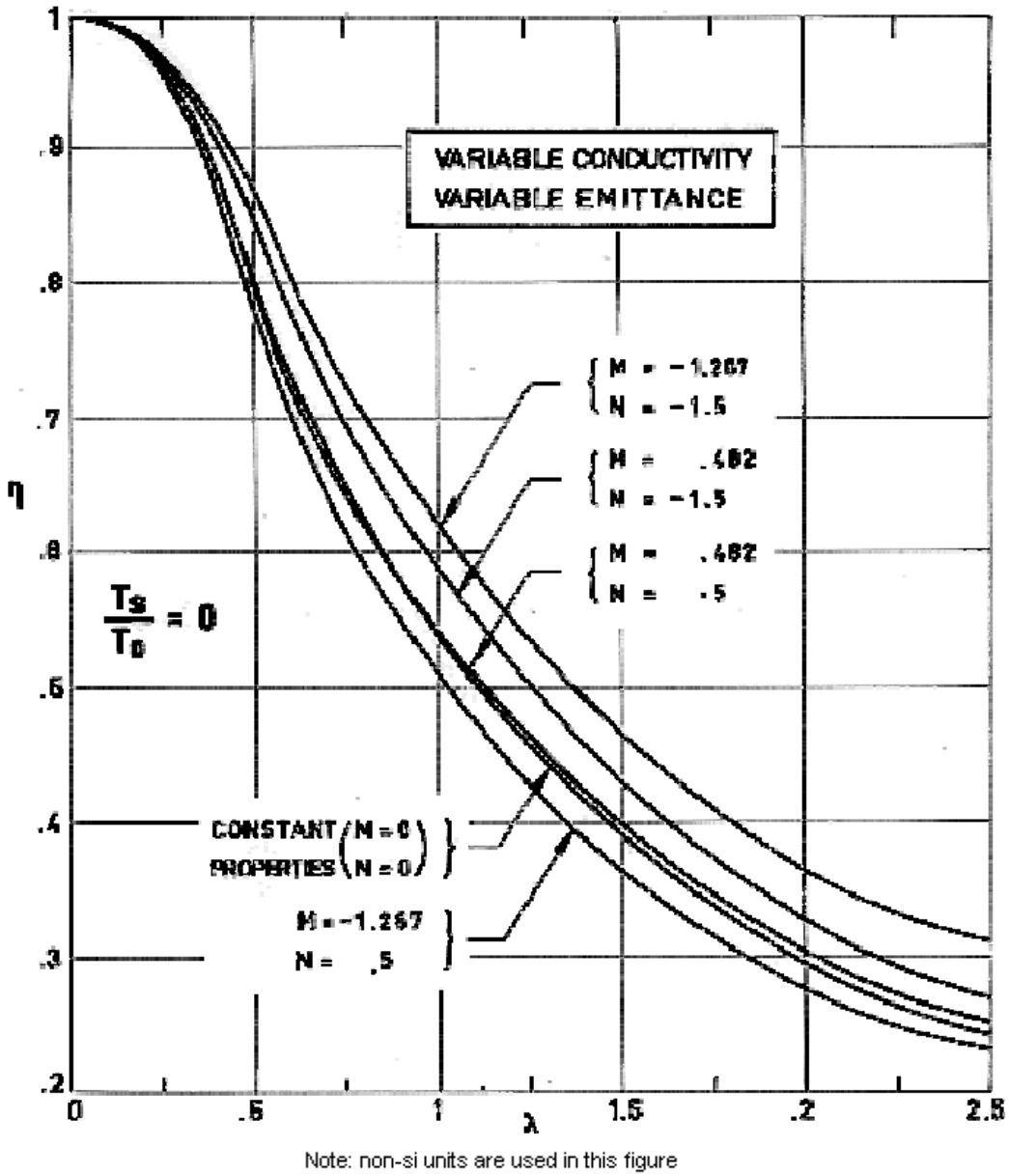

Figure 5-14: Radiating effectiveness, η, vs. conductance parameter, λ, for several values of the conductivity, *M*, and emittance, *N*, slopes. After Stockman & Kramer (1963) [18].

The variables which are assumed to be temperature dependent are the thermal conductivity and the emittance.

The dependence on the temperature is supposed to be given by the following expressions:

$k(T) = k(T_0)\ [1 + M(\tau\text{-}1)]$

$\varepsilon(T) = \varepsilon(T_0)\ [1 + N(\tau\text{-}1)]$

where *M* and *N* are, respectively, the dimensionless slopes of thermal conductivity and emittance.

5.2.6 Heat transfer characteristics of finned-tube radiators

More realistic data, borrowed from Haller (1964) [9], including the contribution to the heat balance of both fins and tubes are given in this clause.

The following assumption have been made:

1. Temperature of the tube surface is constant.
2. Incoming radiation from the external sources is negligible.
3. Fin thickness is neglected in the determination of the view factors from the base surface to the fin.
4. Fin and tube material properties are constant and evaluated at the fin-base temperature.
5. The surfaces act as blackbodies with incident and emitted radiation governed by Lambert's cosine law.
6. The energy input to the fin is composed of heat conduction along the fin from the fin base, and of the incident radiation from the two base surfaces. In the case of the closed-sandwich configuration, additional incident radiation comes from the opposing fin surface. Radiant emission comes from both sides of the fin-tube panel.

The results obtained on the basis of these assumptions are given in **Figure 5-15:** to Figure 5-18.

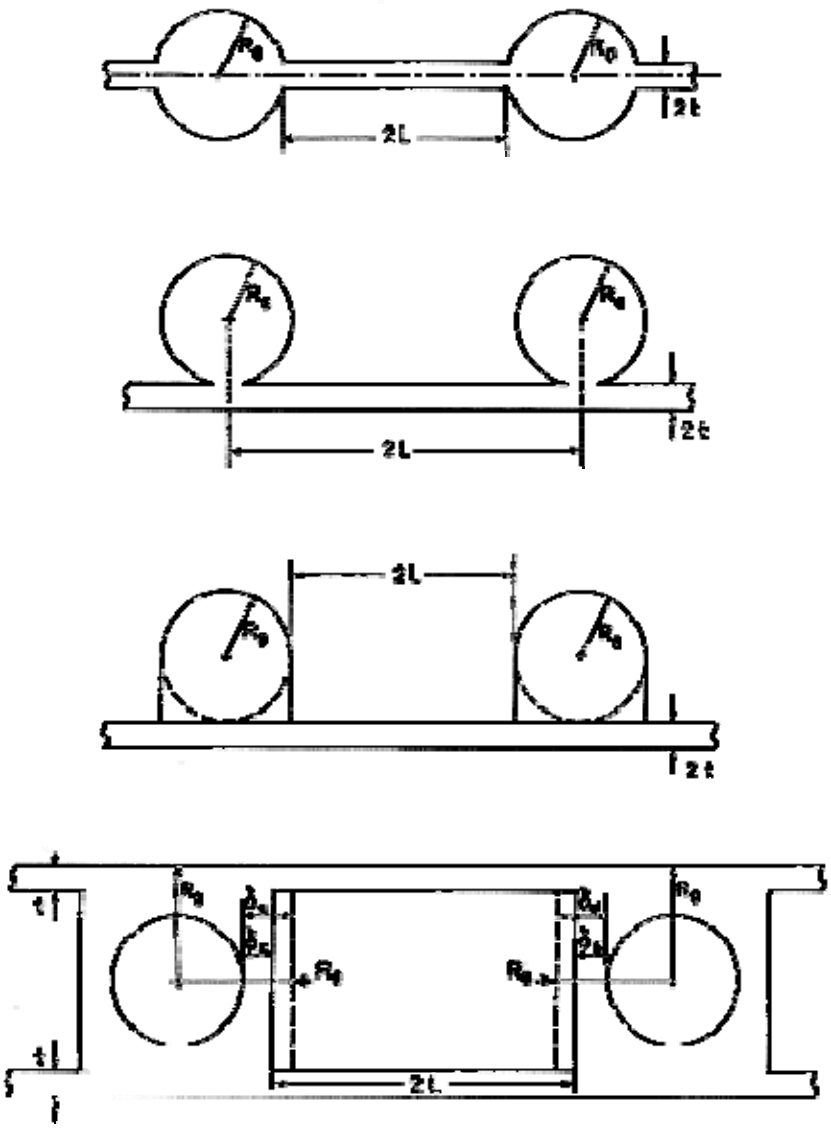

Figure 5-15: Radiating effectiveness, η, vs. ratio L/R_0 for several values of the conductance parameter, λ. Form Haller (1964) [9] (Part 1/2)

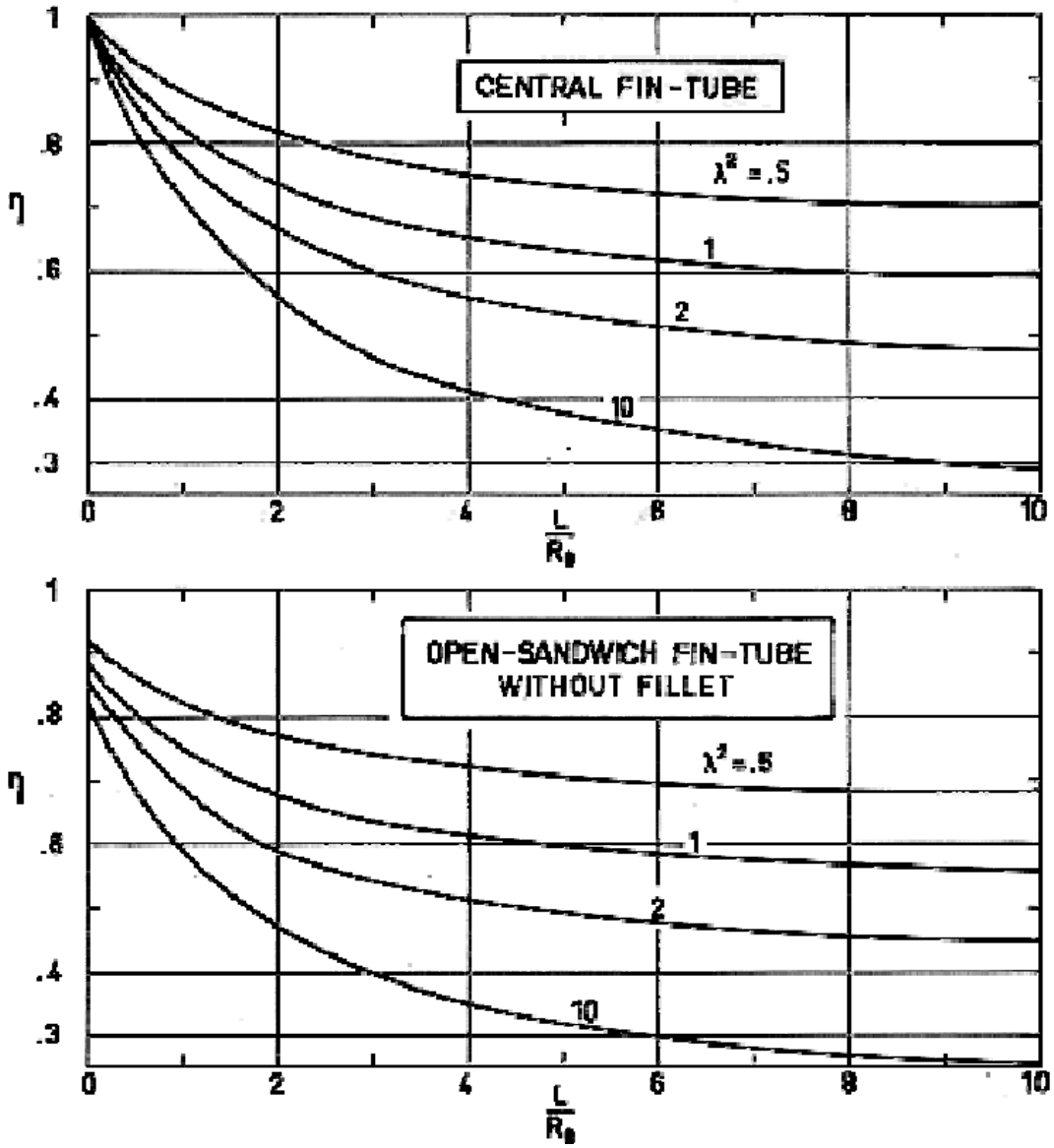

Note: non-si units are used in this figure

Figure 5-15: Radiating effectiveness, η, vs. ratio L/R_0 for several values of the conductance parameter, λ. Form Haller (1964) [9]. (Part 2/2)

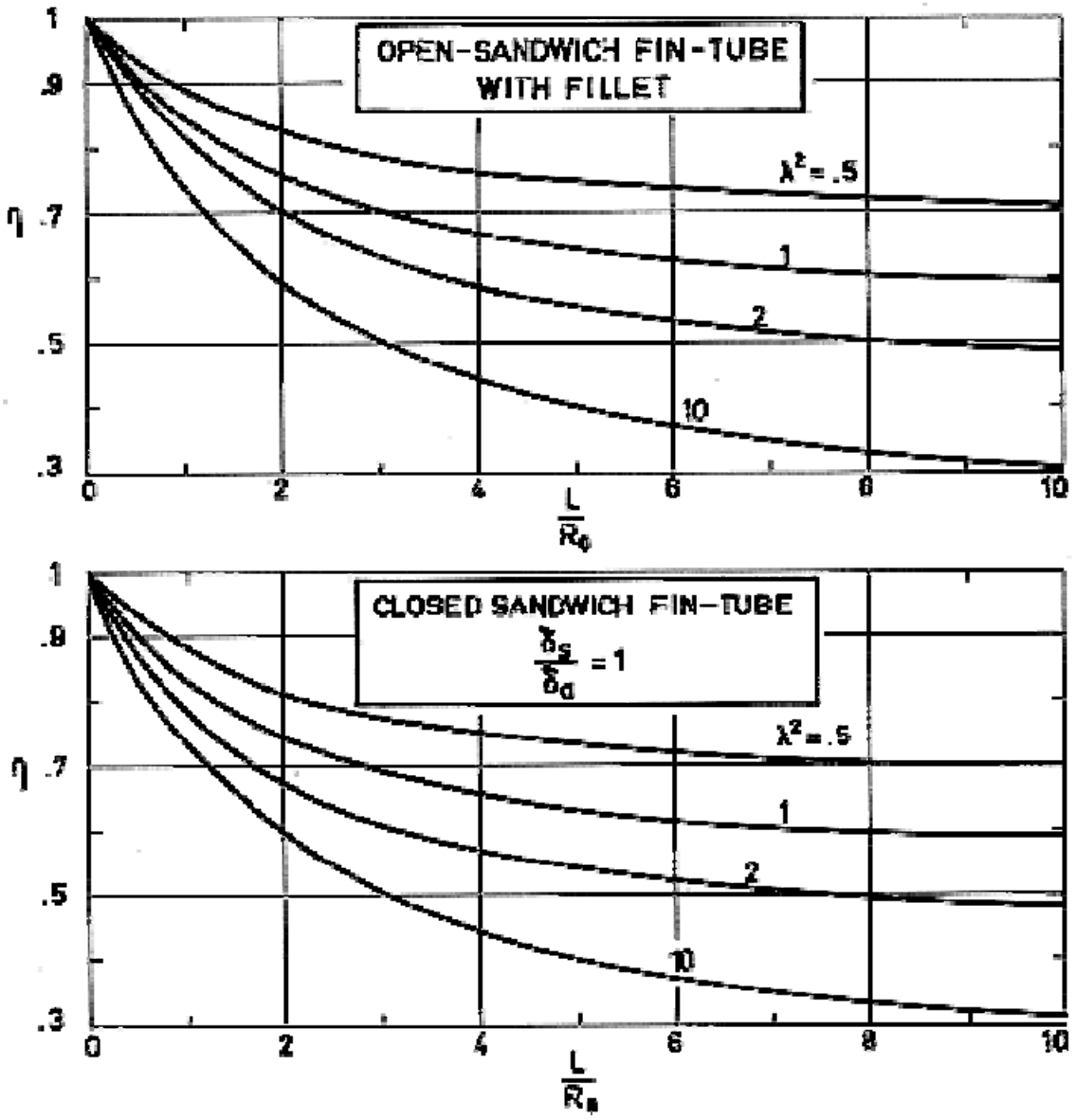

Note: non-si units are used in this figure

Figure 5-16: Radiating effectiveness, η, vs. ratio L/R_0, for several values of the conductance parameter, λ. From Haller (1964) [9].

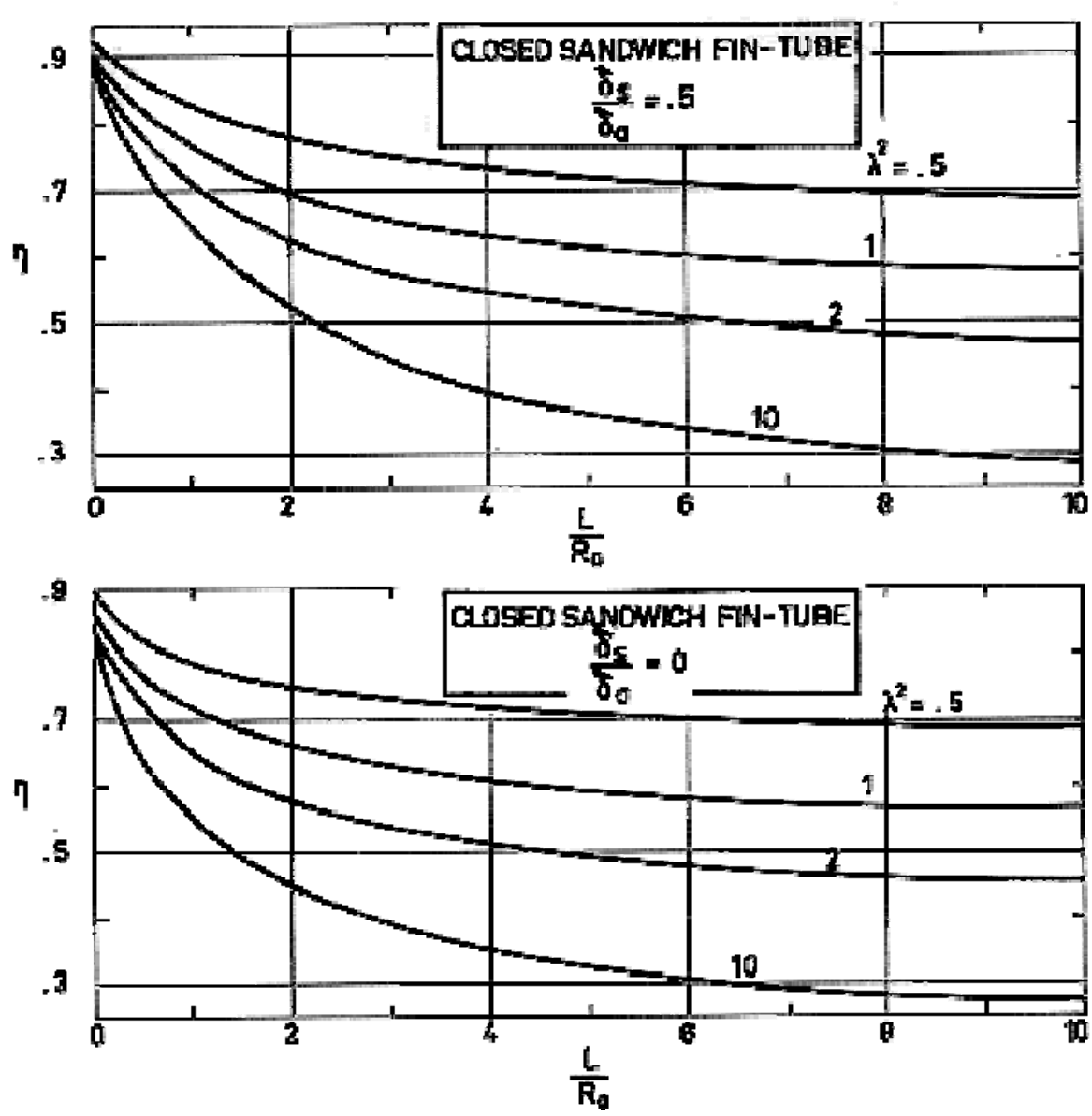

Note: non-si units are used in this figure

Figure 5-17: Radiating effectiveness, η, vs. ratio L/R_0 for several values of the conductance parameter, λ. Form Haller (1964) [9].

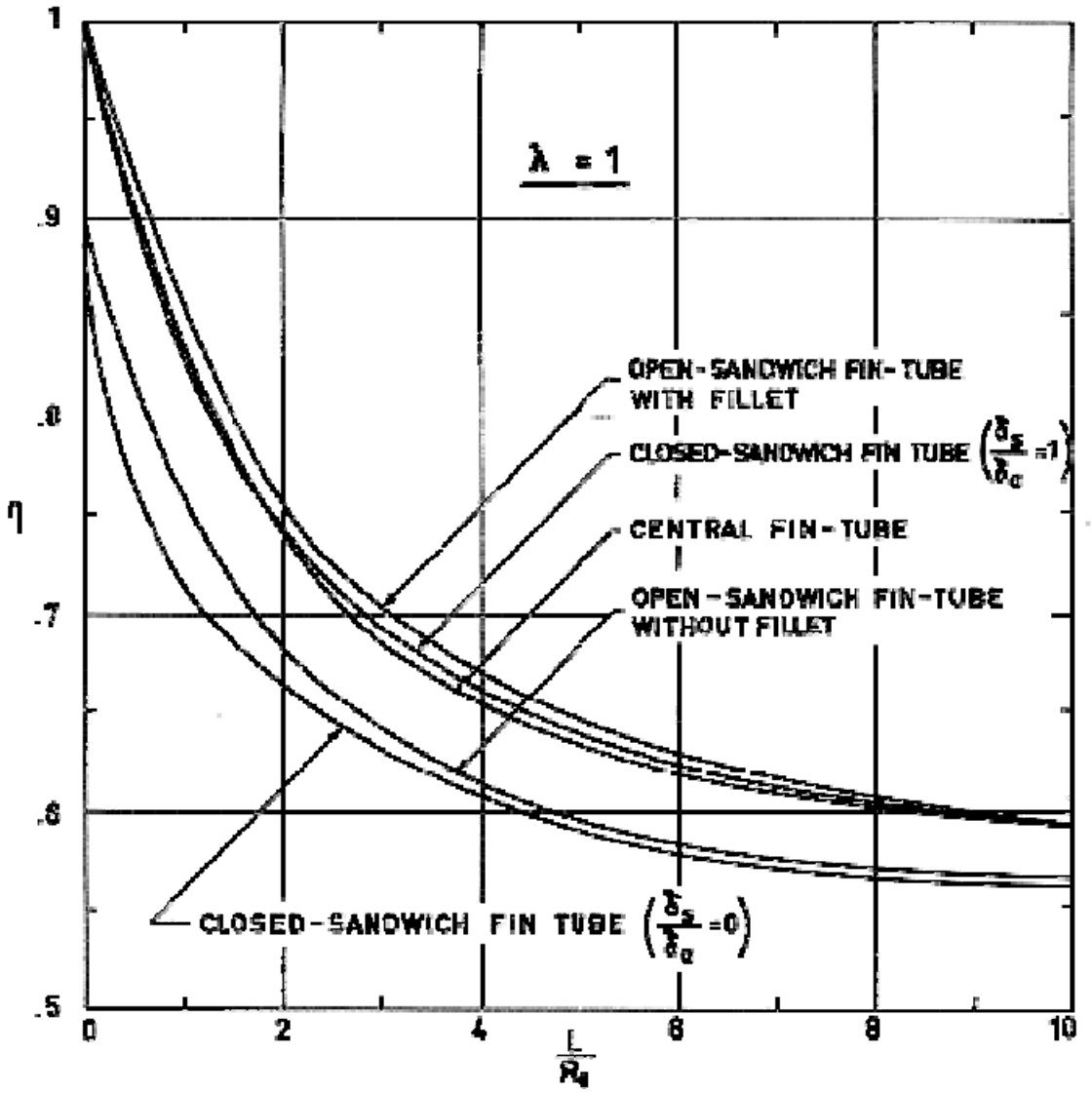

Note: non-si units are used in this figure

Figure 5-18: Comparison of the radiating effectiveness, η, vs. ratio L/R_0 for several fin-tube configurations. After Haller (1964) [9].

5.3 Annular plan form

This clause deals with fin-tube radiators, whose fins are of annular plan form. Either rectangular or triangular fin profiles have been considered.

The assumptions made to obtain the results presented are the following:

1. Temperature of the base surface (tube) is constant.
2. Fin and tube material properties are constant.
3. The surfaces of both fin and tube are gray, diffuse emitters and reflectors.
4. The thermal input to the fin has two parts:
   (a) heat conduction along the fin, and
   (b) radiation coming from the base surface and from the adjacent fins. The radiation from the external sources is assumed to be negligible.

5.3.2 Annular fin of rectangular profile

Sketch:

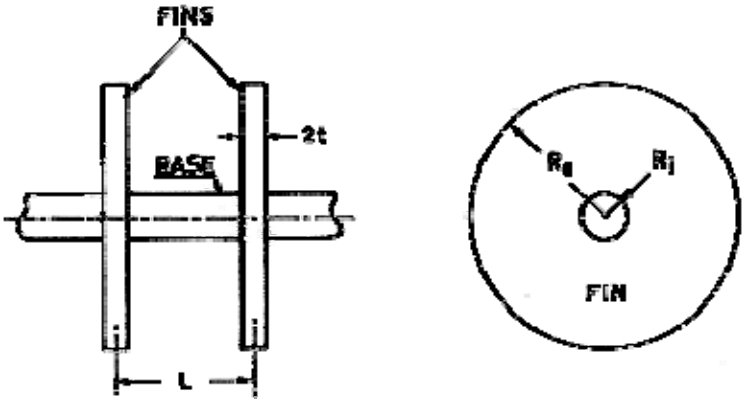

Radiating Effectiveness:

$$\eta = \frac{Q_T}{2\pi R_0^2 \left(\frac{R_i L}{R_0^2} + 1 \right) \sigma T_0^4} \qquad [5\text{-}8]$$

The results are given in Figure 5-19 to Figure 5-21.

Reference: Sparrow, Miller & Jonsson (1962) [17].

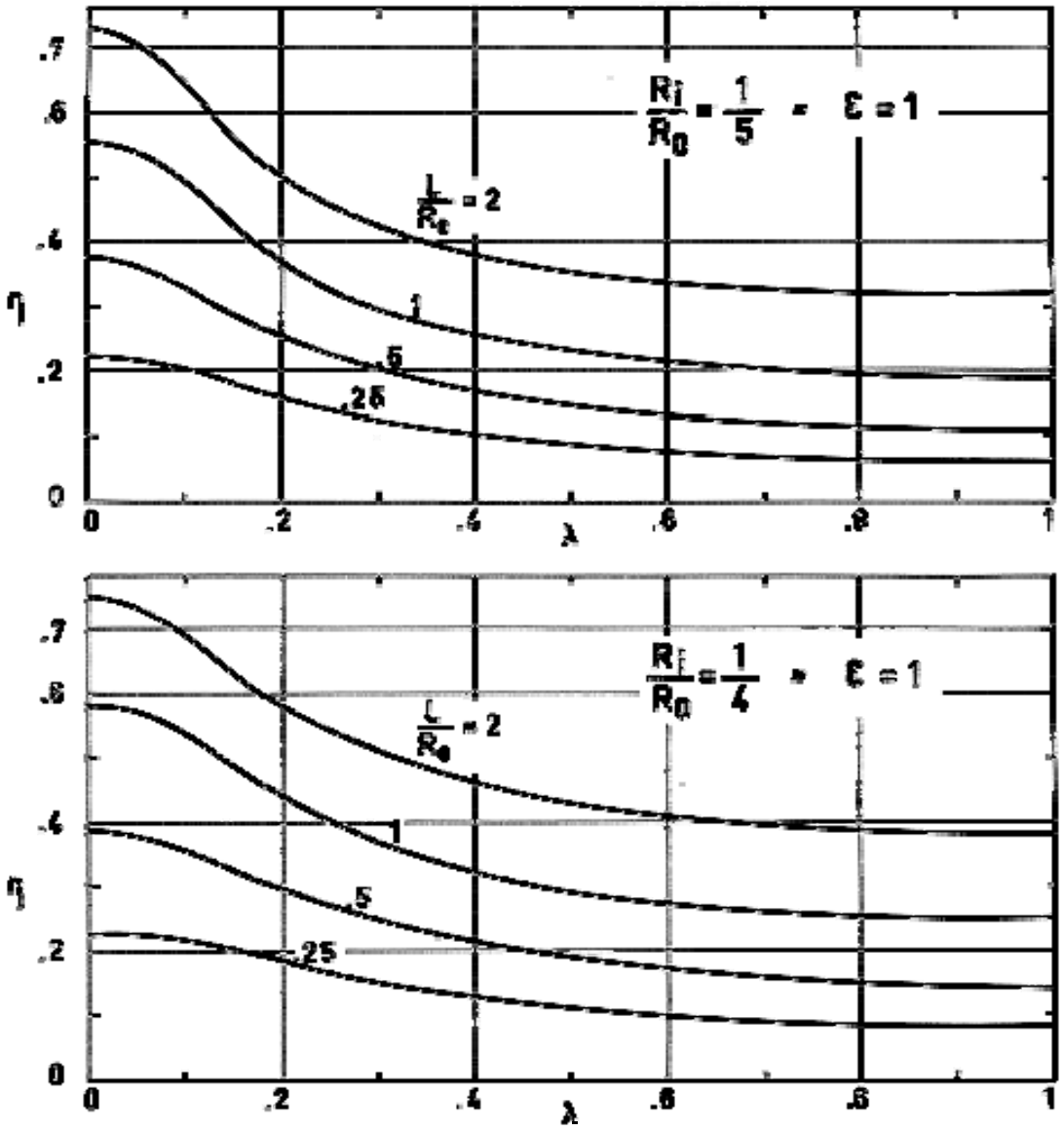

Note: non-si units are used in this figure

Figure 5-19: Radiating effectiveness, η, of annular-finned tube configuration vs. conductance parameter, λ, for several values of L/R_0 and R_i/R_0. Fin of rectangular profile. From Sparrow, Miller & Jonsson (1962) [17].

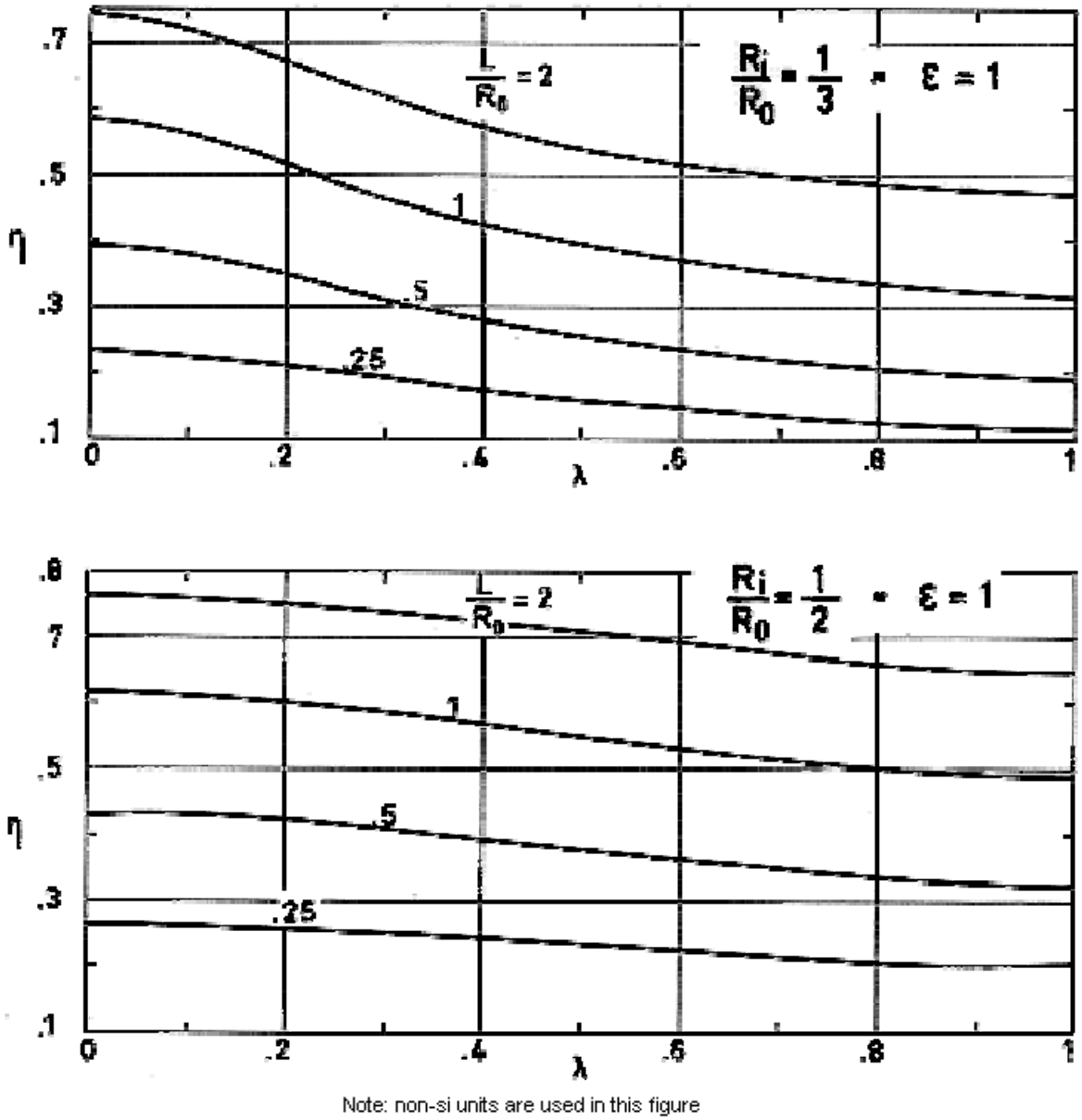

Note: non-si units are used in this figure

Figure 5-20: Radiating effectiveness, η, of annular-finned tube configuration vs. conductance parameter, λ, for several values of L/R_0 and R_i/R_0. Fin of rectangular profile. From Sparrow, Miller & Jonsson (1962) [17].

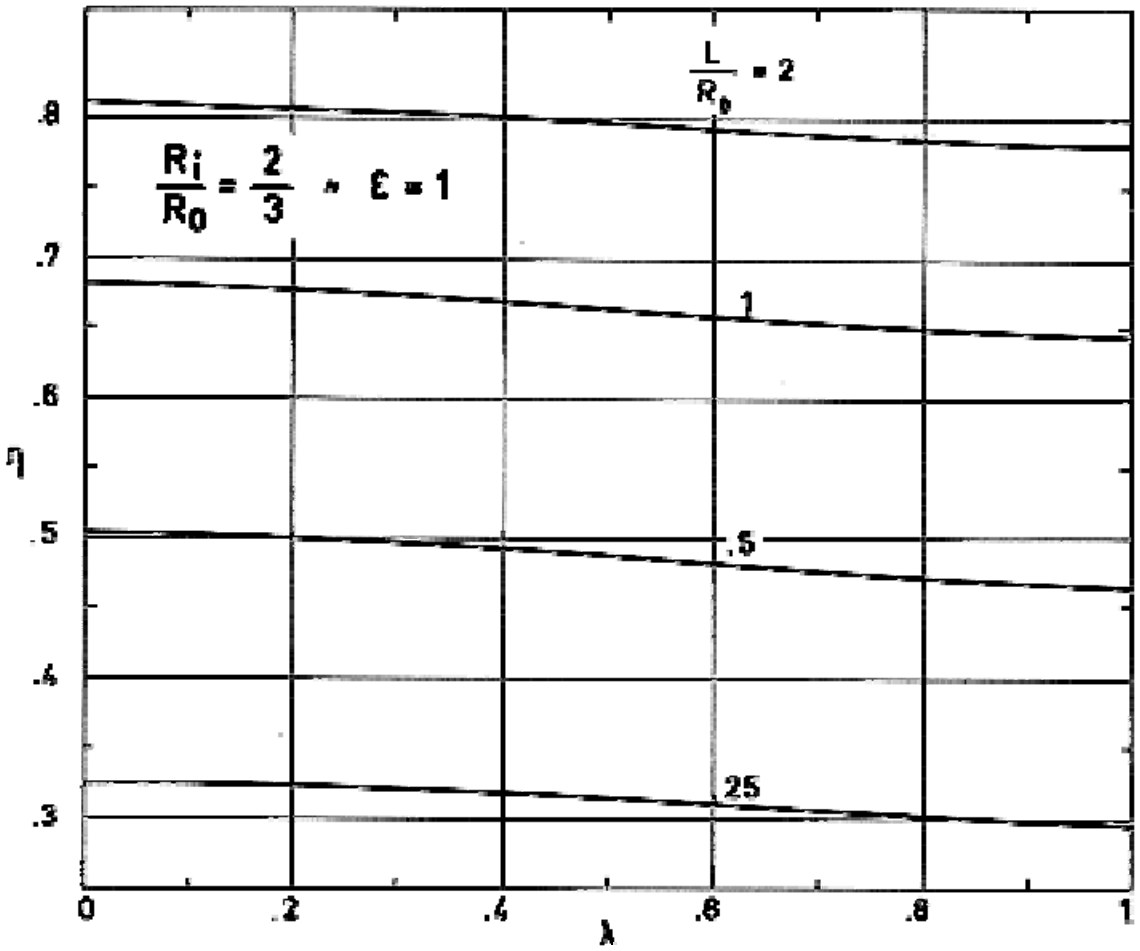

Note: non-si units are used in this figure

Figure 5-21: Radiating effectiveness, η, of annular-finned tube configuration vs. conductance parameter, λ, for several values of L/R_0. Fin of rectangular profile. From Sparrow, Miller & Jonsson (1962) [17].

5.3.3 Annular fin of triangular profile

Sketch:

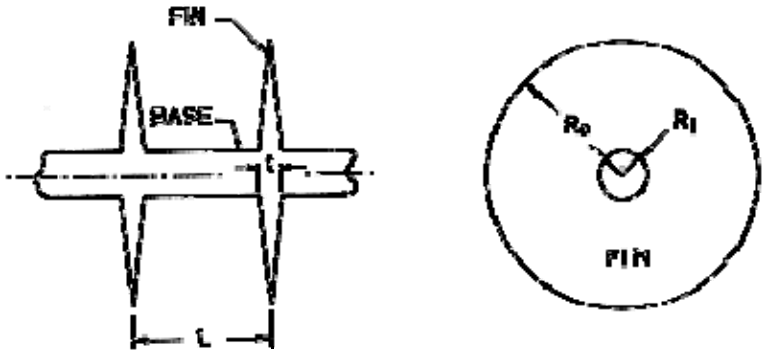

Radiating Effectiveness:

$$\eta = \frac{Q_T}{2\pi R_0^2 \left(\frac{R_i L}{R_0^2} + 1 \right) \sigma T_0^4} \qquad [5\text{-}9]$$

The results are given in Figure 5-22 to Figure 5-25.

Reference: Schnurr & Cotharn (1974) [16].

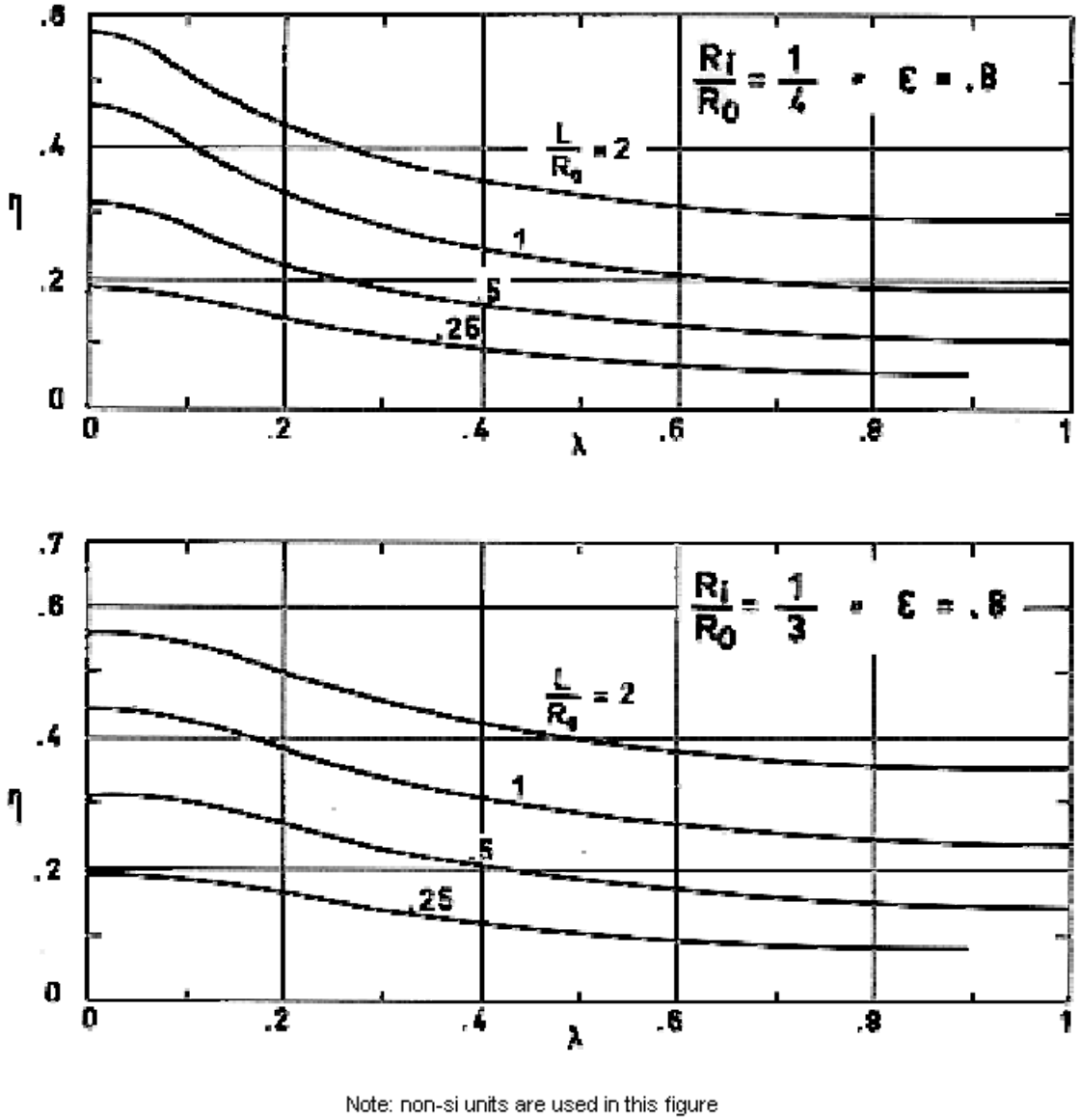

Note: non-si units are used in this figure

Figure 5-22: Radiating effectiveness, η, of annular-finned tube configuration vs. conductance parameter, λ, for several values of L/R_0 and R_i/R_0. Fin of triangular profile. From Schnurr & Cothran (1974) [16].

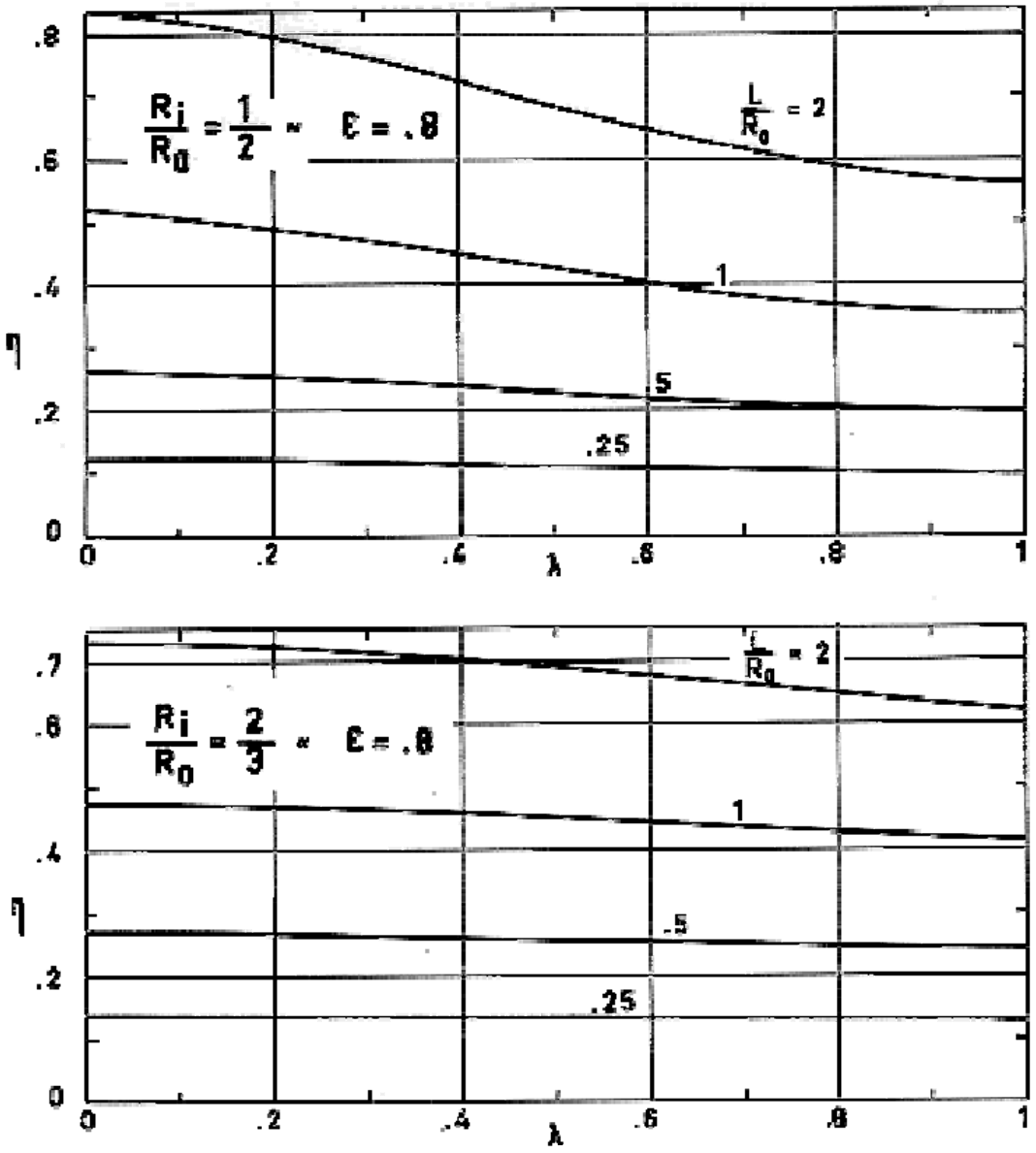

Figure 5-23: Radiating effectiveness, η, of annular-finned tube configuration vs. conductance parameter, λ, for several values of L/R_0 and R_i/R_0. Fin of triangular profile. From Schnurr & Cothran (1974) [16].

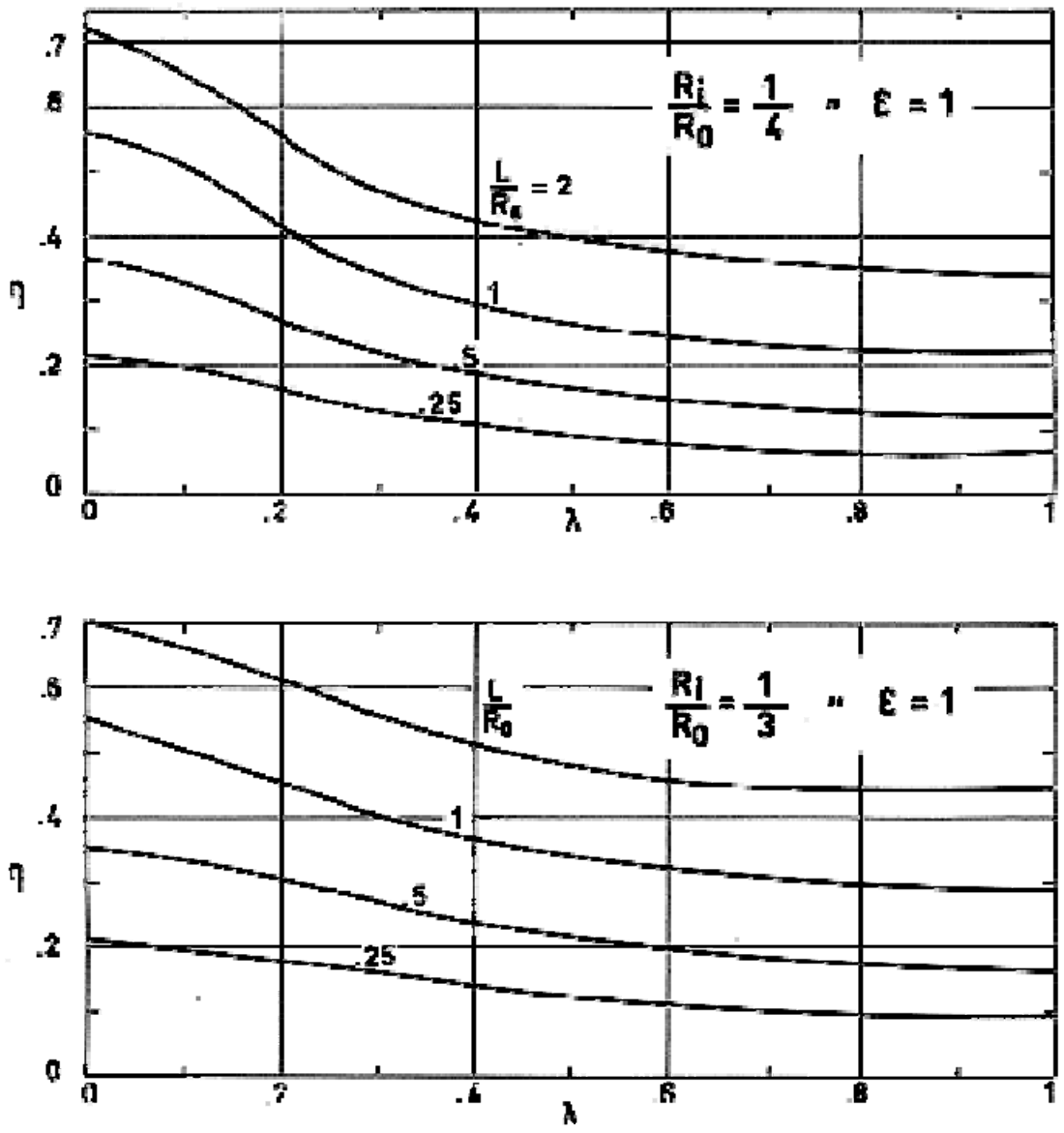

Note: non-si units are used in this figure

Figure 5-24: Radiating effectiveness, η, of annular-finned tube configuration vs. conductance parameter, λ, for several values of L/R_0 and R_i/R_0. Fin of triangular profile. From Schnurr & Cothran (1974) [16].

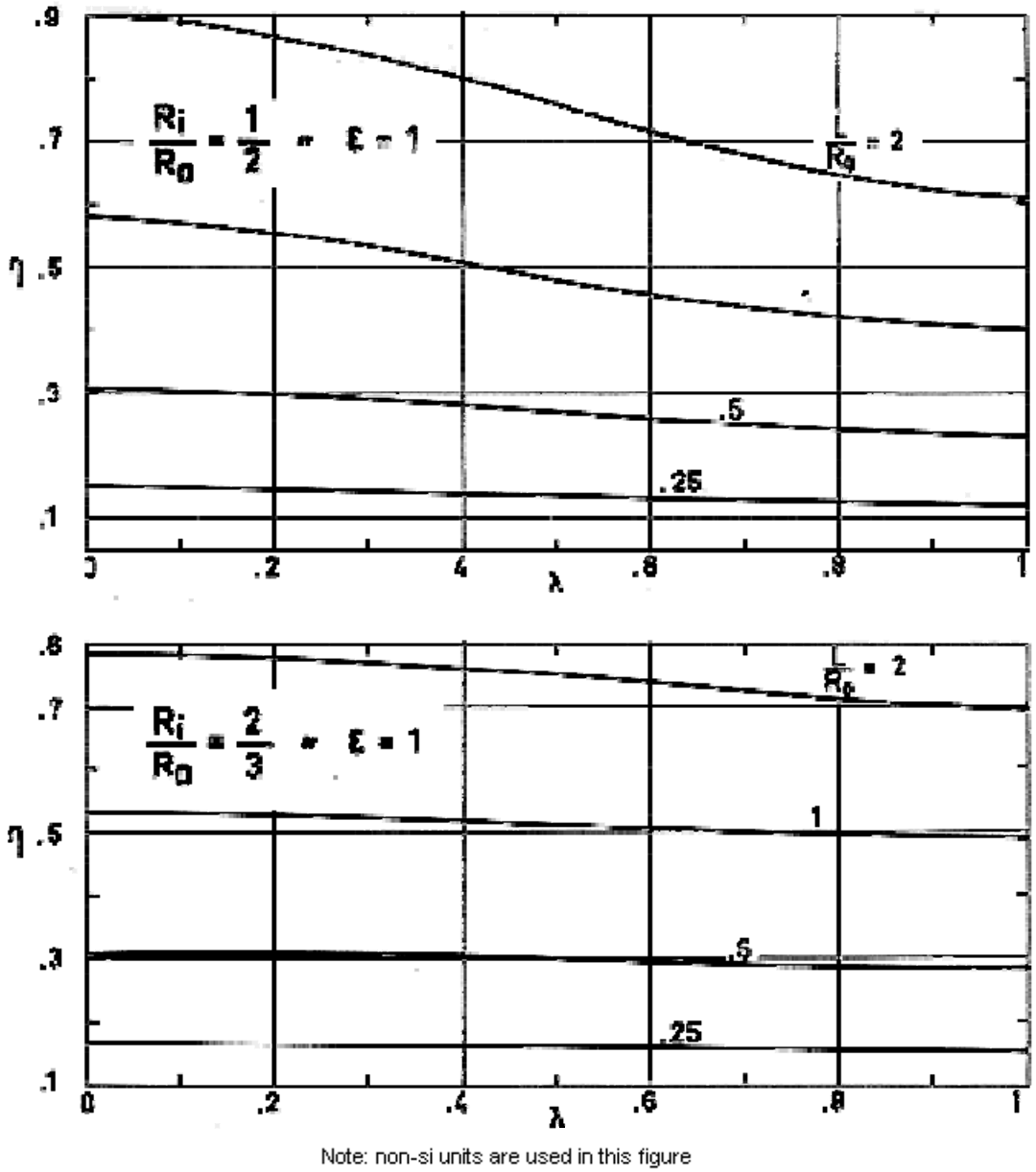

Note: non-si units are used in this figure

Figure 5-25: Radiating effectiveness, η, of annular-finned tube configuration vs. conductance parameter, λ, for several values of L/R_0 and R_i/R_0. Fin of triangular profile. From Schnurr & Cothran (1974) [16].

6
Passive radiant coolers

6.1 General

A method of developing cryogenic temperatures in space is to utilize the low temperature sink of deep space through a passive radiant cooler. This concept is potentially attractive since such a system is completely passive, requires no power, and may be capable of high reliability for extended periods. Passive radiant coolers have been developed for cooling of detectors in electro-optical systems to temperatures in the region between 70 and 200 K.

The efficiency of these coolers is primarily a function of the thermal decoupling from the spacecraft temperature, and the degree of isolation from external radiant fluxes. The type of orbit, the orbit altitude, the orientation of the spacecraft relative to the earth and sun, and the location of the radiator aboard the spacecraft, all significantly influence the design of the radiator.

Passive radiator coolers also present potential problems relative to the contamination of cold surfaces by out gassing from either the spacecraft or the radiator itself.

The main characteristics of passive radiant coolers are:

1. Advantages
   - o They are simple and lightweight.
   - o Do not require continuous power.
   - o Practically indefinite lifetime.
   - o Do not interfere with the detector.
2. Drawbacks
   - o Limited temperature and heat load capacity.
   - o Require proper orbit and location in the spacecraft.
   - o Prone to contamination by out gassing.

   The range of application of this type of coolers is:
   - o Temperature above 50 K.
   - o Geosynchronous or Sun-synchronous orbits.
   - o Heat loads less than 0,1 W with the present technology.
   - o Long missions.

6.2 Radiator configurations

Radiator configuration varies according to mission constraints. In general, the radiant cooler has several stages, however, preliminary analyses developed by Space and Reentry Systems Division of Philco-Ford Corp. (quoted by Donabedian (1972) [5]), on the thermal performance of different types of staged radiators, showed that the thermal performance of such coolers is nearly maximized with three stages, and in some cases with two stages. Additional stages provide negligible thermal improvement and add considerably to the complexity of the design.

In its most usual form, the passive radiant cooler is constructed in two stages. The first stage consists of a conical or parabolic reflector with a highly reflective, specular, inner surface. The purpose of this stage is to shield the patch (the detector stage) from spacecraft and earth, or to reflect shallow-angle sun input out of the cooler before it reaches the patch.

Figure 6-1 shows eight basis radiator designs encompassing single and multistage flat, parabolic and conical surfaces.

When shielding from the spacecraft is not required, and there is no sun input to the radiant cooler, the first parabolic or conical stage can be eliminated. A deployable or fixed door attached to the mouth of the first stage can then be used to block the patch view of the earth. This type of padiant cooler would then assume the configuration shown in Figure 6-2.

A deployable door can be also used with a conical or parabolic type cooler to limit external input or to warm the cooler, door closed, for certain moments during the mission.

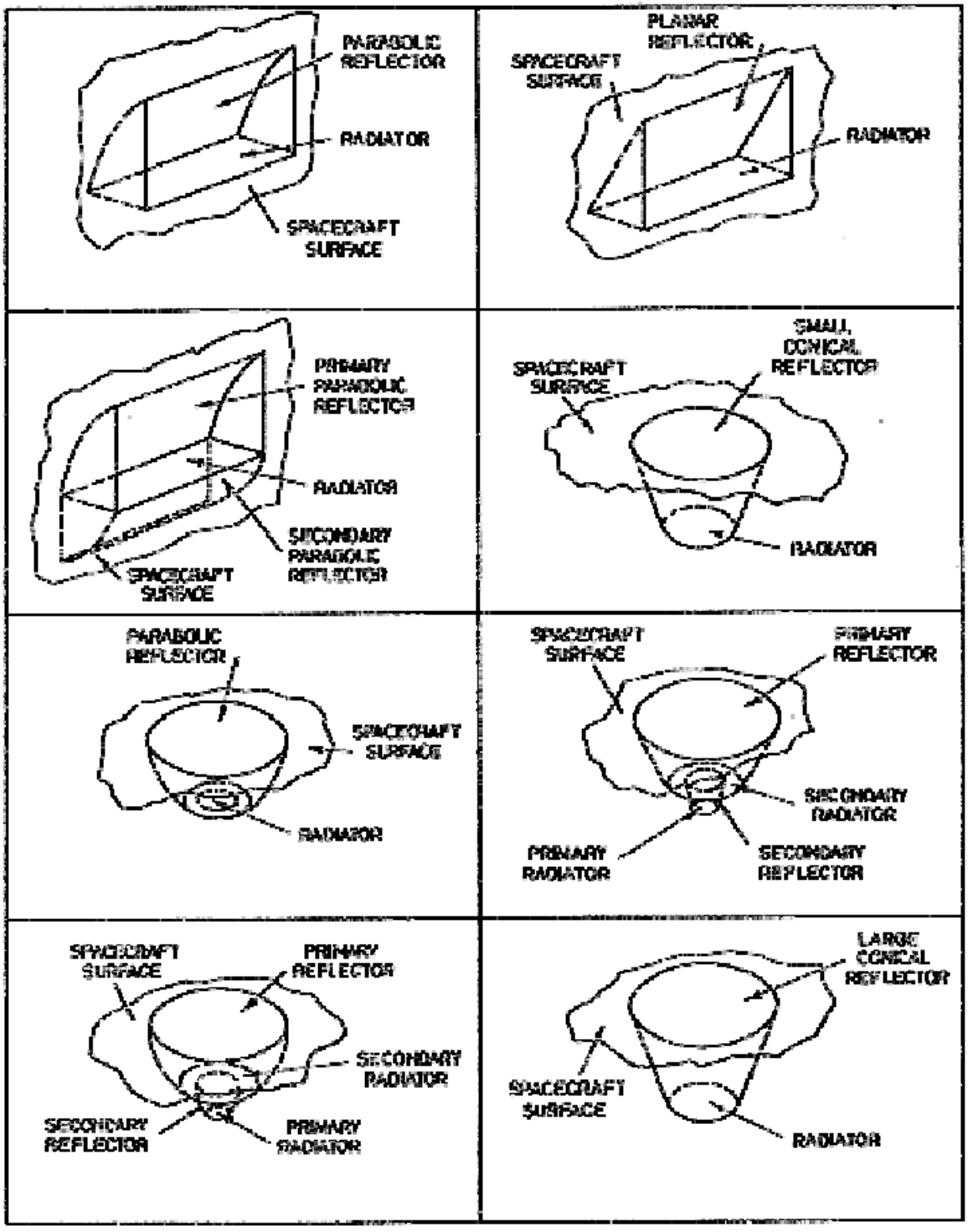

Figure 6-1: Several radiant cooler configurations. From Donabedian (1972) [5].

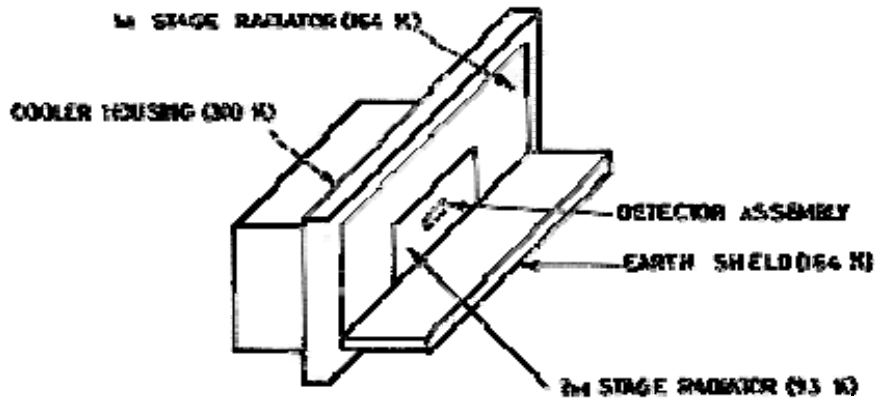

Figure 6-2: Two stage Rectangular "L Shape", ITT Design. From Donohoe, Sherman & Hickman (1975) [6].

There are two alternative philosophies in the design of a passive radiant cooler to perform a given duty. When the cooler is placed in a fixed location on a given spacecraft, it would assume a "mission unique" configuration, this is the case of most passive radiant coolers used onboard NASA satellites. The U.S. Air Force, on the other hand, has employed essentially one cooler design while altering the spacecraft to be compatible with the cooler operation, this is achieved by adding appropriate shielding and/or altering the geometry of the satellite in the neighborhood of the cooler.

6.3 Thermal performances

6.3.1 Thermal efficiency

Thermal efficiency of passive radiant coolers is primarily a function of the thermal decoupling from the spacecraft temperature and the degree of isolation from external heat loads.

Thermal efficiency of passive radiators, η, is defined as:

$$\eta = \frac{Q_L}{A_p \sigma T_p^4} \qquad [6\text{-}1]$$

where Q_L is the heat load from the devices to be cooled, A_p is the patch area, T_p the patch temperature, and σ the Stefan-Boltzmann constant.

The energy balance on the patch, which expresses that the radiant power should be equal to the sum of detector heat load, Q_L, and parasitic loads, Q_E, yields

$$\varepsilon A_p \sigma T_p^4 = Q_L + Q_E \qquad [6\text{-}2]$$

ε being the emittance of the patch.

Combination of [6-1] and [6-2] gives the radiator thermal efficiency:

$$\eta = \frac{Q_L \varepsilon}{Q_L + Q_E} \qquad [6\text{-}3]$$

This equation indicates that in order to increase the efficiency, η, it is desirable to minimize the parasitic heat loads, Q_E, and/or to maximize the patch emittance, ε. Reductions in Q_E can be achieved through high thermal insulation from the satellite and/or shading from the external flux.

Potential heat sources to the cooler are listed in Table 6-1 below.

Table 6-1: Potential Radiant Cooler Heat Sources

Direct radiant heat flux.	* Direct solar energy. * Earth albedo. * Earth emitted thermal energy. * Lunar albedo. * Lunar emitted thermal energy. * Spacecraft emitted thermal energy.
Indirect radiant heat flux.	* Direct radiant heat flux reflected to the radiator by the spacecraft assembly. * Direct radiant heat flux reflected to the radiator by the cooler assembly surface. * Radiator emitted or reflected heat flux reflected back by cooler or spacecraft surfaces. * Radiative heat leaks through insulation.
Conducted and generated heat flux.	* Heat flux trough supports. * Heat flux generated on the radiator surface by electrical resistance losses.

NOTE From Wright (1972) [20].

6.3.2 Patch area

Equation [6-2] gives the minimum theoretical effective area required as a function of the detector heat load, Q_L,the parasitic heat load, Q_E, the patch temperature, T_p, and the patch emittance, ε, for a 0 Kheat sink. The complete assembly is larger because of the shielding system and the structure.

Rearranging Eq. [6-2] yields:

$$\frac{A_p}{Q_L} = \frac{1}{\varepsilon\sigma T_p^4 - \left(Q_E / A_p\right)} \qquad [6\text{-}4]$$

which gives the ratio A_p/Q_L as a function of the patch temperature and the ratio Q_E/A_p. Figure 6-3 shows the variation of A_p/Q_L with T_p for several values of Q_E/A_p. The ratio Q_E/A_p is estimated to range from 1,60 to 3,20 $W.m^{-2}$ of radiator surface, with present technology. To obtain these figures, it has been assumed (Donabedian (1972) [5]) that the heat transfer between the radiator and the supporting structure and vehicle is the only contribution to the parasitic heat load.

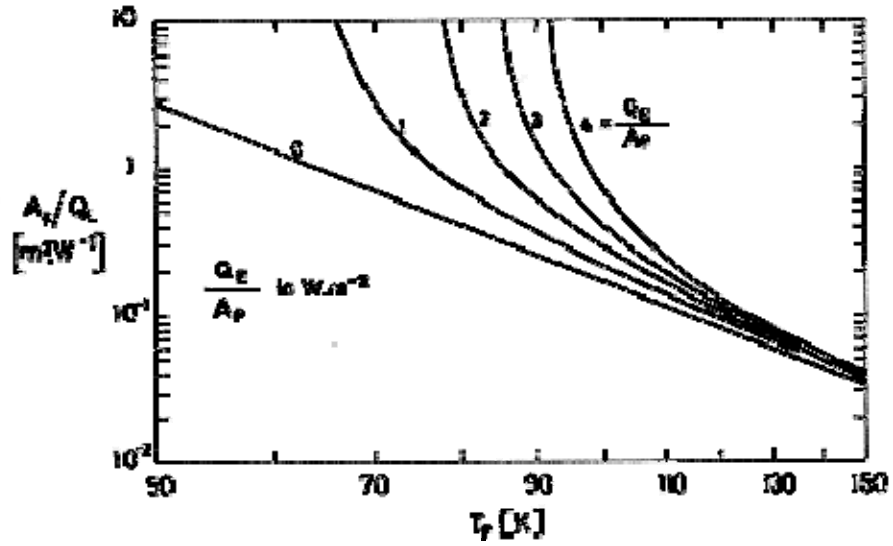

Figure 6-3: Radiator area to detector heat load ratio, A_p/Q_L, vs. patch temperature, T_p, for several values of the ratio Q_E/A_p. From Donabedian (1972) [5].

6.3.3 Thermal stability

Some applications of passive radiant coolers require the detector temperature to be stabilized within some limits (f.e. ± 0,1 K) so that the radiometric sensitivity of the optical system remains constant. This stability can be achieved by bonding a strip heater and temperature sensor on the insulated side of the patch. A heater control circuit should be used to maintain a constant temperature.

The control heater can be also used to prevent icing of the patch during initial cool down and out gassing periods. Once the out gassing has subsided, the heater can be switched to a control mode and the patch cools to its normal operating temperature.

The characteristics of several commercially available electrical heaters are presented in ECSS-E-HB-31-01 Part 11.

6.4 Optimization of cooler geometry

Of **the** available design parameters. A criterion for optimization can be used based on the minimum patch temperature for a given heat load and a fixed cooler volume.
To mathematically express this criterion, the energy balance equations for each stage of the cooler are used, however this does lead to a complicated formulae. This difficulty may be circumvented, in the case of the cone frustrum geometry shown in Figure 6-4, by means of a method, devised by Bywaters & Keeling (1974) [3], which gives near optimum cone angles.

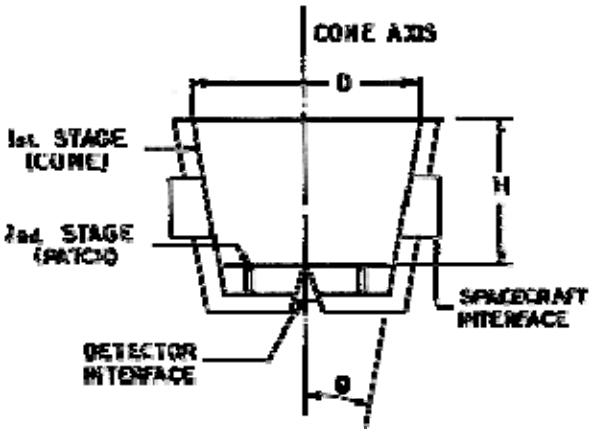

Figure 6-4: Cooler geometry.

Notice that since a volumetric constraint is assumed, the main geometric parameter which would be free for optimization would be the cone angle, θ.

The authors mentioned above assume that the cooler is shaded from both the spacecraft and direct solar rays, and that the cooler axis is normal to the orbital plane. Under these conditions the incident flux comes only from planetary emission and planetary albedo.

The idea of the method consists in calculating the cone angle, θ, which prevents the extreme rays from the limb of the planet from reaching the patch. In other words, the extreme rays determine the cooler field of view as shown in Figure 6-5.

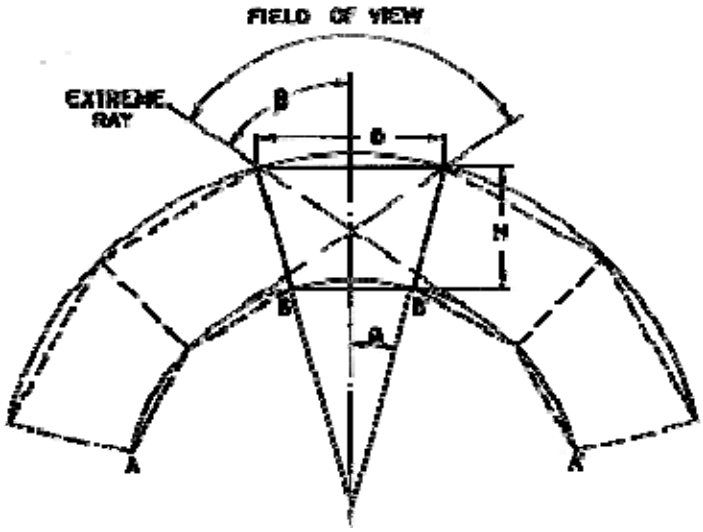

Figure 6-5: Specular images in the cone. From Bywaters & Keeling (1974) [3].

The extreme rays incident upon the cooler cavity at an angle to the cone axis, β, is given by

$$\beta = \cos^{-1} \frac{R_P}{R_P + h} \qquad [6\text{-}5]$$

R_p being the radius of the planet and h the altitude of the orbit, which is assumed to be circular (see insert in Figure 6-7).

The value of the cone angle, θ, that results in a radiator field of view 2β, can be deduced by assuming (which is conservative) that the extreme ray in Figure 6-5 is tangent to the circle AA' defined by multiple reflections of the patch BB' in the mirrors at angle $\pm\theta$. The resulting expression is:

$$\theta + \sin^{-1}\left(1 - 2\frac{H}{D}\tan\theta\right) = \beta \qquad [6\text{-}6]$$

This equation gives the cone angle, θ, required to fully shade the patch from limb rays, once the orbital parameters, R_p and h, and the volume constraint, H/D, are specified.

Figure 6-6 gives the cone angle, θ, versus ratio $R_p/(R_p+h)$ or versus β, for several values of the ratio H/D. Two different lines are plotted for each H/D. The full line correspond to values of θ deduced from Eq. [6-6]. The interrupted line shows the value, θ_{min}, below which the incoming rays directly impinge on the patch. θ_{min} is given by the following expression:

$$\theta_{\min} = \tan^{-1}\left(\frac{H}{D} - \tan\beta\right) \qquad [6\text{-}7]$$

The dotted line in the right upper corner of

Figure 6-6 corresponds to values of θ for zero patch surface area, i.e.:

$$\theta_{\lim} = \tan^{-1}\left(\frac{D}{2H}\right) \qquad [6\text{-}8]$$

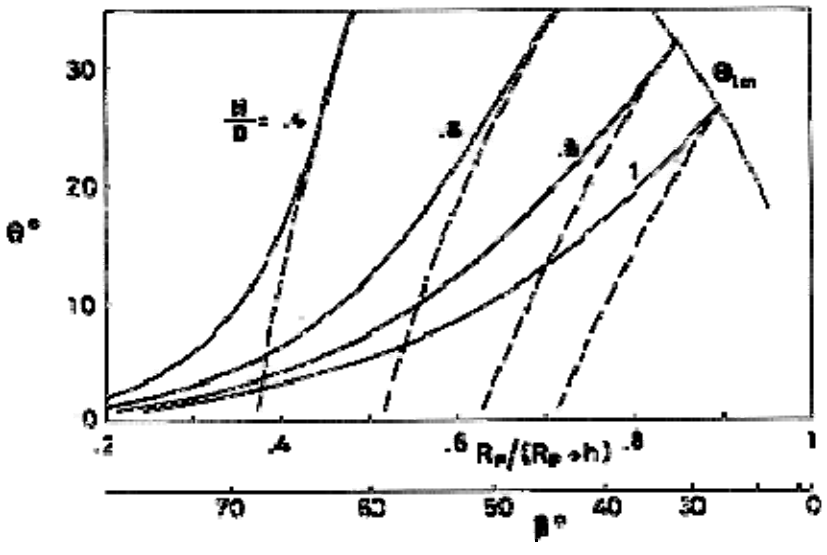

Note: non-si units are used in this figure

Figure 6-6: Cone angle, θ, vs. orbital parameter, $R_p/(R_p+h)$, for several values of the ratio H/D. _____ Values deduced from Eq. [6-6]. --------- Values deduced from Eq. [6-7]. Calculated by the compiler.

The curves given by Eqs. [6-6] and [6-7] divide to whole domain (θ, β) into three different zones, for each value of H/D. That zone to the left of the curve deduced from Eq. [6-6] is fully shaded from planetary radiation. For a given θ, rays with βs larger than those resulting from Eq. [6-7] arrive to the patch without suffering any reflection at the cone walls. Finally, the zone bounded by the curves deduced from Eqs. [6-6] and [6-7] corresponds to rays arriving to the patch after several reflections at the cone walls. In this case, since wall absorption is unavoidable, it could be interesting to know how many reflections suffers a ray before reaching the patch. This can be deduced from the following equation:

$$\frac{\sin(\beta-\theta)}{\sin(\beta+(2m+1)\theta)}+\frac{2H}{D}\tan\theta-1=0 \qquad [6\text{-}9]$$

where m is the number of patch-in-cone reflections taken to limit the cooler field of view.

Results from Eq. [6-9] have been represented in Figure 6-7 for several values of H/D, and for m = 1 and 2. The curves giving θ through, Eq. [6-6] and θ_{min} , through Eq. [6-7], are also represented in this figure.

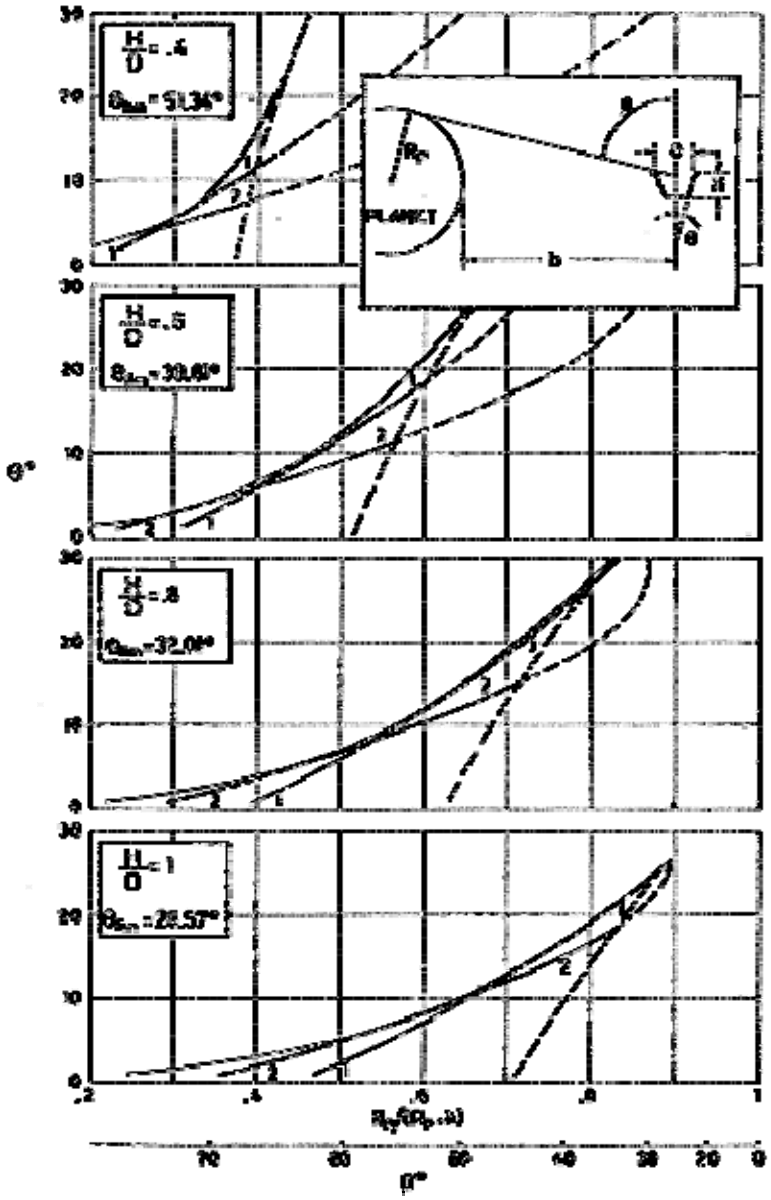

Note: non-si units are used in this figure

Figure 6-7: Cone angle, θ, vs. orbital parameter, $R_p/(R_p+h)$, for several values of the ratio H/D. Numerals on the curves indicate the number, m, of the path-incone reflections taken in Eq. [6-9]. The faint lines correspond to θ values, already shown in Figure 6-6, which limit the zone of validity of the arrival-after-reflection solutions. Calculated by the compiler.

6.5 Degrading effects

Flight data indicate that passive radiant coolers can suffer from contamination of their thermal control surfaces. This contamination, which is due to out gassing from the satellite, changes the optical properties of the surfaces and tends to raise the patch temperature with a corresponding decrease in detector sensitivity. Heaters can be provided to reverse contamination.

A potentially more serious problem is contamination of the optics integrated with the cooler. When contaminants absorb in the same wavelength band as the instrument, optics contamination results in a

net system transmission loss with a decrease instrument sensitivity. Response losses up to 50% in less than a month mission have been observed. These losses do not appear to be completely reversible upon heating. Warm interstage windows can be a satisfactory remedy to prevent optics contamination.

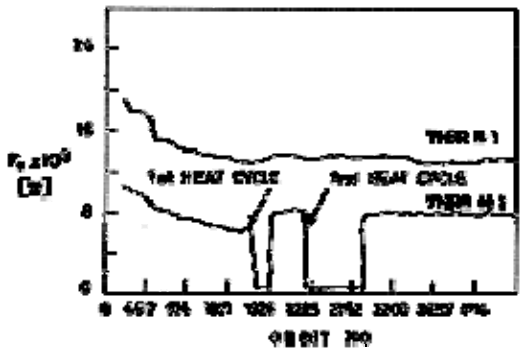

Figure 6-8: Control power, P_c, vs. orbit number of two VHRR-Nimbus V-coolers. From Donohoe et al. (1975) [6].

Flight results for two Very High Resolution Radiometers (VHRR) are shown in Figure 6-8. The proportional control power is used in this figure to indicate the behavior of the cooler thermal control surfaces. The change in the patch control power level, which results from heat cycle on VHRR#2, makes evident the control surface contamination. Notice that a restoration or decontamination of the cooler surfaces takes place. restoration to the earlier values were possibly not achieved because of the moderate decontamination temperature (230 K for 195 orbits).

Larger temperatures were unattainable since the heaters were sized to decontamination from ice formation but not from lower vapor pressure contaminants.

A second heat cycle on VHRR#2 did not achieve any further improvement. VHRR#1 was used as a control and its heaters were not exercised.

Figure 6-9 shows data obtained from the cooler of the Two Channel IR Radiometer (SCMR) developed by ITT (Nimbus V flight). This cooler had heaters, a deployable earth shield (door) and a purge system, all of them designed to minimize contamination effects.

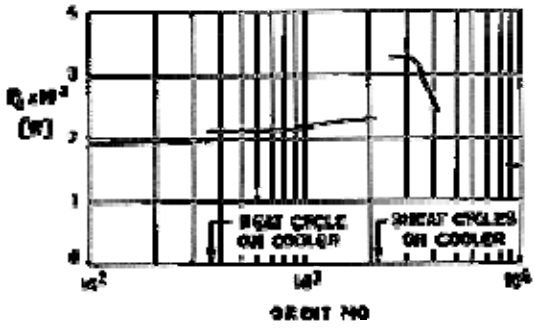

Figure 6-9: Control power, P_c, vs. orbit number. SCMR-Nimbus V-cooler. From Donohoe et al. (1975) [6].

Initial cooling following orbit insertion was postponed for three weeks in order to minimize the effects of spacecraft out gassing on the cooler.

The first heating was performed, during orbit 300, with the door closed and the cone heater on.

For the second heating, which started at orbit 2000, the patch and the cone were heated up to the temperature of the satellite with the door closed three times in succession in order to perform three heating cycles (total time: 600 orbits).

Data for orbit 9000 indicate that there was not permanent degradation of the cooler thermal control surfaces for the two years orbit period.

Figure 6-10 shows the response of SCMR-Nimbus V-IR channels to a constant blackbody calibration source. The data indicate a loss of response which is different for each channel. A possible explanation for the degradation is, in this case, contamination of the optics integrated into the cooler. An electronic failure at orbit 300, when cooling down the instrument, disabled the data link. Hence, the optics contamination, as well as the anti-contamination features of the cooler-optics assembly were not completely evaluated.

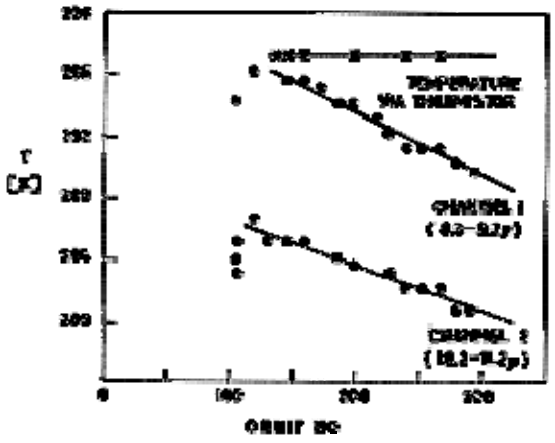

Note: non-si units are used in this figure

Figure 6-10: Target temperature, *T*, vs. orbit number. SCMR-Nimbus V-cooler. From Donohoe et al. (1975) [6].

6.6 Existing systems

DENOMINATION [a]	TYPE
[c]	Cone Cooler
ADL [d]	Cone Cooler
AVHRR	L Shape
HIRS	Cone Cooler
MERC	L Shape
MSS	Cone Cooler
SCMR	Cone Cooler
VHRR	Cone Cooler
VHRR	L Shape
VISSR	Cone Cooler

[a] All data in this table, unless otherwise stated, are from Donohoe, Sherman & Hickman (1975) [6]. Denomination is the same as that used by the authors. Key to abbreviations: ADL: Arthur D. Little; AVHRR: Advanced Very High Resolution Radiometer; HIRS: High Resolution Infrared Sounder; MERC:

[c] From Hulett & Zierman (1970) [10]. Additional details on this cooler are given in clause 6.6.1.

[d] Additional details on this cooler are given in clause 6.6.2.

NOTE For details see the two tables below.

DENOMINATION [a]	[c]	ADL [d]	AVHRR	HIRS	MERC
TYPE	Cone Cooler	Cone Cooler	L Shape	Cone Cooler	L Shape
MANUFACTURER	PHILCO-FORD	ADL			
NUMBER OF STAGES	4	2	2	2	3
ORBIT		Near Polar Sun Synchronous	TIROS-N ($0{,}83 \times 10^6$ m)	NIMBUS (10^6 m)	NIMBUS (10^6 m)
DESIGN STATUS & LAUNCH DATE	Thermal Development Model	Flown	Breadboard 1978	Flight Model 1975	Experimental Model
COOLING	$3{,}5 \times 10^{-4}$ W	10^{-2} W	$3{,}2 \times 10^{-2}$ W	10^{-2} W	2×10^{-3} W

DENOMINATION [a]	[c]	**ADL** [d]	**AVHRR**	**HIRS**	**MERC**
CAPABILITY		at 100 K	at 93 K	at 100 K	at 95 K
FIELD OF VIEW		101º	Anti Sun Side 90ºx180º	± 50º Horizontal –28º Vertical	Anti Sun Side 90ºx180º
RADIATOR AREAS $A_i x 10^4$ [m^2]					
1 st Stage	258	417	420	213	225
2 nd Stage	171	95	77	23	41
3 rd & 4 th Stages	189&207				
HOUSING TEMPERATURE [K]	295	No housing, 300 K Mount Ring	300	300	300
MASS [kg]	0,59	1,59	1,36	4,04	1,36
DIMENSIONS [m]	0,27(Diameter)x0,08	0,30x0,16x0,12	0,35x0,18x0,13	0,18x0,13x0,15	0,23x0,30x0,22
COVER OR SHIELD	No	Cover	Deployable Shield	Deployable Shield	Deployable Shield
CONTROL TEMPERATURE [K]	90-160	Not Specified	105	120	Not Specified
HEAT LOAD SENSITIVITY [b] [$K.W^{-1}$]		400	700	1500	1350

[a] All data in this table, unless otherwise stated, are from Donohoe, Sherman & Hickman (1975) [6]. Denomination is the same as that used by the authors. Key to abbreviations: ADL: Arthur D. Little; AVHRR: Advanced Very High Resolution Radiometer; HIRS: High Resolution Infrared Sounder; MERC:

[b] Detector temperature change per W of heat input.

[c] From Hulett & Zierman (1970) [10]. Additional details on this cooler are given in § 2.6.1.

[d] Additional details on this cooler are given in § 2.6.2.

DENOMINATION [a]	**MSS**	**SCMR**	**VHRR**	**VHRR**	**VISSR**
TYPE	Cone Cooler	Cone Cooler	Cone Cooler	L Shape	Cone Cooler
MANUFACTURER		ITT		RCA	
NUMBER OF STAGES	2	2	2	3	2
ORBIT	Near Polar Sun Synchronous	Near Polar Sun Synchronous	Synchronous Geostationary	Circular Polar	Synchronous Geostationary
DESIGN STATUS & LAUNCH DATE	Engineering Model	Flown 1972	Engineering Model	Flown 1972, 1973	Flown 1974
COOLING CAPABILITY	10^{-3} W at 95 K	10^{-3} W at 110 K	10^{-3} W at 166 K	$1{,}4 \times 10^{-3}$ W at 97 K	2×10^{-3} W at 81 K
FIELD OF VIEW	100º Horizontal 70º Vertical	104º Horizontal 76º Vertical	84º Horizontal 100º Vertical	90ºx180º	130º
RADIATOR AREAS $A_i x 10^4$ [m^2]					
1 st Stage	1315	222	187	309	490
2 nd Stage	64	23	23	180	45
3 rd & 4 th Stages				85	
HOUSING TEMPERATURE [K]	300	250	300	235	300
MASS [kg]	7,26	4,04	2,49	1,49	3,63
DIMENSIONS [m]	0,56x0,56x0,26	0,17x0,25x0,13	0,20x0,38x0,33	0,20x0,18x0,15	0,45(Diameter)x0,22
COVER OR SHIELD	Shield	Shield	Cover (Door)	No	Cover
CONTROL TEMPERATURE [K]	No Commandable Gain	114	120	107	95
HEAT LOAD SENSITIVITY [b] [$K.W^{-1}$]	700	1400	1500	400	1600

[a] All data in this table are from Donohoe, Sherman & Hickman (1975) [6]. Denomination is the same as that used by the authors. Key to abbreviations: MSS: Multi Spectral Scanner; SCMR: Surface Composition Mapping Radiometer; VHRR: Very High Resolution Radiometer; VISSR: Visible and Infrared Spin Scan Radiometer.

[b] Detector temperature change per W of heat input.

6.6.1 Philco-ford passive radiant cooler

A cryogenic radiator intended to cool infrared detector systems for spacecraft applications was developed by PHILCO-FORD Corporation, Electronics Group, Palo Alto, Calif., according to the following requirements:

Detector operating temperature: 90-106 K.

Power dissipation: $3{,}5 \times 10^{-4}$ W.

Lateral and focal plane alignment of detector to optics: within $\pm\ 5{,}08 \times 10^{-5}$ m.

Spacecraft interface temperature : 295 K.

Maximum base diameter: 0,2032 m (arbitrarily fixed).

Details concerning the development of this radiator are given in the following clauses.

Description

The radiator consists of four stages. The first one is a conical-shaped radiator whose aim is to increase the available radiator surface area without increasing its diameter. Each one of the remaining stages is made in the shape of a disc to make easy the manufacturing process. The stages were made of aluminium 5×10^{-4} m thick.

The first stage and the portion exposed to space of each one of the other three stages have a high emittance provided by a black paint with $\varepsilon = 0{,}80$, while all the interior surfaces, of highly polished aluminium, have low emittances ($\varepsilon = 0{,}05$).

Radiation from the high emittance surface of a stage to the low emittance surface of the stage above it was prevented by using a strip of aluminized Mylar around the edge of the upper shield.

The stages are separated by low thermal conductance supports. These supports are of polyurethane foam with a density of 32 $kg.m^{-3}$, and have the shape of a ring of $7{,}62 \times 10^{-2}$ m in diameter and $9{,}5 \times 10^{-3}$ m thick approximately. The foam supports are joined to the discs of the different stages by means of an epoxy adhesive.

The system is shielded from the spacecraft by a truncated cone having a height of $7{,}62 \times 10^{-2}$ m and a cone angle of 60°. This cone is formed by a multilayer insulation having Kapton film shields. To minimize the radiative coupling between the radiator and the spacecraft, the shield surface of the multilayer insulation looking to the radiator is aluminized ($\varepsilon = 0{,}05$) to become specular.

No other external radiation, either direct or indirect, takes place, except that coming from the spacecraft.

The mass of the radiative cooler assembly (lee insulation) is 0,59 kg.

The complete radiative cooler assembly is shown in Figure 6-11, while the staged radiator development model is presented in Figure 6-12.

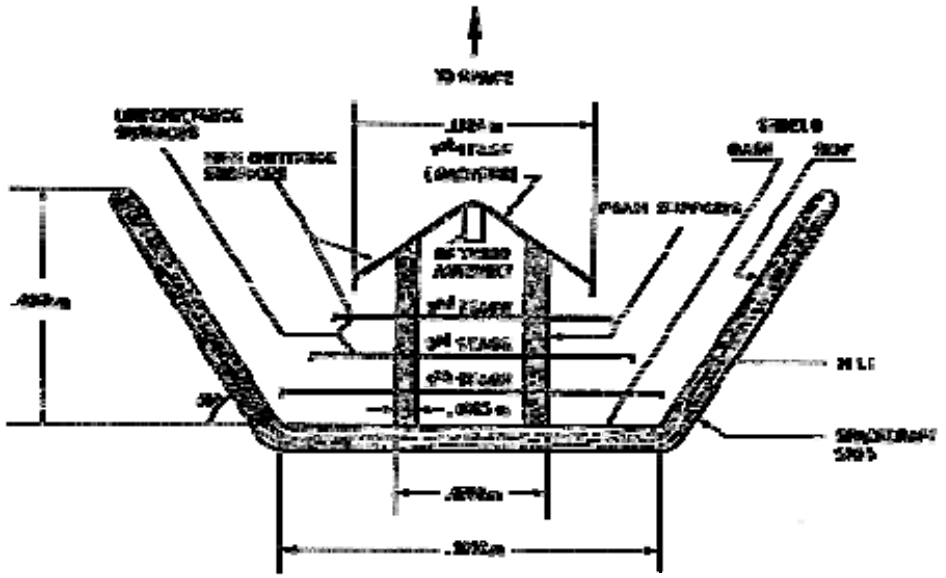

Figure 6-11: Sketch of the PHILCO-FORD cryogenic staged radiator. The shielding strips of the aluminized Mylar, which can be seen in Figure 6-12, are not represented in this Figure. After Hulett & Zierman (1970) [10].

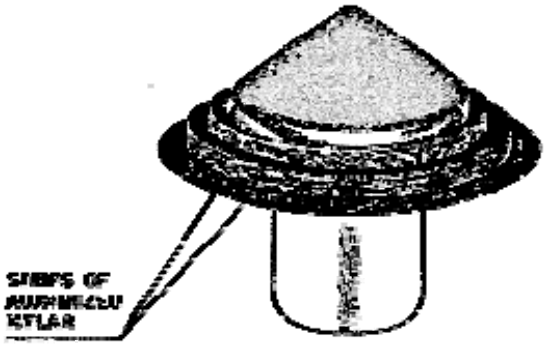

Figure 6-12: PHILCO-FORD cryogenic staged radiator development model. From Hulett & Zierman (1970) [10].

Thermal Analysis and Tests

Thermal analysis of the radiative cooler system were performed using an 8-node computer model. Each one of the four stages is represented by a node, and the multilayer insulation surrounding the system is represented by two nodes, one in the base of the shield and the other one in the side of the shield. The outer space and the spacecraft interface are represented by constant temperature nodes at 0 K and 294 K respectively. The temperatures predicted by the analytical model are presented in Table 6-2.

Table 6-2: Temperatures predicted by the analytical model based on deep space conditions.

Node	Description	Temperature [K]
1	First stage (Radiator)	96
2	Second stage	105
3	Third stage	114
4	Fourth stage	127
5	Shield (Base)	146
6	Shield (Side)	164
7	Spacecraft	294
8	Outer space	0

NOTE From Hulett & Zierman (1970) [10].

Thermal-vacuum tests were conducted on the thermal development model. In the tests the heat sink consisted of a circular aluminium plate kept at constant temperature, and the spacecraft temperature was simulated by a heated enclosure kept at room temperature. the temperature of the radiator (first stage) was both measured in the tests and calculated by using the 8-node thermal model with the same boundary conditions (sink and spacecraft temperatures) as in the test.

The measured and predicted radiator temperature values are compared in Table 6-3.

Table 6-3: Boundary Temperature and Resulting Radiation First Stage Temperature.

TEST N°	HEAT DISSIPATION [W]	TEMPERATURE [K]			
		BOUNDARY CONDITIONS		RESULTS FIRST STAGE	
		SINK	SPACECRAFT	MEASURED	CALCULATED
1	0	96	294	120	118
2	0,1	96	296	131	129
3	0,183	93	294	137	138
4	0	96	325	121	120

NOTE From Hulett & Zierman (1970) [10].

6.6.2 Arthur D. Little passive radiant cooler

A two-stage passive radiator designed to cool an infrared detector operating in the 90-110 K temperature range, was developed by ARTHUR D. LITTLE, Inc., Cambridge, Mass., according to the following requirements:

Detector operating temperature: Should be below 107 K, with a maximum detector power of approximately 10^{-2} W.

Maximum clear filed of view to space: Approximately 101.

Mass: Less than 1,6 kg.

Orbital conditions: Designed for operation in near-polar earth orbits at altitudes greater than $7{,}4 \times 10^5$ m, with a 3-axis stabilized spacecraft.

Environmental power input: The external power absorbed by the radiator from the spacecraft, earth and direct sunlight is less than 0,93 W.

Engineering details concerning this radiator are given in the following clauses.

Description

The assembly consists of an outer stage, an inner stage, a mounting ring, an insulation system, and low thermal conductance supports.

The outer stage is a truncated conical structure with a flange area at its large end and a bulkhead closure at the small end. The basic cone surface is reinforced with integral circular stiffening rings and three axially oriented ribs 120 apart.

This outer stage is machined from a solid billet of 6061-T6 aluminium and its inner conical surface is plated with electroless nickel and then lapped in order to obtain an specular surface of low emittance, thence minimizing the radiant heat input to the inner stage.

The inner stage element is mounted within the small end of the outer stage structure by means of three low thermal conductance support elements, located 120 apart, whose aim is to thermally uncouple both stages. The inner stage is machined from a solid disc of 6061-T6 aluminium, heat treated after rough machining to obtain dimensional stability. The emittance of the top surface of such stage is high in order to radiate to space the heat load on the stage.

The mounting ring serves to support the outer stage at three points around its circumference. This mounting ring is also machined from 6061-T6 aluminium.

The assembly is supported by low thermal conductance supports in order to minimize the heat load from the spacecraft.

The outer and inner stages are insulated from the spacecraft interface by multilayer insulation. The insulation comprises alternate layers of aluminized Mylar with nylon mesh spacers.

A sketch of the diametral section of the assembly is given in Figure 6-13.

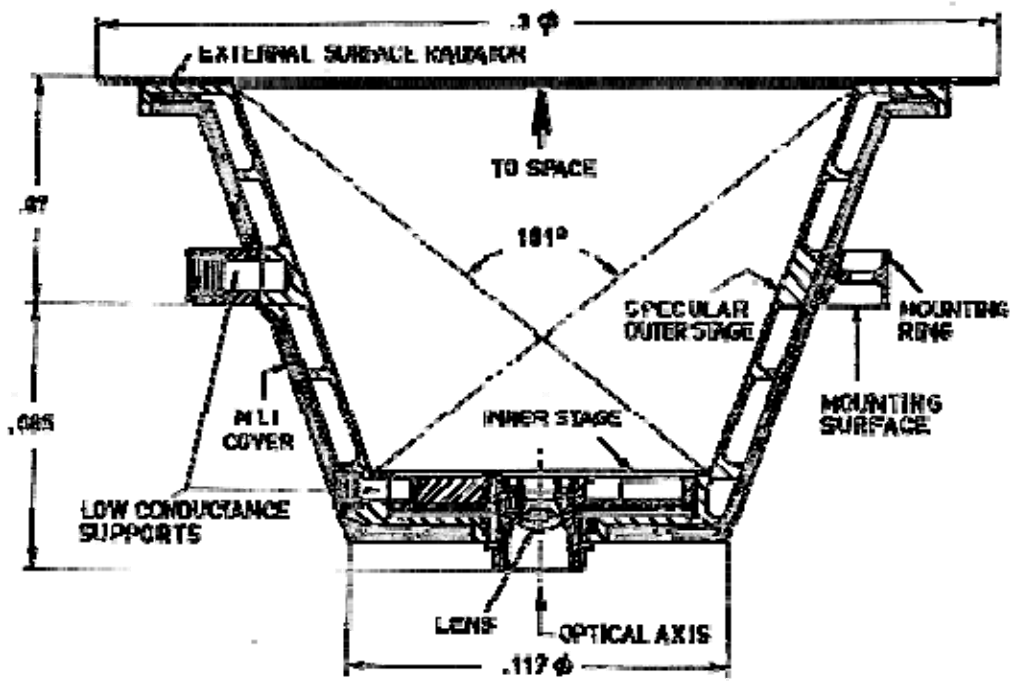

Note: non-si units are used in this figure

Figure 6-13: Schematic diagram of the ADL Spaceborne passive radiator. All the dimensions are in m. From ARTHUR D. LITTLE [2].

Flight Data

Predicted temperatures of the inner stage are compared in Figure 6-14 with those corresponding to the first 800 h of flight.

The detector temperature was operating at approximately 104 K, 3 K below the maximum allowable temperature. The outer stage cone temperature was approximately 199 K.

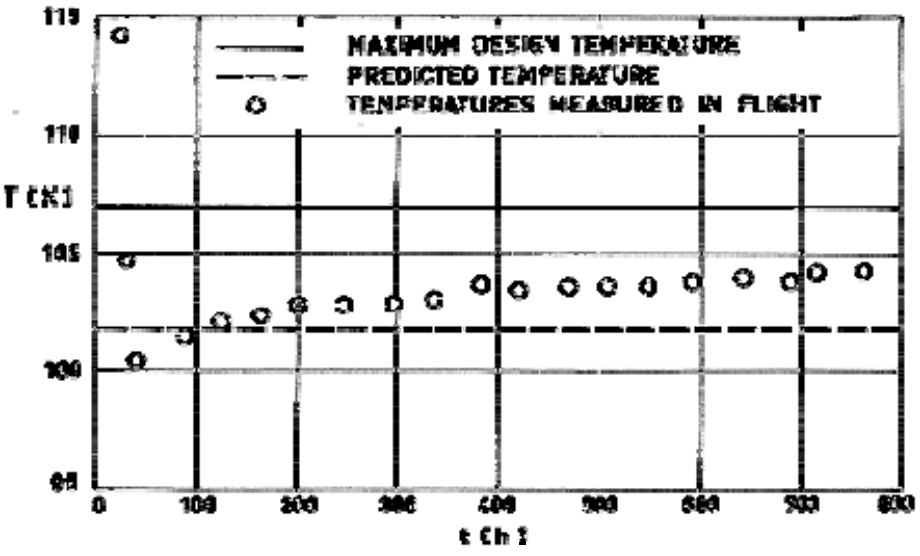

Figure 6-14: Inner stage temperature, *T*, of the ADL spaceborne passive radiator vs. orbital time, *t*. From Gabron, McCullough & Merriam (1971) [8].

6.6.3 Two-stage Meteosat radiometer cooler

A two-stage cone cooler has been developed by CNES, Toulouse (France) to provide cooling to the three channel high resolution radiometer which constitutes the main scientific payload onboard Meteosat. This radiometer has been developed by Engins Matra, Vélizy (France).

Meteosat consists of two cylindrical bodies concentrically stacked. The radiometer is located in the main cylindrical body, which is covered with solar cells. One of the six standard solar panels covering the satellite surface has a large aperture for the radiometer telescope.

The spacecraft is spin stabilized, the spin axis being normal to orbit (equator) plane. The line East-West Scanning is provided by the spin (100 rpm), and the North-South scanning by rotation of the complete telescope, by ± 9°, around an axis normal to the spin.

The passively cooled infrared detector is fixed to the spacecraft structure.

The radiometer-radiant cooler overall configuration is shown in Figure 6-15. See Peraldi (1972) [13] for a description of the scanner operating method.

A baffle, surrounding the telescope, thermally insulates the radiometer from the spacecraft. During handling, ground transportation and launching phases the radiometer is closed, sealed and pressurized with dry nitrogen. Two protective covers, one behind the baffle, the other at the top of the radiator, were sequentially released in orbit, two weeks after orbit acquisition, so that the instrument outgasses before cooling.

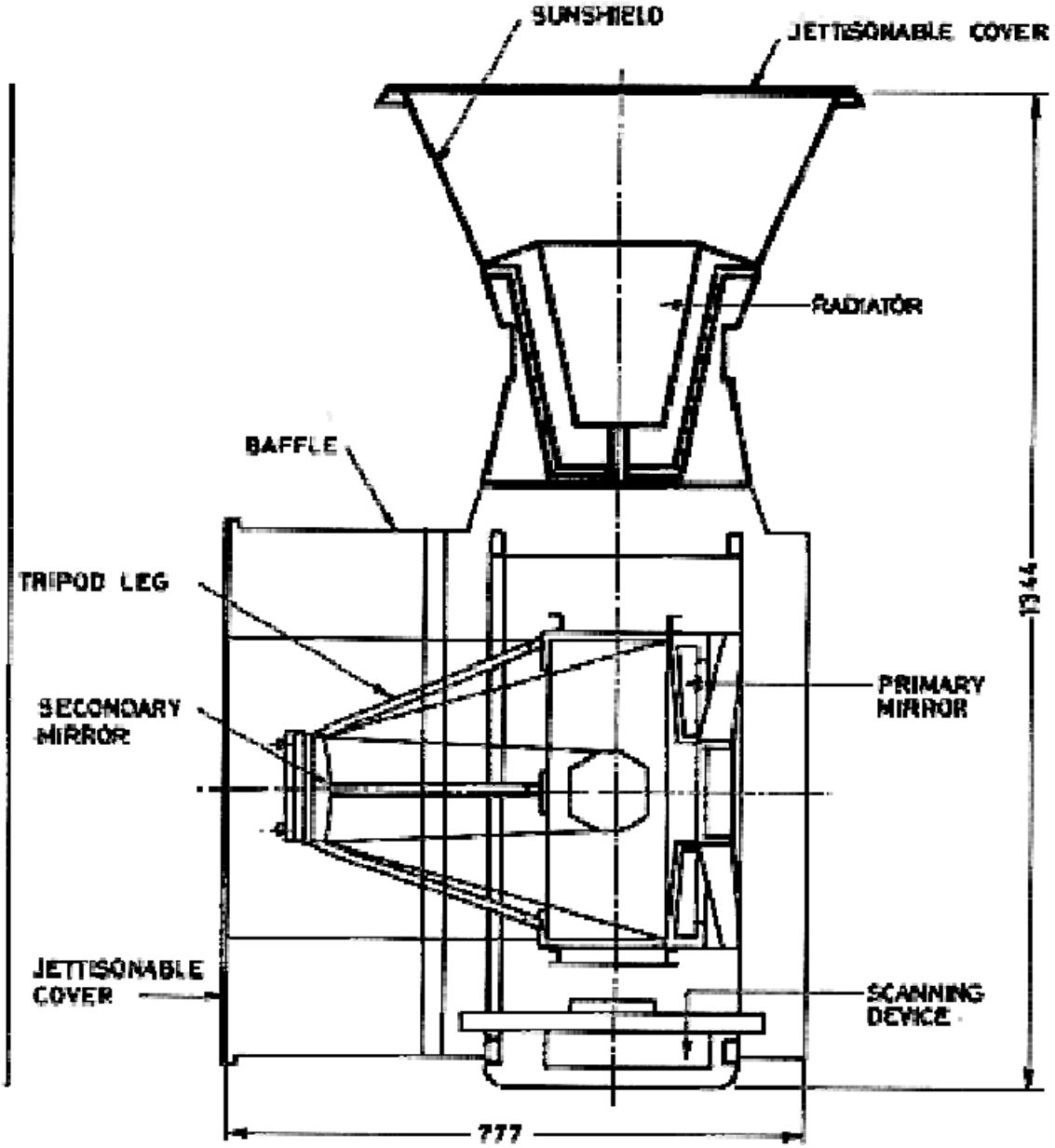

Figure 6-15: Sketch of the Meteosat radiometer and radiant cooler. The dimensions are in mm. After Peraldi (1972) [13] and ESA (Brochure on the Meteosat System).

Detector operating temperature is close to 90 K.

Total mass of the radiometer, including radiant cooler, is 61 kg. Radiometer average consumption is 27 W.

Aside from Meteosat, the cooler was tested onboard a small technological satellite, SRET 2, orbited on June 5th, 1975, by Soviet launcher. Table 6-4 gives orbital and attitude data for both satellites.

Table 6-4: Orbital and Attitude Parameters for SRET 2 and Meteosat 1.

Parameters	SRET 2 [a]	METEOSAT 1
Launching Date	June 5, 1975	Nov. 23, 1977 [b]
Apogee [km]	40871	35692 [b]
Perigee [km]	401	34913 [b]
Inclination [Degrees]	63,5	0,73 [b]
Period [min]	736,5	1440
Spin Axis	In the Ecliptic Plane	Normal to Equatorial Plane.
Spinning Rate [rpm]	> 60	100 [c]
Spin Axis-Sun Direction Angle [Degrees]	0 to 180	67 to 113
Spin Axis-Satellite/Earth Direction Angle [Degrees]	~90	~90 [c]

[a] Data from Rolfo (1976) [15].

[b] From Taylor (1978) [19].

[c] From Peraldi (1972) [13].

Description

The following description of the cooler mainly corresponds to that flown onboard SRET 2 (Rolfo (1976) [15]). This cooler is identified as "SRET 2 Cooler" in contradistinction to "Meteosat Cooler" when differences are note worthy.

In order to avoid direct Sun illumination of the cooler cold stage a sunshield much bigger than the effective radiator itself is used, Figure 6-16.

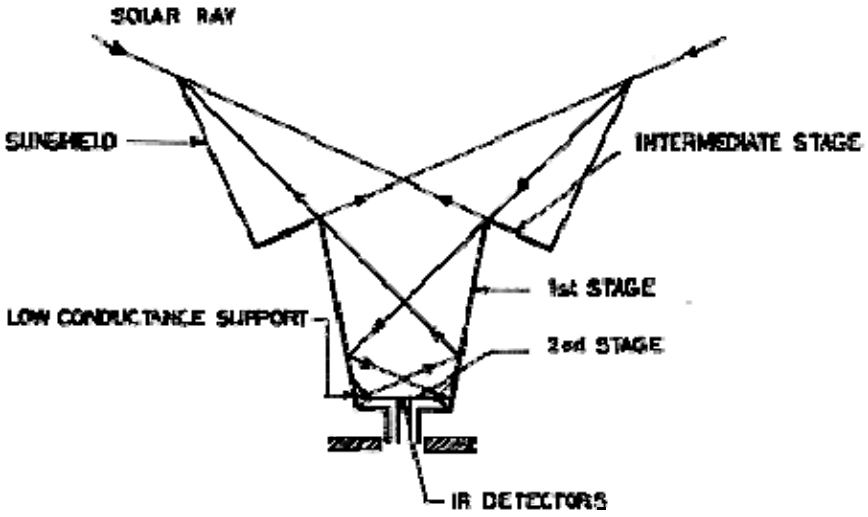

Figure 6-16: Configuration of the Meteosat cooler showing how the incident solar rays are reflected back into space. From Peraldi (1972) [13].

The sunshield consists in a frustrum polished and coated with vacuum deposited aluminium on its inner surface, and white-painted with PSG 120 (see ECSS-E-HB-31-01 Part 6, clause 5.2.4) on its outer surface. The frustrum is not a part of the radiator, rather it is fixed to the spacecraft structure.

The radiator itself is a two-stage design. The first stage, lower cone, which operates at about 150 K, is an aluminium frustrum. Its internal part is polished and coated with vacuum deposited aluminium. The external part is only polished.

The second stage, cold stage or patch, the normal operating temperature of which is about 90 K, is a flat disc, 0,11 m in diameter, made of beryllium coated with golden tape on its lower part and with PSG 120 white paint on its upper part.

The most critical problem of the radiant cooler assembly is that of minimizing the thermal conductance between first and second stage, but still using supports able to withstand the loads resulting from the launch phase. Several tricks have been considered to solve this problem, among them:

1. Peraldi (1972) [13] mentions a system which consists of a mesh of thin glass wires, and was designed by Bertin (France).
2. Pyramidal, low conductance, supports made of fiber-glass and epoxy resin, used in the SRET 2 Cooler (Rolfo (1976) [15]).
3. Tension ties (see ECSS-E-HB-31-01 Part 14, clause 6.3.1) used in the Meteosat Cooler, Figure 6-17.
4. In addition to the thermal conduction through the supports, other major thermal inputs to the second stage are radiation from the radiometer structure, detector wires and screening.

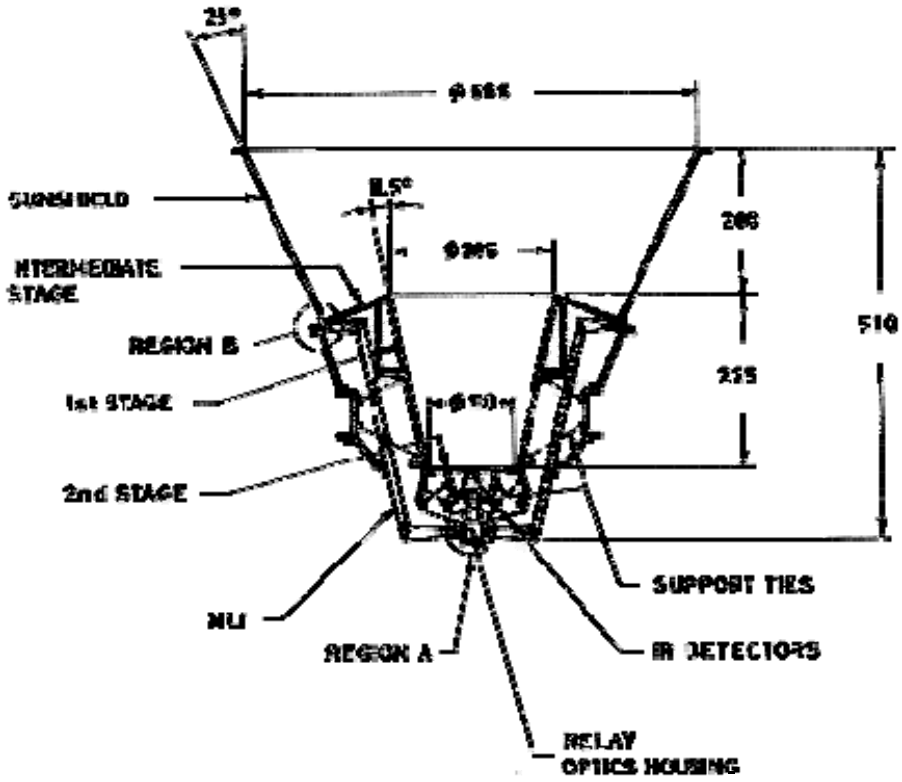

Figure 6-17: Schematic of the Meteosat Cooler. From Reynolds & Kieffer (1979) [14]. All the dimensions, which are given in mm have been estimated by the compiler. A and B are kept for latter reference (see below Thermal Test for Meteosat Cooler).

An intermediate stage is placed between the radiator itself and the sunshield. This stage has its internal part polished, and its external part white-painted with PSG 120.

In the SRET 2 Cooler first and intermediate stages were attached to the satellite by a cylinder made of fiber-glass and resin, and radiatively insulated by an MLI, Figure 6-18.

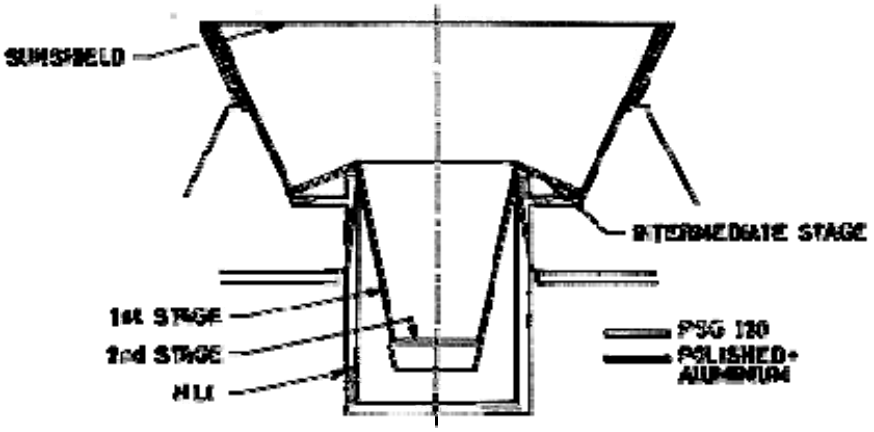

Figure 6-18: Schematic of the SRET 2 Cooler. From Rolfo (1976) [15].

Thermal Tests on the SRET 2 Cooler

Temperatures of the main components of the cooler were continuously monitored in flight by redundant thermistors. Results up to one year in orbit are shown in Figure 6-19. Calculated values are deduced from a thermal model based on the nominal thermal radiation properties given in Table 6-5: Nominal Thermal Radiation Properties

Table 6-5: Nominal Thermal Radiation Properties

Surface	Coating	ε	ρ_{IR}	α_s	ρ_s	Comments
Sunshield (Outer)	PSG 120	0,87	0,13	0,19	0,81	ε assumed to be constant.
Sunshield (Inner)	Polished + Aluminium	0,035	0,025	0,12	0,03	ρ is the diffuse reflectance.
Intermediate Stage	PSG 120	0,87	0,13	0,19	0,81	ε assumed to be constant.
First Stage	Polished + Aluminium	0,025	0,025	0,12	0,03	ρ is the diffuse reflectance.
Second Stage	PSG 120	0,87	0,13	0,19	0,81	ε assumed to be constant.

NOTE From Rolfo (1976) [15].

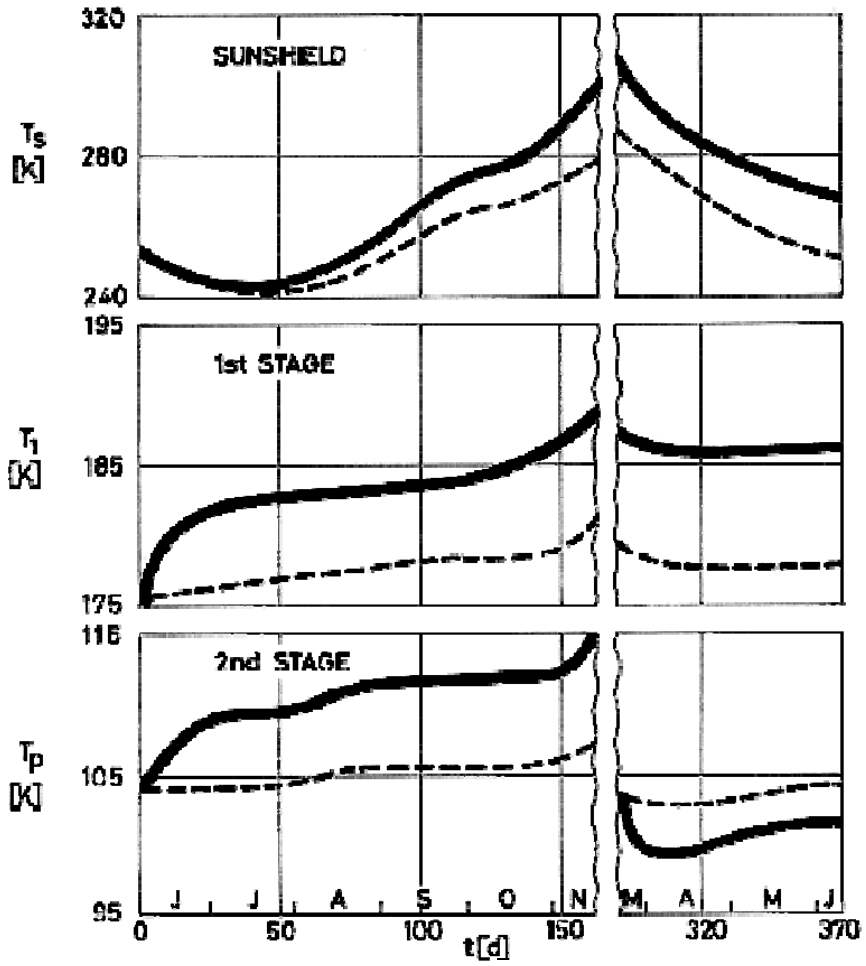

Figure 6-19: Temperature of the sunshield, T_s, first stage, T_1, and second stage, T_p, of the SRET 2 Cooler, vs. orbital time, t. Solid line: measured in orbit; dashed line: calculated on the basis of nominal thermal radiation properties, Table 6-5: Nominal Thermal Radiation Properties. From Rolfo (1976) [15].

Four different periods appear in Figure 6-19, namely:

1. From June 5, 1975 to October 20, 1975.

   Angle between spin axis and Sun direction above 90°.

   Sunshield and cooler under albedo radiation.

   First and second stage temperatures increase at first during three weeks, then remain almost constant.

   Thermal properties of the outer surfaces which appear in the thermal balance and which are not assumed to be constant or estimated otherwise are:

   ε for polished surfaces.

   ρ_{IR} for polished surfaces. This property has not an appreciable influence on the temperature and cannot be calculated accurately. In any case, it has been assumed that the values for the sunshield and first stage are the same.

   New values of thermal radiation properties are given in Table 6-6: Thermal Radiation Properties after June 28, 1975

Table 6-6: Thermal Radiation Properties after June 28, 1975

Surface	Coating	ε	ρ_{IR}	α_s	ρ_s	Comments
Sunshield (Outer)						α_s from another experiment onboard SRET 2.
Sunshield (Inner)	Polished + Aluminium	0,13	0,04	0,32	0,056	
Intermediate Stage						
First Stage	Polished + Aluminium	0,041	0,04	0,15	0,056	
Second Stage						

NOTE From Rolfo (1976) [15].

Empty boxes should be filled as in Table 6-5: Nominal Thermal Radiation Properties. Heavy contoured boxes are filled with values calculated after the next period, ending November 15, 1975.

Recalculated temperatures, based on the new values of the thermal radiation properties, agree with experimental values within 1 K from June 28 to November 15.

During launching the satellite and the cooler were close to the cryogenic tanks of the launcher and, thus, their temperatures were low (between 243 and 263 K). After fairing ejection the satellite outer surface heated up whereas the cooler temperature decreased. Most of the out gassing material deposited on the sunshield (yielding a large ε increment) and much less on the first stage. The resulting values remained constant over three months indicating that ε changes were truly due to contamination; this is partially confirmed by the fact that the ρ_{IRS} remained small.

2. From October 20, 1975 to November 15, 1975.

   Angle between spin axis and Sun direction below 90°, reaching 65° on November 15.

   The sunshield inner face is partially illuminated by the Sun.

   Thermal properties of the outer surfaces which appear in the thermal balance and which are not assumed to be constant or estimated otherwise are:

   α_s and $\rho_s = 1-\alpha_\sigma$ for PSG 120.

   α_s and ρ_s for polished surfaces.

   Six unknown values for only three equations. It is assumed that PSG 120 does not degrade and that the ρ_{sS} for both polished surfaces are equal. Heavy contoured values, Table 6-6: Thermal Radiation Properties after June 28, 1975, were calculated this way.

3. From November 15, 1975 to March 22, 1976 (not represented in Figure 6-19).

   Angle between spin axis and Sun direction below 65°.

   Solar rays impinge directly into the first stage and cooler temperature raises up to about 400 K on first and second stage, and up to 315 K on the sunshield. This resulted in decontamination of the surfaces.

4. After March 22, 1976.

   Angle between spin axis and Sun direction above 65°.

   Cooler temperature decreases again.

   New values of thermal radiation properties are given in Table 6-7: Thermal Radiation Properties after March 22, 1976 Empty boxes as in Table 6-5: Nominal Thermal Radiation Properties.

Table 6-7: Thermal Radiation Properties after March 22, 1976

Surface	Coating	ε	ρ_{IR}	α_s	ρ_s	Comments
Sunshield (Outer)	PSG 120			0,5	0,5	α_s from another experiment onboard SRET 2.
Sunshield (Inner)	Polished + Aluminium	0,10	0,04	0,24	0,05	
Intermediate Stage	PSG 120			0,5	0,5	
First Stage	Polished + Aluminium	0,15	0,002	0,12	0,03	
Second Stage	PSG 120			0,5	0,5	

NOTE From Rolfo (1976) [15].

Notice, in particular, the value $\varepsilon = 0{,}015$ for the first stage, which is smaller than the initial value given in Table 6-5: Nominal Thermal Radiation Properties. This seems to indicate that contamination occurred before ground testing. The quoted value, $\varepsilon = 0{,}015$, is similar to those given for vapor deposited aluminium, when measured in vacuum (see Table 6-2, p. G 1-20).

Thermal Tests of the Meteosat Cooler

An analysis of inflight performance of radiometer and cooler has been made by Reynols & Kieffer (1979) [14].

Ice deposition on the cold optics caused signal reductions both during the winters of 1977-78 and 1978-79. Diagnostic techniques were devised to differentiate the various phenomena (contamination or other) leading to radiometer signal reductions. The signal level was restored by heating the optical elements above the ice sublimation point, confirming the diagnostic that the origin of the malfunction was ice deposition. It has been conjectured that water vapor comes from region A of the MLI, Figure 6-17, during the short period of winter when this region is hotter than 173 K.

Regarding contamination of thermal control surfaces, the major concerns were ice deposition and UV induced polymerization.

Contamination was detected by monitoring the temperature evolution in only three points (placed in the sunshield, first and second stage, respectively). Even this very reduced amount of information can be helpful if combined with some analytical model of the system. It was a priori known that the temperature of the second stage is controlled by that of the first stage, and the temperature of the first stage is similarly controlled by that of the sunshield with a second order contribution from the

radiometer. Then, a good diagnostic technique, which presents the advantage of being independent of seasonal temperature fluctuations, consists in plotting second stage vs. first stage temperature, and first stage vs. sunshield temperature, comparing the plots to those obtained in ground tests. Results, from Reynolds & Kieffer (1979) [14], are given in Figure 6-20.

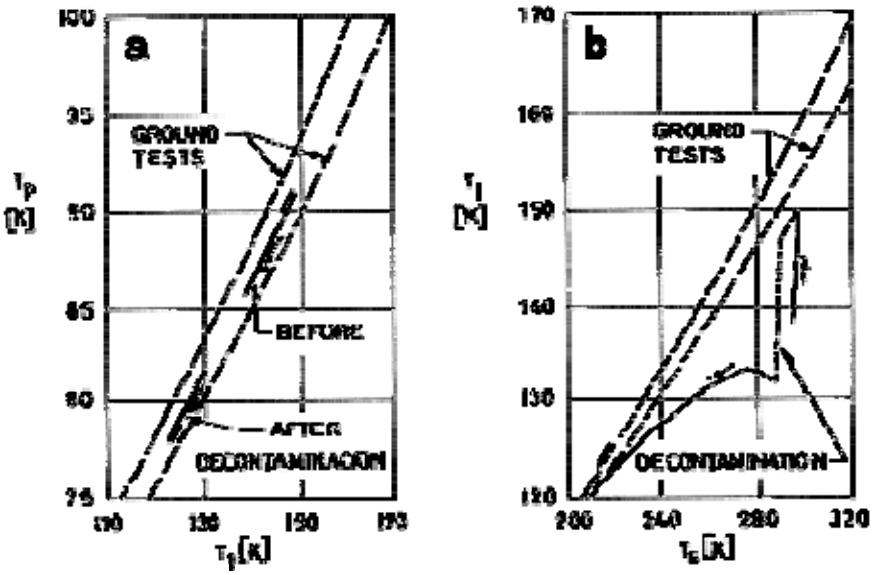

Figure 6-20: Relative temperature evolution of the Meteosat Cooler. a) Second stage temperature, T_p, vs. first stage temperature, T_1. b) First stage temperature, T_1, vs. sunshield temperature, T_s Arrows indicate the direction of temperature evolution. From Reynolds & Kieffer (1979) [14].

Although the second stage is actively maintained at 90 K in normal operation, the system was allowed to free-run during the first six months. Since that time the non-controlled temperature has been extrapolated from the knowledge of the thermostat reference signal.

Figure 6-20a, second stage vs. first stage temperature, indicates that the inflight data more or less follow the ground tests curves. No measurable degradation resulted.

Figure 6-20b, which shows first stage vs. sunshield temperatures, evidences, on the contrary, a departure in the nominal temperature. The total time elapsed correspond approximately to the first six months in orbit, starting early December 1977. A very rapid contamination in winter continued, after a decontamination in late January 1978, at a rate which decreased into the summer period.

Again water vapor, presumably coming from region B of the MLI, Figure 6-17, and condensed on the first stage, was the main contaminating material.

Similar but less dramatic results, since the contaminating source was being depleted, were observed in the following year.

6.6.4 Two-stage heat-pipe radiator

A large two-stage heat-pipe radiator was developed for ground testing in order to verify the thermal performance and structural integrity of large passive cryogenic radiant coolers (Wright (1980) [21]).

The design requirements that applied to the Cryogenic Radiator Test Unit (CRTU) were the following:

Cooling capability of 5 W at an average radiator temperature of 70 K ± 2 K.

Temperature drop from the radiator to a heat source located 1 m from the radiator to be less than 3 K.

Shielding capable of preventing direct solar impingement on the radiator in a geosynchronous orbit.

Ability to withstand the dynamic launch environment imposed by the Shuttle orbiter or by a Titan launch vehicle.

Compatibility with a 2,74 m diameter design envelope, like Titan III booster.

Design operational life expectancy of at least five years.

The CRTU should also be designed for later addition of a third-stage radiator.

Details concerning this radiator are given in the following.

Description

The CRTU, the overall configuration of which is shown in Figure 6-21, consists of two radiator stages, insulation blankets, sun and side shields, heat pipes, a structural support pan, and structural mounting supports.

The first stage is mounted off the structural support pan by means of low thermal conductance support posts. The second stage is similarly supported off the first stage. Forty-layer MLI blankets are located between the pan and first stage and second stage.

The radiator stages are made from $1{,}27 \times 10^{-2}$ m thick Aluminium honeycomb with $0{,}25 \times 10^{-3}$ m faces heets. The first stage radiator is rectangular measuring 2,1 m by 3,86 m. Three sides are bent upwards to form the sun and side shields (see Figure 6-21). The sunshield is 0,38 m high and is angled up 60 degrees from the plane of the radiator. The side shields are angled up 90 degrees from the plane of the radiator and are triangular.

The second stage MLI covers all but 0,9 m^2 of the first stage and 0,4 m^2 of the sunshield. The exposed areas are coated with a high emissivity black paint ($\varepsilon = 0{,}9$).

The second stage radiator is rectangular and measures 1,83 m by 3,76 m. The exposed surface area is 6,88 m^2 and is also coated with high emissivity black paint.

Heat is transferred from the heat source to the radiator via two transport heat pipes (for redundancy), and distributed over the radiator surface by a distributor heat pipe.

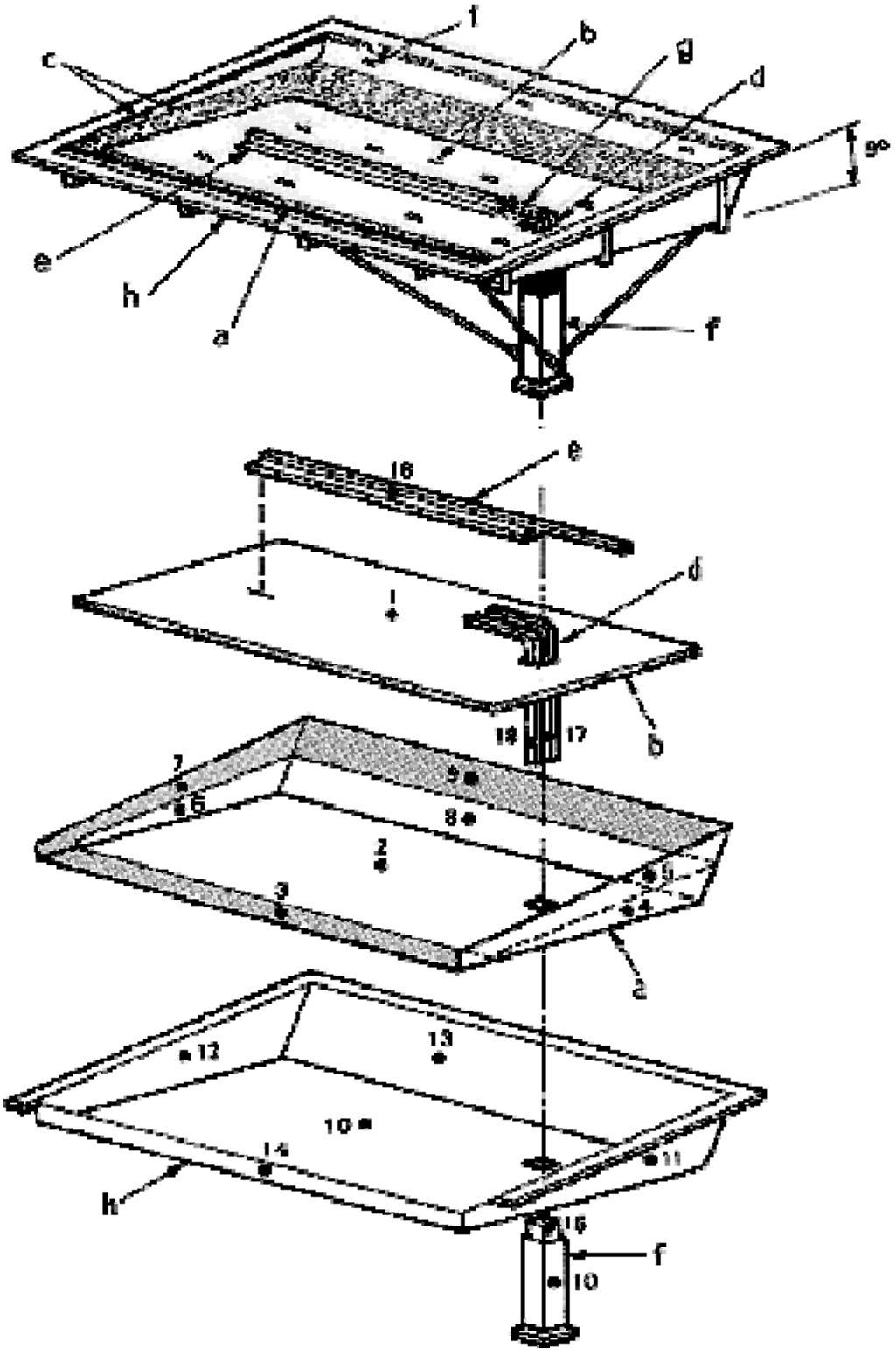

Figure 6-21: CRTU configuration. Numbers indicate the position of the nodes used in the numerical modeling. a) First Stage Radiator; b) Second Stage Radiator; c) MLI; d) Transport HPs (2); e) Distributor HP; f) HP Thermal Shroud; g) Thermal Clamp Block; h) Structural Support Pan; i) Support Post Housings. From Wright (1980) [21].

The transport heat pipes are L-shaped, they measure 1 m by 0,25 m and are normal to the plane of the radiator. Insulation is achieved through an MLI and an Aluminium thermal shroud.

The distributor heat pipe, 2,4 m long, is mechanically and thermally coupled to the transport heat pipes by a thermal clamp block, and bonded along the centerline of the radiator. This heat pipe uses oxygen as working See the dimensions in Figure 6-22.

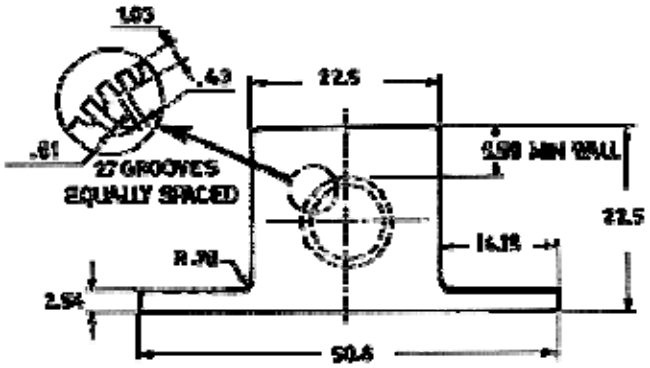

Figure 6-22: Distributor heat pipe geometry. All dimensions are in mm. From Wright (1980) [21].

The structural support pan is a riveted Aluminium sheet metal structure that supports the radiator and simulates the spacecraft interface. It is stiffened with zee-section longerons and intercostals to provide a rigid structure to which the radiator stages can be attached.

Shielding

Radiator shielding requirements for the CRTU are those for a geosynchronous satellite. The primary axis of the spacecraft is assumed to be in the direction of the velocity vector, Figure 6-23. In the generalized configuration shown in Figure 6-23 the orbit plane is inclined to the equatorial plane at an angle *i*. The plane of the radiator is tilted above the orbit plane such that the radiator looks above the Earth's horizon. For six months of the year, the earth-Sun vector is below the orbit plane; for the other six months it is above the orbit plane. The radiator can be shielded from any direct solar incidence by erecting a shield, the shadow angle of which is equal to the angle ϕ, between the Earth-vehicle vector and the vehicle-horizon vector. When the Sun moves above the orbit plane, the spacecraft is yawed 180 degrees such that the radiator faces south instead of north. This yaw maneuver should be repeated at six-month intervals.

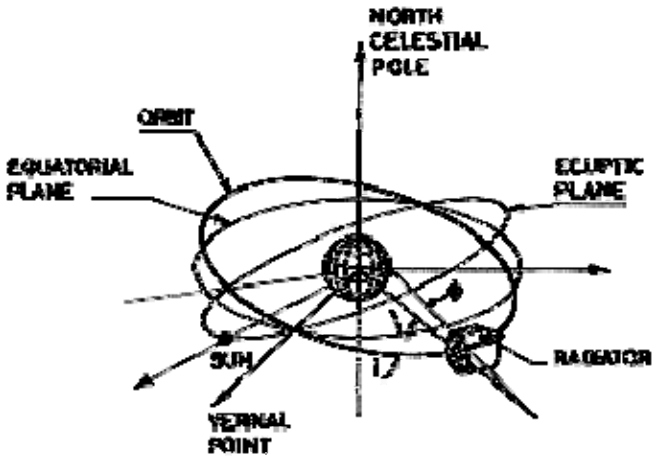

Figure 6-23: Orbital and radiator shielding geometry. Fromm Wright (1980) [21].

At geosynchronous altitude, the required shield angle, ϕ, is 8,5 degrees; however, an angle of 9 degrees was selected to provide some design margin for attitude control variations.

Supporting

In addition to withstanding the structural loads imposed by launch, the primary design considerations for the structural supports are thermal shrinkage of the radiator and parasitic heat leakage through the supports. Maximum axial and lateral acceleration load factors of 13 g and 8 g respectively were used for determining the design (static) loads. Calculation of dynamic loads was based on typical vibration input levels for the Titan III C and the Shuttle vehicles.

Because of the size of the radiator, up to $2x10^{-2}$ m of lateral deflection of the radiator stages due to thermal contraction should be accommodated by the structural supports. As a result, the selected design approach was to support the radiator stages along two sides with rod-end-type post to allow shrinkage in two dimensions. Rod-end standoff posts were also used in the direction perpendicular to the plane of the radiator. A post spacing of approximately 1 m was selected as a compromise between both the structural load on each post and the number of penetrations through the insulation. A typical post configuration is shown in Figure 6-24. The post are made of fiber-glass with spherical rod-end bearings. Side support posts have a thermal conductance of $5,1x10^{-5}$ $W.K^{-1}$, whereas standoff posts have a thermal conductance of $1,5x10^{-4}$ $W.K^{-1}$.

Total mass of the CRTU is 145 kg including heaters, wiring and instrumentation. Of the total, the structural support pan, which is not mass-optimized, accounts for approximately 62 kg. For in flight application, however, the radiator may be directly attached to the spacecraft structure, and no support pan would be required.

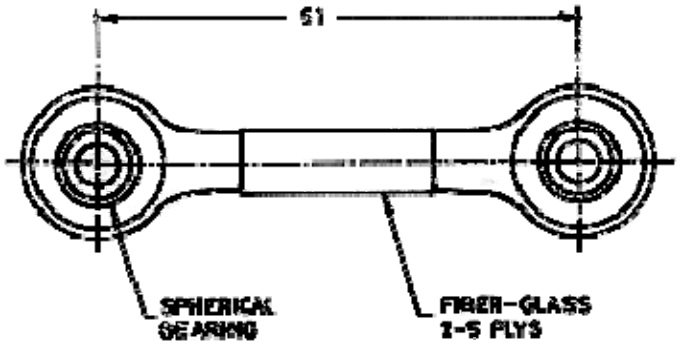

Figure 6-24: Structural support post configuration. Distance between centers in mm. From Wright (1980) [21].

Thermal Test

A thermal balance test in vacuum was conducted to study the behavior of the CRTU in a simulated space environment. The tests aimed at assessing:

1. the cooling capability of the system, as mentioned in clause 6.6.4.
2. The performance of the radiator for various heat loads to the second stage.
3. The effect on the second stage temperature of adding up to 20 W heat to the first stage.
4. The sensitivity of the second stage temperature to the sunshield temperature.
5. The performance of MLIs and structural support posts.

The tests were conducted in the Mark I space chamber, Arnold Engineering Development Center, Tennessee. See Anon (1968) [1] for a description of this facility.

The test setup is shown in Figure 6-25. A gaseous-helium cooled shroud, simulating the deep space, is placed above the radiator. The shroud is finned, black-painted ($\varepsilon \geq 0{,}95$), and kept at 20 K ± 5 K during the tests. An MLI closeout curtain is located around the periphery between the CRTU and the shroud to prevent impingement on the radiator surfaces of the radiation from the chamber or from the supporting structure.

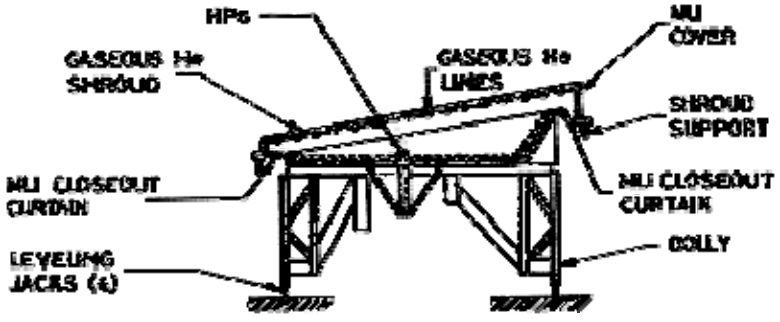

Figure 6-25: Thermal balance test setup. From Wright (1980) [21].

Direct solar impingement was not simulated since it is assumed to be prevented by the sunshield.

The CRTU was instrumented with 50 chromel-constantan thermocouples (ANSI Type E) and 6 diode temperature sensors. The thermocouples are attached to various locations on the first and second

stages, HPs, structural support pan and sunshield. The maximum error of the thermocouple system is ± 1 K. The silicon diode temperature sensors are used to provide temperature data at critical locations on the CRTU such as the HPs, their accuracy is better than 0,1 K.

Heat input from simulated detector focal plane is supplied by a standard cartridge-type heater. Heater power is measured to an accuracy better than 0,02 W. Heater power to the first stage is supplied through a row of Kapton film heaters (see the existing systems of electrical heaters developed by MINCO PRODUCTS) bonded to the bottom of the first stage radiator just underneath the exposed edge. Similar heaters are used on the structural support pan and on the back of the sunshield to keep them at the desired temperature during the tests.

Eight tests conditions were run. They are summarized in Table 6-8. Under all test conditions, the vacuum chamber pressure was less than $1{,}3 \times 10^{-3}$ Pa. The structural support pan was kept at an average temperature of 290 K ± 5 K. Each test condition was held for the number of days indicated in the table to ensure near steady-state conditions at the end of each test run. End-of-run test results also are summarized in Table 6-8.

Table 6-8: Results of the CRTU Thermal Vacuum Test

Test Run	Heat Load [W]		Pan/Side Shield Temp. [K]	Sunshield Temp. [K]	Days	End of Run Temperature [K]	
	1 st Stage	2 nd Stage				1 st Stage	2 nd Stage
1	0	5	290	290	3	106,09	70,80
2	0	0	290	290	2	103,32	45,24
3	20	5	290	290	2	147,71	71,78
4	0	7	290	290	2	107,31	76,53
5	0	3	290	290	2	104,12	62,84
6	20	10	290	290	2	147,77	84,51
7	0	5	290	325	2	104,81	70,52
8	0	5	290	290	2	105,94	70,97

NOTE From Wright (1980) [21].

A thermal mathematical model consisting of 21 nodes was used to simulate CRTU performance and to correlate test results. The SINDA lumped capacity network computer programme was used to generate the data. The locations of the nodes are shown in Figure 6-21. Fifteen diffusion nodes represent the major structural elements of the radiator, whereas 3 zero-capacitance nodes simulate the outer layers of the exposed MLI surfaces. Three boundary nodes (not shown in the figure) are used to represent the space sink (helium shroud), the spacecraft boundary (structural pan) and the sunshield. The performance of the HPs are simulated by empirical data determined from testing. Empirical data for the MLI performance thermal conductivity, k_{eff}, (see clause J 3-1)

$$k_{eff} = 2{,}4\times10^{-10}\left(T_H + T_C\right) + 4{,}2\times10^{-13}\,\frac{T_H^4 - T_C^4}{T_H - T_C} \qquad [6\text{-}10]$$

Similar expressions of the effective thermal conductivity can be found elsewhere, see for instance ECSS-E-HB-31-01 Part 14.

For analysis of test results either the above value of k_{eff} or twice this value were used.

The experimental results have been compared in Figure 6-26 to predictions via the above mentioned thermal mathematical model. Cases considered are those in Table 6-8 involving a heat load to the second stage only, with a constant sunshield temperature, T_s = 290 K, namely Test Runs 1, 2, 4, 5 and 8. Ordinates are fin-root temperatures of the second stage skin adjacent to the distributor HP (node 1 in Figure 6-21). These temperatures correspond to steady-state conditions and were deduced by an appropriate correction to the end-of-run temperatures. The corrective term accounts for the temperature rate of change at the end of the test run and for the variation of the emissive power of the second stage with temperature.

Numerical predictions were based on MLI conductivities of either k_{eff} or $2k_{eff}$, and on several models of the fin effectiveness of the second stage, as indicated in the caption of Figure 6-26. This fin effectiveness is defined in clause 4.

Results from the remainder cases are summarized in Table 6-9. Predictions are based on $2k_{eff}$ and a temperature-dependent fin effectiveness.

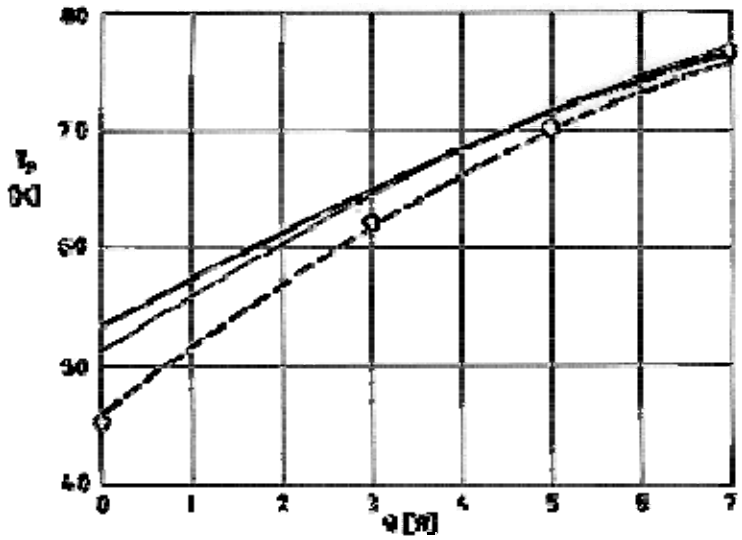

Figure 6-26: Temperatures, T_p, of CRTU second stage vs. second stage heat load, Q. Solid thick line: Predicted. $2k_{eff}$. $\eta = 0{,}8$; solid thin line: Predicted. $2k_{eff}$. $\eta = \eta(T)$; dashed line: Predicted. $2k_{eff}$. $\eta = \eta(T)$; Circles: Measured. From Wright (1980) [21].

Table 6-9: Predicted and Measured Temperatures for CRTU Second Stage.

Test Run	Stage	Predicted Temperature [K]	End of Run Temperature [K]
3	2 nd 1 st	75,3 163,5	71,8 147,7
6	2 nd 1 st	86,6 145,6	84,5 147,8
7	2 nd 1 st	71,9 112,8	70,5 104,8

NOTE From Wright (1980) [21].

7
Active radiant coolers

7.1 Existing systems

7.1.1 Ge active radiator with liquid metal coolant

An aluminium space radiator panel utilizing a liquid metal coolant was designed, fabricated, and tested by GENERAL ELECTRIC Co., Philadelphia, Pa.

Such a radiator would be suitable for the primary heat rejection system of SNAP-8 Rankine cycle power system, or for advanced technology power systems using Brayton cycles.

Description

The radiator panel is a portion of a conical surface of rectangular plan form (1,2x1,8 m) as shown in Figure 7-1. Its construction is consistent with the use of the radiator as a portion of the primary spacecraft structure.

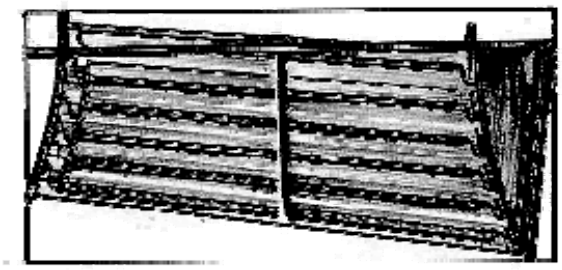

Figure 7-1: GE radiator panel rear surface. From Cockfield & Killen (1970) [4].

The material used are the following:

Tube armor: Aluminium 99,5% pure. Its composition was chosen with the two-fold aim of obtaining a high thermal conductivity and the possibility of welding to the fin material.

Tube: Stainless steel 316 compatible with the liquid metal coolant.

Fin: Aluminium 6061-0. It was milled with a welding land for each tube element. Iron titanate was plasma-sprayed onto the fins in order to obtain a high emittance. an uniform emittance approaching 0,9 was thus obtained.

Liquid coolant: Nak.

The fin-tube configuration and its relevant dimensions are given in Figure 7-2 and Table 7-1 respectively.

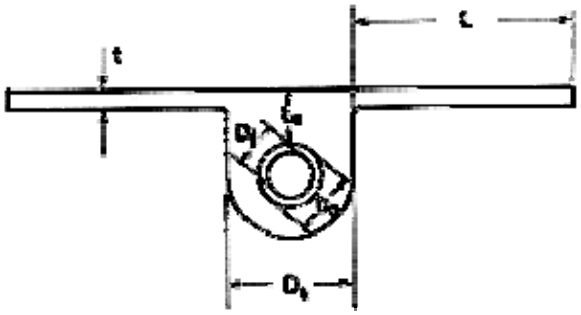

Figure 7-2: Schematic diagram of the fin-tube configuration. From Cockfield & Killen (1970) [4].

Table 7-1: Relevant Dimensions of the Radiator

Fin Thickness, t	$1{,}27 \times 10^{-3}$ m
Fin Length, L	$8{,}433 \times 10^{-2}$ m
Tube Armor, t_a	$1{,}143 \times 10^{-2}$ m
Liner Outer Diameter, D_O	$5{,}334 \times 10^{-3}$ m
Liner Inner Diameter, D_i	$4{,}572 \times 10^{-3}$ m
Tube Outer Diameter, D_t	$1{,}118 \times 10^{-2}$ m

NOTE From Cockfield & Killen (1970) [4].

Test Method

The panel was instrumented with 170 Thermocouples which were either flame sprayed or spot welded to the radiator.

Preliminary tests were conduced in air, outside the vacuum chamber, at temperature up to 422 K, with the panel in vertical position.

In the vacuum chamber tests, the panel was placed horizontally and its back side was insulated to minimize heat losses. The chamber wall temperature was maintained at approximately 294 K during all tests, while the pressure level was 5,33 Pa or less. Tests were conducted over a range of coolant inlet temperatures from 422 K to 644 K and a range of flow rates from 0,09 to 0,295 $kg.s^{-1}$. Total test chamber time was 550 h, including a continuous run of 175 h at design conditions during which no degradation in performance was observed.

The experimental values of the fin temperature profiles for several root temperatures are shown in Figure 7-3. The Figure 7-4 shows the position of the testing points together with the temperaturevalues which were obtained in a particular case.

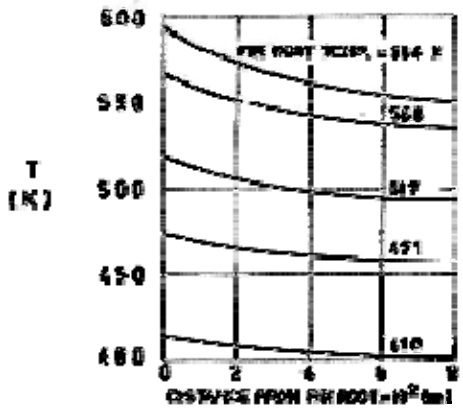

Figure 7-3: Fin temperature, T, vs. distance from the root. Vacuum operation. Sink Temperature 294 K. From Cockfield & Killen (1970) [4].

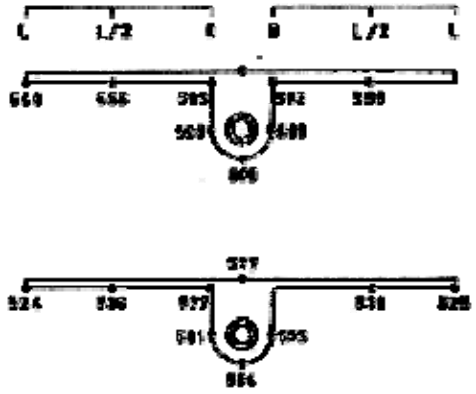

Figure 7-4: Typical values of the fin-tube temperatures. Numbers indicate temperatures in K. From Cockfield & Killen (1970) [4].

The fin effectiveness deduced from the experimental temperature profiles are compared in Table 7-2 with the values obtained analytically by using the Lieblein method (Lieblein (1959) [12]).

Table 7-2: Comparison of analytical and experimental fin effectiveness

FIN ROOT TEMPERATURE [K]	FIN EFFECTIVENESS	
	OBTAINED ANALYTICALLY	OBTAINED FROM THE MEASURED TEMP. FIELD
594	0,78	0,80
568	0,80	0,82
517	0,84	0,84
471	0,87	0,87
403	0,91	0,91

NOTE From Cockfield & Killen (1970) [4].

Bibliography

[1] Anon., "Test Facilities that Outguessed the Future", Cryogenic Engineering News, Vol. 3, Dec. 1968, pp. 28-30.

[2] ARTHUR D. LITTLE, "Spaceborne Passive Radiator Cooler Model 101", Technical Data Sheet, Arthur D. Little, Inc., Cambridge, Massachusetts.

[3] Bywaters, R.P., Keeling, M.C., "Multistage Radiative Coolers for Spacecraft Sensors", in "Advances in Cryogenic Engineering", Vol. 19, K.D. Timmerhaus, Ed., Plenum Press, New York, 1974, pp. 490-499.

[4] Cockfield, R.D., Killen, R.E., "Testing of an Aluminium Radiator with Liquid Metal Coolant", in "Heat Transfer and Spacecraft Thermal Control", Progress in Astronautics and Aeronautics, Vol. 24, J.W. Lucas, Ed., The MIT Press, Cambridge, Massachusetts, 1971, pp. 601-613.

[5] Donabedian, M., "Survey of Cryogenic Cooling Techniques", Air Force Report No. SAMSO-TR-73-74. The Aerospace Corporation, El Segundo, California, Oct. 1972, pp. 4-1 to 4-11.

[6] Donohoe, M.J., Sherman, A., Hickman, D.E., "Radiant Coolers-Theory, Flight Histories, Design Comparisons and Future Applications", AIAA Paper No. 75-184, AIAA 13th Aerospace Sciences Meeting, Pasadena, California, Jan. 20-22, 1975.

[7] ESA, "The Meteosat System", ESA, Paris, France.

[8] Gabron, F., McCullough, J.E., Merriam, R.L., "Spaceborne Passive Radiator for Detector Cooling", Conference of American Society of Mechanical Engineers, Society of Automotive Engineers, and American Institute of Aeronautics and Astronautics, San Francisco, California, July 1971.

[9] Haller, H.C., 1964, "Comparison of Heat-Rejection and Weight Characteristics of Several Radiator Fin-Tube Configurations", NASA TN D-2385, July 1964.

[10] Hulett, R.H., Zierman, C.A., "Staged Radiator Design for Low Temperature Spacecraft Applications", in "Heat Transfer and Spacecraft Thermal Control", Progress in Astronautics and Aeronautics, Vol. 24, J.W. Lucas, Ed., The MIT Press, Cambridge, Massachusetts, 1971, pp. 614-629.

[11] Krebs, R.P., Winch, D.M., Lieblein, S., "Analysis of a Megawatt Level Direct Condenser-Radiator", in "Power Systems for Space Flight", Progress in Astronautics and Aeronautics, Vol. 11, M.A. Zipkin and R.N. Edwards, Eds., Academic Press, New York, 1963, pp. 475-504.

[12] Lieblein, S., "Analysis of Temperature Distribution and Radiant Heat Transfer Along a Rectangular Fin", NASA TN D-196, 1959.

[13] Peraldi, A.L., "The Meteosat Dual-Channel Radiometer", in "Infrared Detection Techniques for Space Research", V. Manno and J. Ring, Eds., D. Reidel Publishing Company, Dordrecht, Holland, 1972, pp. 93-99.

[14] Reynolds, M.L., Kieffer, J., "Meteosat Cleanliness Control Achievements", in ESA SP-145, "Spacecraft Materials in Space Environment", Proceedings of a Symposium held at ESTEC, Noordwijk, The Netherlands, Oct. 2-5, 1979, pp. 181-184.

[15] Rolfo, A., "In Flight Results of a Cryogenic Cooler Designed for Meteosat", IAF 76-210, XXVII Congress International Astronautical Federation, Anaheim, California, Oct. 10-16, 1976.

[16] Schnurr, N.M., Cothran, C.A., "Radiation from an Array of Gray Circular Fins of Trapezoidal Profile", AIAA Journal, Vol. 12, No. 11, Nov. 1974, pp. 1476-1480.

[17] Sparrow, E.M., Miller, G.B., Jonsson, V.K., "Radiating Effectiveness of Annular-Finned Space Radiators, Including Mutual Irradiation between Radiator Elements", Journal of the Aerospace Sciences, Vol. 29, No. 11, Nov. 1962, pp. 1291-1299.

[18] Stockman, N.O., Kramer, J.L., "Effect of Variable Thermal Properties on One-Dimensional Heat Transfer in Radiating Fins", NASA TN D-1878, May 1963.

[19] Taylor, J.W.R., "Jane's all the World's Aircraft, 1978-1979", Macdonald and Jane's Publishers, Ltd., London, 1978, p. 657.

[20] Wright, P.E., "Refrigeration Systems for Spacecraft", RCA Advanced Technology (A 73-23781, 10-14), Radio Corporation of America, Moorestown, New Jersey, 1972, pp. 50-55.

[21] Wright, J.P., "Development of a 5 Watt 70º K Passive Radiator", AIAA Paper No. 80-1512, AIAA 15th Thermophysics Conference, Showmass, Colorador, July 14-16, 1980. Also published in "Heat Transfer and Thermal Control", Progerss in Astronautics and Aeronautics, Vol. 78, A.L. Crosbie, Ed., American Institute of Aeronautics and Astronautics, New York, 1981, pp. 429-451.